université PARIS-SACLAY

NNT : 2017SACLS452

Thèse de doctorat

Structure et fonction de protéines bactériennes à domaine FIC

Thèse de doctorat de l'Université Paris-Saclay
Préparée à l'Université Paris-Sud

École doctorale n°569 innovation thérapeutique : du fondamental à l'appliqué (ITFA)
Spécialité de doctorat: Biochimie et biologie structurale

Thèse présentée et soutenue à Cachan, le 11 décembre 2017, par

Simon Veyron

Composition du Jury :

Herman van Tilbeurgh Professeur, Université Paris-Sud (–FAAM)	Président
Pedro Alzari Professeur, Institut Pasteur (– UMR 3528)	Rapporteur
Jean-Michel Jault Directeur de recherche, IBCP (– UMR 5086)	Rapporteur
Isabelle Broutin Directrice de recherche, LCRB (–UMR 8015)	Examinateur
Yves Méchulam Directeur de recherche, École Polytechnique (– UMR 7654)	Examinateur
Jacqueline Cherfils Directrice de recherche, ENS Paris-Saclay (– UMR 8113)	Directeur de thèse
Gérald Peyroche Maître de conférences, ENS Paris-Saclay (–UMR 8113)	Invité

Université Paris-Saclay
Espace Technologique / Immeuble Discovery
Route de l'Orme aux Merisiers RD 128 / 91190 Saint-Aubin, France

Table des matières

Université Paris-Saclay
Espace Technologique / Immeuble Discovery
Route de l'Orme aux Merisiers RD 128 / 91190 Saint-Aubin, France

Remerciements

Je vais tout d'abord commencer par remercier Jacqueline. Ces 3 années de thèse ont été mouvementées mais je pense que nous avons trouvé un très bon rythme de travail. Je te remercie tout d'abord pour la confiance que tu m'as accordée. Que ce soit pour les horaires de travail ou la possibilité de faire telle ou telle expérience, tu m'as permis de trouver mon rythme, d'accomplir mon travail comme il me semblait être le mieux et de mener la recherche que je voulais tout en m'encadrant et remettant dans le droit chemin quand nécessaire. Je te remercie également pour la formation exceptionnelle dont j'ai pu bénéficier dans cette équipe, de l'environnement de travail et des opportunités que tu m'as accordées en m'acceptant en thèse, ne serait-ce que pour tout les congrès et workshops auquel j'ai pu participer ! Enfin, je te remercie de m'avoir écouté quand j'avais besoin de parler avec toi, quelques soient tes disponibilités. J'espère que tu as apprécié cette thèse autant que moi et que tu en es aussi satisfaite que moi.

Je remercie également Gérald d'avoir été là pour prendre part à nos discussions, échanger sur les différentes expériences et pour l'attention et la patience infinie dont tu as fait preuve malgré des nombreuses obligations.

Je tiens ensuite évidemment à remercier chaque membres du Jury d'avoir accepter de venir assister à ma thèse, de prendre le temps d'étudier ce document et d'évaluer ces 3 années de travaux.

Je remercie les équipes des différentes lignes de lumière au synchrotron Soleil où j'ai eu la chance de passer de nombreuses heures et en particulier Léo et Pierre de Proxima 1 pour leur aide ainsi que Gilles qui a coordonné notre BAG pendant tout ce temps.

Je remercie particulièrement Codjo Hountondji, Anne et Soria qui m'ont encadrés en stage volontaire il y a déjà 7 ans pour m'avoir fait découvrir le monde de la recherche et m'avoir orienté vers le bon Master. Je remercie également les deux responsables de ce master formidable qu'est Ingénierie des biomolécules, Philippe Minard et Herman van Tilbeurgh et surtout les amis de promotion Adeline, Clément, Dimitri et Margarida, sans qui ces 2 années auraient été bien compliquées.

Ces 3 années ne se seraient pas passées aussi bien sans l'équipe Small GTPases

d'abord au LEBS puis au LBPA. J'ai eu la chance de travailler avec des personnes formidables et toujours là pour m'aider à travailler ou à faire une pause. Je remercie donc particulièrement François Peurois le râleur, en face de moi et toujours là pour discuter, pour donner son avis sur une expérience et pour s'occuper de stagiaires ! Tu as un don pour l'enseignement, j'espère que tu y parviendras. Lulu, ma voisine de bureau, toujours là pour m'aider et me soutenir également, ne serais-ce qu'en choix de musique pour contrer François et ses goûts douteux. Yann l'encyclopédie et mon camarade de synchrotron et de bière de fin de journée. Si j'ai des doutes dans le futur, je sais où tu habites maintenant ! Je n'oublie pas non plus Christian et Noelia qui complètent l'équipe synchrotron, Wenhua, Ilham et Mahel qui étaient toujours là pour discuter et le reste de l'équipe que je voyais moins (Marie-Hélène et surtout Jorge).

Je tiens également à remercie Valérie qui nous a quitté lors de notre déménagement au LBPA pour m'avoir encadré lors de mon stage, pour tout ce que tu m'as appris et pour ta bonne humeur, Agata, la maman du synchrotron et Sarah, dernier membre du labo 106 et ma camarade de Jeanne Mas !

Je remercie également tous les membres du LBPA, j'ai eu la chance de bien m'entendre avec tout le monde mais tout particulièrement Olivier, Fred, Martine, Marie-Christine, Malcolm et Naïma.

Je remercie bien évidemment mes parents, mon frère, ma sœur et mes amis de m'avoir soutenu même sur la fin de la thèse, particulièrement Jeff, François, Pierre et Coline, copains d'amour de toujours et pour toujours.

Je n'ai pas de mots pour remercier assez Coralie-Anne qui partage ma vie depuis presque le début de cette aventure. Je te remercie pour toutes ces années, tout ces souvenirs et pour ton amour et ton soutien (presque) infini. Quoique j'écrive, ce ne sera pas suffisant mais ma vie ne serait pas la même sans toi.

Problématique de la thèse

Les protéines FIC, pour filamentation induced by cAMP, ont été découvertes il y a 30 ans chez *Escherichia coli* et sont aujourd'hui identifiées comme une famille de transférases très répandues dans le domaine bactérien. Ces dernières années, ces protéines sont devenues de plus en plus étudiées de par leur incroyable plasticité et aujourd'hui plus de 20 000 gènes codants une protéine FIC ont été identifiés par annotation automatique, mais seulement quelques exemples ont été étudiés.

Les membres de cette famille se caractérisent tout d'abord par leur activité de modification post-traductionnelle d'une protéine cible avec une molécule contenant un phosphate, modification ayant pour effet d'activer ou d'inactiver la fonction de la cible. Ainsi, qu'une FIC soit impliquée dans une fonction interne à la cellule ou qu'elle soit une toxine de pathogène une régulation fine est mise en œuvre. Si cette régulation des FICs est encore peu étudiée, 2 sous-familles sont décrites : les modules toxine-antitoxine et les FICs autorégulés par un glutamate.

Les modules toxine-antitoxine sont constitués de protéines FICs qui sont inactivées par la formation d'un complexe avec une antitoxine et dont l'activation requiert la dissociation.

Les FICs autorégulées sont des protéines portant une hélice alpha positionnant un glutamate dans leur site actif. Ces protéines sont décrites comme étant inhibées pour la fixation de l'ATP et l'activité d'AMPylation à proprement parler par ce résidu, les études publiées sur les protéines de cette famille exploitent donc toujours une mutation de ce résidu glutamate. Cependant, une étude récente a montré que la protéine FIC humaine HYPE est capable de dé-AMPyler sa cible BIP lorsqu'elle n'est pas mutée pour ce glutamate. Ce résultat suggère que cette mutation pourrait donc ne pas avoir pour seul effet d'activer constitutivement l'activité AMPylase, mais pourrait également impacter l'activité « dé-AMPylase ». Cette découverte ouvre de grandes perspectives sur l'étude de ces protéines si elle s'avérait transposable à d'autres membres de cette sous-famille et suggère que l'étude de FICs à glutamate régulateur non mutés pourrait révéler des informations encore inconnues sur le mécanisme.

Si ces deux familles regroupent la majorité des FICs décrites, de nombreuses autres protéines ont un mode de régulation différent. Parmi celles-ci, l'effecteur de la bactérie *Legionnela pneumophila* AnkX, toxine à domaine FIC qui catalyse le transfert d'une molécule de phosphocholine sur une petite protéine G de la famille des Rab. Cette modification post-traductionnelle est retirée par une seconde toxine de *Legionella* et des études

suggèrent que la proximité membranaire pourrait jouer un rôle régulateur lors de l'activité de modification de la petite GTPase.

La problématique de ma thèse a donc été d'étudier les régulations de protéines à domaine FIC d'un point de vue fonctionnel et structural.

Dans ce manuscrit, je présente dans un premier temps une synthèse bibliographique sous la forme d'une revue sur l'état de l'art de la famille des protéines FIC. Pour cette revue, j'ai choisi un fil conducteur portant sur la complémentarité des stratégies expérimentales utilisées pour étudier ces différentes protéines (Article 1).

Cette revue est suivie de la présentation des résultats de l'étude d'une nouvelle FIC à glutamate régulateur, dont j'ai réussi à élucider le mécanisme de dé-modification en combinant analyses biochimiques et cristallographiques. Ces résultats sont présentés sous forme d'un manuscrit d'article en cours de soumission (Article 2), complété par de résultats supplémentaires.

Ensuite, je présente une étude biochimique et structurale menée sur AnkX et axée sur sa régulation par les membranes et dont les résultats sont présentés sous forme d'un d'article en cours de rédaction (Article 3) et de résultats supplémentaires.

Enfin, la mise au point et l'exploitation d'une méthode d'étude des petites protéines G aux membranes sans l'utilisation de modification lipidique, qui a fait l'objet d'une publication à laquelle j'ai participé activement, sont présentées (Article 4).

I. Les multiples facettes des protéines à domaine FIC

A. Introduction

Les protéines à domaine FIC ont été découvertes il y a 30 ans chez *Escherichia coli* mais le domaine de recherche sur ces protéines n'a vraiment commencé à être exploré qu'il y a une dizaine d'années. Aujourd'hui il est établi que la famille des protéines FIC est très majoritairement bactérienne, un seul membre ayant été identifié chez les animaux.

Cette famille est caractérisée par un domaine catalytique à structure tridimensionnelle hélicoïdale très conservée, appelé domaine FIC ou Fido, présentant le motif signature de la famille. Ce domaine porte l'activité de modification post-traductionnelle d'une protéine cible avec une molécule contenant un phosphate, à savoir le phosphate lui-même (phosphorylation), des nucléotides monophosphates (ex : AMP, réaction d'AMPylation), ou d'autres composés (ex : phosphocholine, réaction de phosphocholination). Dernièrement, il a été montré que la seule protéine FIC humaine connue (HYPE ou FICD) présente une activité de modification mais également de dé-modification.

Aujourd'hui, les protéines FIC ont été décrites comme étant impliquées dans différents processus cellulaires. Ainsi, des exemples de toxine sécrétée ciblant des protéines de la cellule infectée comme les petites GTPases impliquées dans la dynamique du cytosquelette ou dans le contrôle du trafic vésiculaire de la cellule hôte ont été identifiés. Des FICs impliquées dans la régulation de la réponse au stress ont également été décrits montrant que les membres de cette famille ont un rôle d'interrupteur moléculaire.

La caractérisation d'une nouvelle protéine FIC passe donc par l'identification de ses substrats, donneur de groupement d'une part et protéine cible d'autre part, l'étude de ses effets et l'analyse de sa régulation. Ces questions s'appliquent à toutes les FICs et sont parfois peu comprises.

Dans un premier temps, une analyse *in silico* permet d'identifier une nouvelle protéine FIC et une analogie de séquence de formuler des hypothèses sur son activité. Si les marqueurs bio-informatiques existants ne permettent pas d'identifier avec certitude l'activité d'une protéine, l'alignement avec les structures des autres FICs caractérisées peut permettre de formuler de nouvelles hypothèses sur les substrats de la protéine une fois la structure de la protéine connue.

La structure des protéines FIC est donc une source précieuse de données, la conservation du site actif présentant des informations sur la reconnaissance du substrat.

Parmi les structures résolues, on peut noter celle d'IbpA en complexe avec sa cible

modifiée (AMP-Cdc42, forme AMPylée de la protéine Cdc42), la seule à ce jour qui donne des informations sur la reconnaissance de la protéine cible par l'enzyme, ou encore le travail réalisé sur les modules toxine/antitoxine, Doc/PhD d'une part et FicTA d'autre part. La structure a montré que l'antitoxine bloque stériquement l'accès au site actif en se complexant avec la toxine et que dans le cas des modules FicTA, l'antitoxine empêche la fixation du substrat ATP en positionnant un glutamate dans le site actif de la toxine FicT. La comparaison des structures du complexe FicTA et du complexe FicT-ATP ont permis de montrer que le glutamate positionné dans le site actif par l'antitoxine se localise à la place qu'occupe le phosphate gamma de l'ATP dans le complexe FicT-ATP, empêchant donc sa fixation dans une conformation catalytique. Ce mécanisme de régulation des toxines FicT par leur antitoxine a été étendu à une sous-famille dont les membres présentent ce glutamate dans le site actif de manière intramoléculaire, la sous-famille des FICs à glutamate régulateur, aussi appelé glutamate inhibiteur dans la littérature. L'étude de certaines de ces protéines par mutation de ce résidu a montré que l'activité d'AMPylation en présence d'ATP était bien inhibée par le glutamate et les études structurales ont confirmé que seul son déplacement permet la fixation de l'ATP en position catalytique. La protéine humaine HYPE présentant une activité de dé-AMPylation fait partie de cette sous-famille et une étude récente suggère que le glutamate régulateur serait impliqué dans cette dé-AMPylation.

La caractérisation de l'activité est effectuée *in vitro* avec des protéines recombinantes purifiées. Les FICs présentent une activité d'auto-modification ce qui permet de faire des tests d'activité sans connaître la cible. La grande majorité des FICs décrites ayant une activité de transfert de nucléotide monophosphate à partir d'un nucléotide triphosphate, la plupart des études d'activité utilisent des nucléotides radioactifs pour le phosphate alpha et une analyse des produits de la réaction par SDS-PAGE et autoradiographie. Cette méthode peut également être utilisée pour rechercher et identifier une cible en analysant l'effet sur des extraits cellulaires ou pour confirmer une cible putative en procédant à l'aide de protéines recombinantes.

Lorsque nécessaire, des systèmes à plusieurs composants peuvent même être reconstitués *in vitro,* comme il a été réalisé avec Doc où la reconstitution du système de traduction à permis l'identification d'EF-Tu en tant que protéine cible ou l'utilisation de membranes artificielles pour pouvoir réaliser des cinétiques de l'activité d'AnkX.

La caractérisation de l'effet de la modification post-traductionnelle catalysée par une FIC nécessite parfois de procéder à des analyses *in cellulo* ou *in vivo*. Ainsi, l'identification de cible et la

caractérisation de l'effet de l'activité de certaines protéines FIC ont été obtenues par des études d'infection (cas de plusieurs toxines) ou par expression ectopique du gène. Nous pouvons citer l'effecteur de *Legionella* AnkX qui va cibler les petites protéines G Rab1 et Rab35 et détourner la voie de recyclage endosomale durant l'infection, les toxines VopS et IbpA dont la fonction durant l'infection va être de perturber le cytosquelette de la cellule hôte ou encore la protéine HYPE humaine dont l'étude a révélé que son activité était impliquée dans la réponse au stress du réticulum endoplasmique par contrôle de l'activité de la chaperone BIP.

L'analyse du principe et des apports de ces différentes méthodes d'analyses des protéines FIC a fait l'objet d'une revue présentée ci-après.

FIC proteins: from bacteria to human and back again

Simon Veyron, Gérald Peyroche and Jacqueline Cherfils

CNRS and Ecole normale supérieure Paris-Saclay, Cachan, France

Abstract

The founder of the FIC (Filamentation induced by cyclic AMP) family is a thermosensitive mutant of an E.coli protein discovered in the early 80's, which impairs bacterial division under stress conditions leading to filamentation. However it is only during the last decade that FIC proteins were defined as a large family comprised of a variety of enzymes found in bacteria and a single member found in animals. The *air de famille* of FIC proteins stems from a domain of conserved 3-dimensional structure with a signature catalytic sequence, which catalyzes the post-translational modification (PTM) of proteins by a phosphate-containing compound. In bacteria, examples of FIC proteins include the toxin component of toxin/antitoxin modules (Doc/PhD and VbhT-VbhA), toxins secreted by pathogenic bacteria to divert small GTPases of the host cell (AnkX, IbpA and VopS), and a vast majority of proteins of unknown functions comprised of a FIC domain either alone or decorated with other domains. FIC proteins of known function catalyze primarily PTM by AMP (IbpA, VopS, VbhT) but they are not intrinsically restricted to this PTM. Other PTMs carried out by FIC proteins include UMP (FIC protein from a plant pathogen), phosphate (Doc) and phosphocholine (AnkX). Recently, studies on animal FICD (also called HYPE) revealed a new twist in the FIC landscape. FICD was shown to catalyze both AMPylation and de-AMPylation of the BIP chaperone, and both activities are required for the unfolded protein response in the endoplasmic reticulum. FICD shares structural features with bacterial FIC proteins, raising the possibility that some of them may also encode such dual activities. In this review, we discuss how complementary bioinformatics and experimental approaches have fertilized each other to generate and prove hypothesis regarding the PTM, protein substrate and regulation of FIC proteins from bacterial pathogens to animals, with a particular emphasis on the central contribution of structural biology.

FIC proteins: from the air de famille to function

FIC proteins are widespread in bacteria, with a single member found in animals. They have attracted considerable interest over the last decade for their functions in bacterial stress responses and in infections (reviewed in [1-4]) and recently in proteostasis control in animal cells (reviewed in [5]). The air de famille of FIC proteins stems from a domain of conserved 3-dimensional structure with a signature sequence that catalyzes the post-translational modification (PTM) of proteins by a phosphate-containing compound. This domain was called Fido (FIC domain) as an umbrella term to refer to FIC proteins and other proteins with the same overall fold [6]. In bacteria, genes coding for FIC proteins are often found in mobile genomics islands which may have facilitated their spreading across bacterial species [7].

A commonality of FIC proteins with known functions is that they carry out the post-translational modification (PTM) of target proteins by a phosphate-containing compound, and this enzymatic activity is entirely comprised in the FIC domain. This function was not known when the first FIC gene was discovered in E. coli 30 years ago, in which a point mutation was found to impair cell division under stress conditions (cyclic AMP in growth medium at high temperature), leading to filamentation [8, 9]. This now anecdotal observation led to naming this gene fic-1 for Filamentation Induced by cAMP, and later to extend the name to the conserved FIC domain [10, 11] and eventually to the entire family [6]. The product of fic-1 gene was recently characterized as the toxin component of a toxin/antitoxin (TA) module structurally related to the VbhT-VbhA TA module and has now been renamed EcFicT [12]. The function of EcFicT has not yet been elucidated. However, the related *Pseudomonas fluorescen*t Fic-1 inhibits DNA replication by adding AMP to DNA gyrase [13], a reaction coined AMPylation or adenylylation, and ectopic expression of *Bartonella schoenbuchensis* VbhT in E.coli disrupts DNA topology by adenylylation of DNA gyrase and topoisomerase [14]. Thus, it is plausible that EcFicT also functions in controlling DNA replication.

It took more than 3 decades for the FIC family to be brought into limelight, following the landmark discoveries that toxins carrying a FIC domain are secreted by bacterial pathogens to divert small GTPases in infected cell by AMPylation [10, 11]. *Vibrio parahaemolyticus* VopS [10] and *Histophilus somni* IbpA [11] both AMPylate small GTPases of the Rho family, which inactivates them leading to the collapse of the actin cytoskeleton. This reaction uses ATP as donor for AMP, which is transferred to hydroxyl-containing

residues on the target protein (tyrosine, serine or threonine). While AMPylation was briefly thought to be the unifying reaction in the family (reviewed in [15]), alternative enzymatic activites were soon discovered, including phosphocholination of Rab small GTPases by the type IV *Legionella pneumophila* effector AnkX [16], phosphorylation of the GTPase-related elongation factor EF-Tu by the plasmid-borne toxin-antitoxin Doc/PhD module in *E. coli* [17, 18], and addition of UMP to plant immune kinases by a FIC protein from the plant pathogen *Xanthomonas campestris* [19]. The reaction landscape of FIC proteins was accordingly extended to the more general function of transferring a phosphate-containing compound to a target protein leading to signaling roadblocks (reviewed in [2, 3]. In an unexpected twist, the sole animal protein with a FIC domain, called HYPE or FicD, was recently shown to carry out both the addition [20, 21]and removal [22, 23] of AMP from the endoplasmic reticulum chaperone BIP. De-AMPylation depends on a glutamate located outside the catalytic FIC motif itself [23], which is structurally conserved in FicD/Hype and a subset of bacterial FIC proteins where it is thought to serve an autoinhibitory function [24].

Currently, our understanding of many aspects of FIC proteins remains fragmentary. What is the protein substrate, the PTM donor (referred to as the co-factor hereafter) and the primary post-translational modification (PTM) carried out by individual FIC proteins? How are animal and bacterial FIC proteins regulated? Is de-AMPylation also found in bacterial FIC proteins? Ultimately, what is the function of the still predominantly uncharacterized bacterial FIC proteins? In this review we discuss how complementary bioinformatics and experimental approaches have been used to generate and prove hypothesis regarding the PTM, protein substrate and regulation of FIC proteins from pathogens to humans, with a particular emphasis on the central contribution of structural biology.

Bioinformatics: analyzing phylogeny and predicting mechanisms.

High-throughput sequencing of bacterial genomes identified potential coding genes for proteins with FIC signatures in a large number of bacterial species, including free-living, host-associated, commensal and pathogenic species. For example, as of 2017 the PFAM database reports about 7500 sequences that contain a FIC domain, organized in 96 architectures found in >2300 bacteria, 360 eukaryotes and 71 archae species (**Figure 1**). In many cases, these genes were annotated in the databases as "Filamentation induced by cAMP protein" or "adenosime monophosphate-protein transferase". While the first annotation is now mostly anecdotal, the second annotation may be somewhat misleading as enzymatic activities other than AMPylation continue to be discovered. We suggest that unknown genes should therefore better be annotated as "uncharacterized FIC family protein" to reflect that fact. Sequence databases have provided a rich material to classify FIC proteins and investigate their phylogeny [1, 6, 7, 10, 11, 14, 24] and to forge hypothesis about regulatory mechanisms [24]. However, predicting whether a FIC protein of unknown function is an actual AMPylator based on its sequence alone still remains uncertain. We discuss below how structural biology highlights functional diversity encoded in FIC sequences, while experiments using recombinant proteins and cell assays have remained the primary approaches for discovering the enzymatic activities and functions of individual FIC proteins.

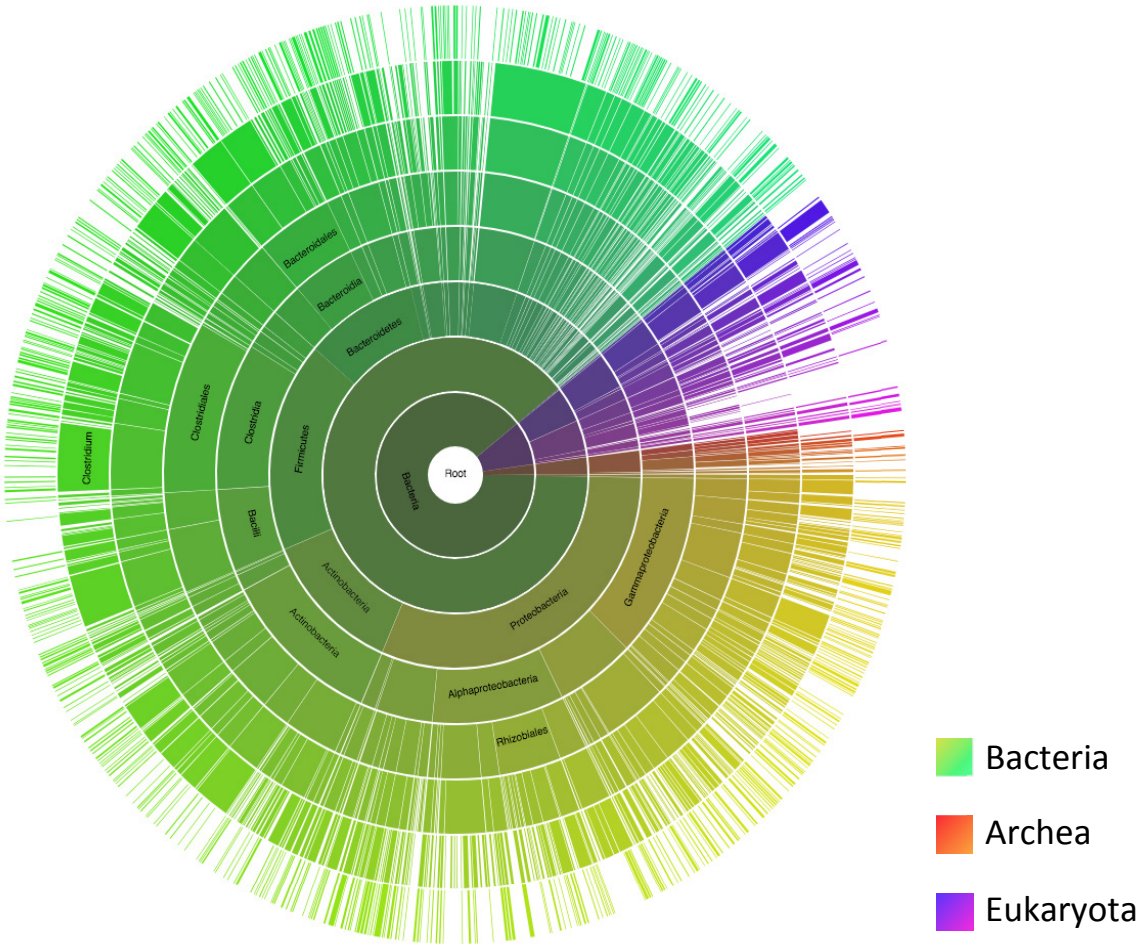

Figure 1: A graphical representation of the distribution of the Fic genes (PF02661) across taxonomic levels. Reproduced from the EMBL-EBI PFAM server (http://pfam.xfam.org/family/Fic#tabview=tab7) [25]. The distribution among the eight major taxonomic levels is shown, starting with superkindom in the center of the sunburst, and then centrifuges circles corresponding successively to kingdom, phylum, class, order, family, genus and species. Each circle is subdivided in coloured arcs corresponding to superkingdoms and/or kingdoms. The longer the arc, the higher the number of species harboring at least one FIC gene. On the most outside circle, one line corresponds to one species, irrespectively of the number of FIC genes (one or more) unraveled in its genome. It should be noted that except for bacteriophage P1 Doc/PhD found in E.coli, FIC proteins have not been identified in viruses.

Structural biology: dissecting mechanisms and inspiring regulation hypothesis.

The first high-resolution structures of a FIC protein were those of single domain FIC proteins from *Helicobacter pylori* and *Neisseria meningitidis*, which were determined as part of Structural Genomics Initiatives in 2006 (PDB entries 2G03 and 2F6S, which have no associated publications). However, the structure of FIC proteins only began to be discussed with the structure of the Doc/PhD toxin/antitoxin complex[25] and soon afterwards with the discovery of AMPylating FIC toxins from pathogenic bacteria [10, 11, 26]. As of today, the structures of >20 FIC proteins have been determined, several of them in complex with a co-factor bound to the active site, while only one has a bound protein substrate (**Table 1** and references therein). These structures established the remarkable conservation of the FIC domain and of the FIC motif (HPFx[D/E]GNGR, with variations) that carries the invariant catalytic histidine (**Figure 2A**). Importantly, they identified a variety of structural features that explain the mechanism of PTM modifications and they irrigated the field with fruitful hypothesis (reviewed in [1-3]). We present below some of the milestone structures that shaped our current understanding.

How FIC proteins bind to their protein substrate was elucidated by the structure of *Histophilus somni* IbpA bound to AMPylated Cdc42, a small GTPase that regulates actin cytoskeleton dynamics [26]; as of today, it remains the only structure of a FIC protein bound to a protein substrate (**Figure 2B**). This structure revealed that the target residue (here, a tyrosine from the small GTPases CDC42) is presented into the active site as an extended peptide that binds to a β-hairpin that is structurally conserved in FIC proteins. In Cdc42, the target peptide is the so-called switch 1, a flexible region in small GTPases, and it is distorted to bind the β-hairpin. It is plausible that intrinsic flexibility is a general feature of regions that are modified by FIC proteins. The IbpA/Cdc42 structure also revealed that IbpA interacts with Cdc42 with regions outside the FIC domain, which explains its narrow specificity. Other structures of Fic proteins, such as the bacterial toxin VopS [27], carry non-FIC domains in the vicinity of their active site, which, as seen in IbpA, may contribute to the specific recognition of their protein target. Conversely, single-domain FIC proteins do not carry elements outside their active site to recognize their targets. The substrate of these proteins has remained unknown, and the possibility that they modify peptides rather than proteins cannot be excluded. Domains appended to the FIC domain can also have localization functions. Using small angle X-ray scattering (SAXS), a method to observe the structure of proteins in

solution, we found that the AnkX toxin has a horseshoe shape that allows it to bind simultaneously to membrane-attached Rab GTPases by its FIC domain and to the membrane by its C-terminal domain (Veyron et al., our unpublished observations). These findings are consistent with the observation that AnkX binds to membranes in cells by elements located in its C-terminal half [28].

Structures of FIC proteins bound to co-factors (defined as the diphosphate-containing substrate used for PTM) or reaction products revealed both common and unique features of co-factor recognition and processing (reviewed in [1-3]; **Table 1** and **Figure 2C**). Notably, the structure of *Legionella pneumophila* AnkX in complex with intact CDP-choline, the co-factor for the phosphocholination of the small GTPase Rab1, showed that the FIC motif recognizes solely the diphosphate moiety of the co-factor, while the cytidine and choline moieties are recognized by elements located both upstream and downstream the FIC motif (**Figure 2D**) [29]. Likewise, residues in contact with the adenine moiety of ATP vary greatly between FIC proteins with AMPylation activity. This diversity explains why predicting the nature of the co-factor has remained difficult based on sequences only. In the future, a complementary strategy to discover co-factors of FIC proteins could be through structure-based docking, an approach that docks and ranks small molecules into crystal structures or structural models and is widely used in drug discovery to identify small molecules that bind to protein targets (reviewed in [30]); in the case of FIC proteins, our current knowledge suggests that this approach could be restricted to diphosphate-containing compounds.

Because FIC proteins appear to carry out reactions that stall major cellular processes, an important issue is whether they are regulated, and in which case, what are the modalities of this regulation. The structures of plasmid prophage Doc/PhD [25, 31] and of *Bartonella* VbhT/VbhA [24] toxin/antitoxin modules provided a general principle for inhibition of FIC toxins by their cognate antitoxins, in which the catalytic site of the toxin is obstructed by the antitoxin. Accordingly, dissociation of the antitoxin releases inhibition. Remarkably, comparison of VbhT/VbhA structure with the crystal structure of a single domain FIC protein from Neisseria led to the discovery of a structurally equivalent glutamate that wedges into the active site in trans in VbhT and in cis in monomeric FIC proteins [24] **(Figure 2E).** Several structures of glutamate-containing FIC proteins with bound ATP highlighted that this nucleotide binds in a non-canonical binding mode [32, 33] or in a manner where only the ADP moiety is visible [24], suggesting that the glutamate conflicts with the binding of ATP in

a catalytically-competent conformation. Furthermore, mutation of the glutamate unleashed a potent AMPylation activity in these proteins, leading to the hypothesis that this residue is auto-inhibitory for the AMPylation reaction [24]. This hypothesis fueled intense research to discover signals or interactions able to trigger inhibition release. In the case of single domain FIC proteins, recurrent observation of oligomers in the crystal led to propose that this large group of bacterial FIC proteins are regulated by oligomerization, thereby enabling auto-AMPylation as a means to displace the auto-inhibitory glutamate [34]. In an unexpected twist, animal HYPE/FicD proteins were recently shown to support the removal of AMP from the BIP chaperone in cells [20, 21] and this was dependent on the same structurally conserved glutamate [23]. This raises the intriguing possibility that single domain FIC proteins and other proteins with an inhibitory glutamate may also have similar dual activities. However, a major question remaining is the nature of the cellular cues able to undergo variations that are large enough to promote the switch from the AMPylation reaction to the de-AMPylation reaction.

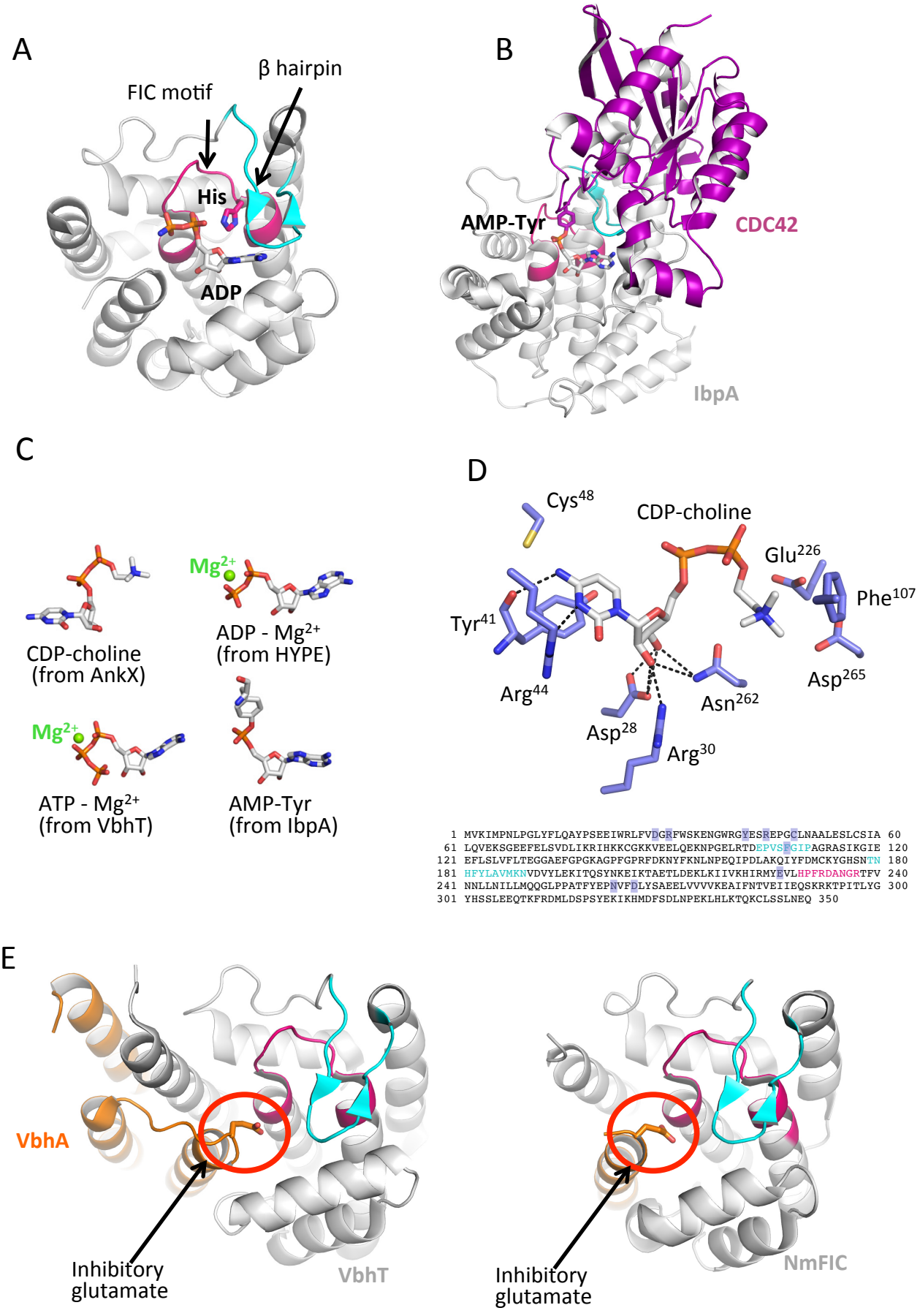
A
FIC motif
β hairpin
His
ADP
B
AMP-Tyr
CDC42
IbpA
C
CDP-choline
(from AnkX)
Mg2+
ADP - Mg2+
(from HYPE)
Mg2+
ATP - Mg2+
(from VbhT)
AMP-Tyr
(from IbpA)
D
Cys48
CDP-choline
Glu226
Phe107
Tyr41
Arg44
Asn262
Asp265
Asp28
Arg30
1 MVKIMPNLPGLYFLQAYPSEEIWRLFVDGRFWSKENGWRGYESREPGCLNAALESLCSIA 60
61 LQVEKSGEEFELSVDLIKRIHKKCGKKVEELQEKNPGELRTDEPVSEGIPAGRASIKGIE 120
121 EFLSLVFLTEGGAEFGPGKAGPFGPRFDKNYFKNLNPEQIPDLAKQIYFDMCKYGHSNTN 180
181 HFYLAVMKNVDVYLEKITQSYNKEIKTAETLDEKLKIIVKHIRMYEVLHPFRDANGRTFV 240
241 NNLLNILLMQQGLPPATFYEPNVFDLYSAEELVVVVKEAIFNTVEIIEQSKRKTPITLYG 300
301 YHSSLEEQTKFRDMLDSPSYEKIKHMDFSDLNPEKLHLKTQKCLSSLNEQ 350
E
VbhA
Inhibitory
glutamate
VbhT
Inhibitory
glutamate
NmFIC

Figure 2. Structural features of FIC proteins.

A- The canonical FIC domain, exemplified by the structure of NmFIC-ADP. The Fic motif is in pink and the catalytic histidine shown, the β-hairpin is in cyan. A bound co-factor (ATP) is shown in stick representation. The same color coding is used in the other panels. All PDB entries and references are given in **Table** 1.

B. The structure of the *Histophilus* IbpA toxin bound the small GTPase Cdc42. Cdc42 is in purple and the FIC proteins in grey. The AMPylated tyrosine of Cdc42 is shown in a circle

C: Examples of co-factors found in crystal structures. AMP-Tyr is from Histophilus IbpA in complex with AMPylated Cdc42, ADP-Mg^{2+} is from human HYPE carrying a mutation of the inhibitory glutamate, ATP-Mg^{2+} is from Bartonella VbhT in complex with VbhA carrying a mutation of the inhibitory glutamate, CDP-choline is from Legionella AnkX carrying a mutation of the catalytic histidine. The FIC domain is in the same orientation in all views.

D: The active site of Legionella AnkX, showing elements from outside the FIC motif that recognize the cytosine and choline moieties of CDP-choline. Below, the sequence of AnkX, highlighting these residues in blue. The β-hairpin, which in AnkX is interrupted by an insertion, is in cyan and the FIC motif is in red.

E: Comparison of the structure of the VbhA-VbhT complex (left panel) and NmFIC (right panel). The inhibitory helix is located in the antitoxin in the VbhA-VbhT complex, and is in C-terminus in NmFIC (in orange). The inhibitory glutamate is circled in red.

Cell free assays with recombinant proteins: characterizing activities of FIC proteins

Biochemical assays using purified recombinant proteins have played a central role in characterizing the protein substrates and the co-factors of FIC proteins. Radiolabeling, in which the FIC protein is incubated with radioactive co-factors followed by autoradiography, is the standard assay to report on the activity of FIC proteins towards candidate protein targets. It was used to confirm the AMPylation activities of VopS [10] and IbpA [11] towards Rho GTPases (**Figure 3A**), the phosphocholination of Rab1 and Rab35 GTPases by AnkX [16, 29], and the AMPylation of BIP by FicD/Hype [21, 22]. Likewise, the de-AMPylation activity of FicD was established directly using recombinant FicD and purified BIP chaperone [23]. Surprisingly, FicD is also capable of AMPylating Rho GTPases in *in vitro* assays [11], but a phenotype suggesting that it inactivates Rho GTPases in cells has not been described. Recombinant proteins have also been used to identify or confirm candidate targets using cell extracts treated with ATP followed by mass spectrometry. This approach confirmed that

recombinant bacterial VopS AMPylates human Rho GTPases in cell extracts [10], and it revealed that the chaperone BIP is the substrate of human FicD using a hyperactive mutant in which the inhibitory glutamate had been mutated [22]. In a different setup, phosphorylation of the elongation factor Ef-Tu by Doc was discovered by radiolabeling using *in vitro* translation systems [17, 18].

Autoradiography is also the standard assay to identify candidate co-factors. For example, it showed that IbpA and VopS both use ATP and CTP to modify eukaryotic Cdc42 *in vitro*, while VopS but not IbpA can use GTP [35]. Another method to compare candidate co-factors has been the thermal shift assay (TSA), which is based on the assumption that natural co-factors will bind more strongly to the protein thereby increasing its thermal stability [32]). It should be noted that this assay is moderately sensitive and may not always yield accurate dissociation constants. A shortcoming in characterizing the activity of FIC proteins is that the natural co-factor, the natural protein target or both are often not known. A convenient readout for activity has therefore been the analysis of auto-modifications using autoradiography ([6, 19, 23, 24, 26, 32, 35-37]; Veyron, unpublished results). It should be emphasized that it has remained unclear whether auto-modifications are functionally important. In the case of single-domain FICs, indirect evidence based on mutants of the regulatory glutamate suggested that auto-modifications facilitate their conversion to an AMPylation-competent conformation [24, 34]. Auto-AMPylation was also observed in Pseudomonas Fic-1, which is related to the VbhT/VbhA TA module, and mutations of auto-AMPylation sites reduced its ability to modify DNA gyrase [13]. Conversely, study of autophosphocholination of AnkX by time-resolved Fourier transform infrared spectroscopy using caged compound suggested that is not relevant for catalysis [38] and some AnkX constructs with potent phosphocholination activity were not auto-modified[29]. This points to a possible promiscuity of FIC proteins under non-natural conditions, and to potentially different usages of auto-modifications by FIC proteins.

Gaining quantitative insight into the efficiency of FIC proteins is important to understand their regulation and this requires that their kinetics can be monitored. Kinetics of Rab GTPases phosphocholination by AnkX was measured using fluorescence, using either the signal from protein tryptophanes or from a fluorescent co-factor [36] (**Figure 3B**). Alternatively, ATP labeled by a fluorescent probe attached to the adenine base was used to monitor the de-AMPylation activity of FicD towards the BIP chaperone by following the

change in fluorescence anisotropy [23]. The kinetics of some FIC proteins being very slow, detection of the reaction product by antibodies that recognize modified residues can be used for semi-quantitative kinetics. For example the kinetics of Cdc42 AMPylation by VopS was assayed by measuring the incorporation of radiolabeled AMP at several time points [27]; similarly, the phosphocholination kinetics of Rab1 and Rab35 and the stimulatory effect of membranes by AnkX were determined using an anti-phosphocholine antibody (Veyron et al., our unpublished results). In the future, a systematic determination of kinetics appears highly desirable to quantify the efficiency, specificity and regulation of FIC proteins.

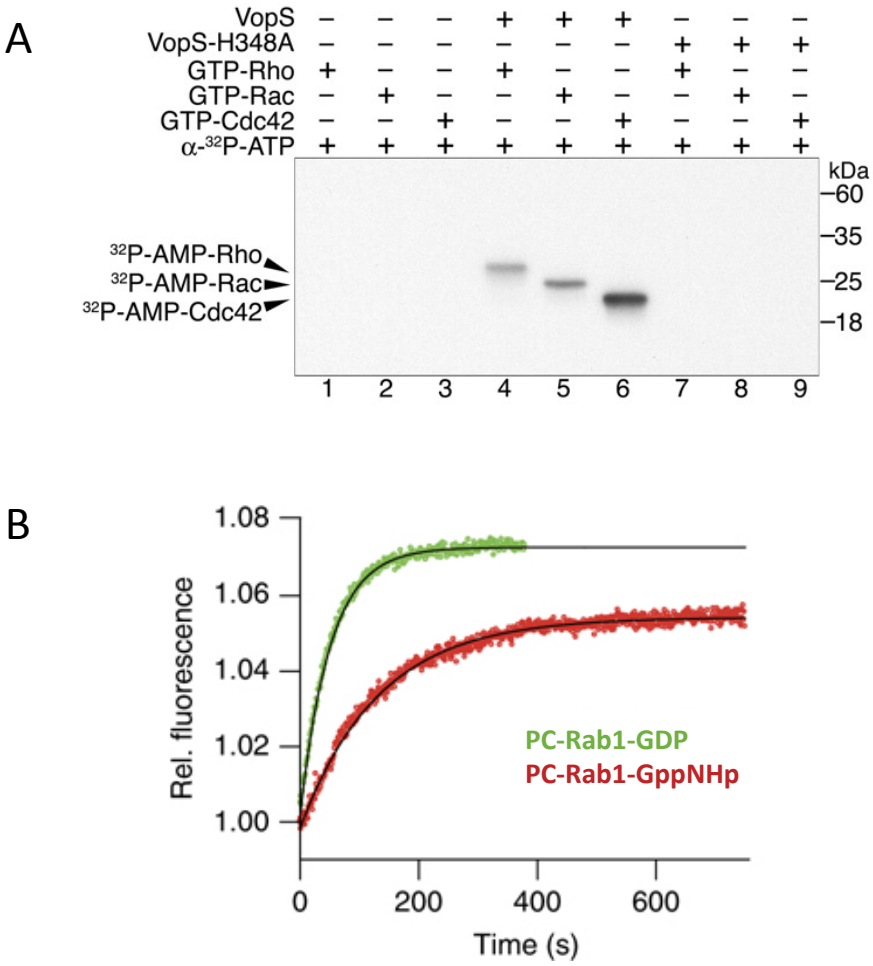

Figure 3: *In vitro* characterization of FIC proteins activity. A) *In vitro* AMPylation of Rac-family GTPases by recombinant VopS. Recombinant human GTPases (Rac, Rho, CdC42), active VopS from V. parahaemolyticus, and inactive VopS harboring a mutation of the catalytic histidine were expressed in E.coli and purified. VopS constructs lacked the N-terminal secretion signal. GTPases loaded with GTP were then incubated with recombinant VopS proteins in the presence of radiolabelled ATP. Proteins were separated by SDS-PAGE and analyzed by autoradiography. Controls in which VopS was omitted were performed (lanes 1-3). Reprinted with permission from [10]. B) AnkX phosphocholination kinetics analysis by intrinsic fluorescence measurement. Rab1b was loaded with GTP or with the non-hydrolysable GppNHp analogue. Addition of AnkX to solutions containing loaded Rab1b results in an exponential increase of tryptophane fluorescence (λexc = 297nm and λem=340nm). The curves can be fitted by mono-exponentials, allowing the determination of the catalytic efficiencies kcat/KM ($9.8x10^4$ $M^{-1}S^{-1}$ and $9.8x10^4$ $M^{-1}S^{-1}$ respectively). Reprinted with permission from [36].

Cell-based and in vivo assays : profiling PTM landscapes and characterizing functions.

A primary use of cell-based assays has been to generate and test functional hypothesis regarding how FIC proteins manipulate cell signaling. In most cases, investigations of FIC functions have been carried out through heterologous expression in cells. For example, phenotypes resulting from ectopic expression of VopS and IbpA guided the identification of their protein targets [10, 11]. Both toxins were shown to disrupt the actin cytoskeleton, a hallmark of the inactivation of Rho GTPases; this led to the discovery that these toxins inactivate Rho GTPases by AMPylation (**Figure 4 A**). Deletion and ectopic expression of FicD and mutant FicD in human cells, which resulted in AMPylation patterns that could not be explained by a simple AMPylation function, was instrumental in guiding the discovery that its primary function is the de-AMPylation of the BIP chaperone in the ER [23] (**Figure 4B**). Heterologous expression of animal FicD in yeast induced a heat shock response; this guided the subsequent characterization of a cytosolic activity of FicD in human cells [39]. For various bacterial FIC proteins that cannot be investigated directly in the species that express them, ectopic expression in *E. coli* has been used as a convenient proxy to investigate their functions and this allowed to identify candidate protein targets (e.g., DNA gyrase and topoisomerase as targets of VBHT, [14]). It cannot be excluded that their actual protein

substrate is not present in *E.coli* or that alternative substrates are picked up out of a possible specificity leakage in non-natural conditions.

Infection studies in cells were pivotal to the discovery that Legionella AnkX modified Rab GTPases by phosphocholination, reasoning that Legionella effectors interfere with the Rab machinery and that FIC proteins are enzymes that carry out PTMs [16]. This prompted the analysis of Rab GTPases by mass spectrometry following infection of macrophages by different Legionella strains, including one that did not secrete AnkX [16]. More recently, ectopically expressed AnkX was shown to localize on endosomal membranes using immunogold transmission electron microscopy and confocal microscopy, eventually revealing that it disrupts endosomal recycling in the course of infection [28]. In another cell infection study, the Doc/PhD toxin-antitoxin module of the pathogen *Salmonella typhimurium* was shown to be required for the formation of macrophage-induced non-replicating persisters [40].

Finally, there has been only few *in vivo* studies to date. In one study, the *C. elegans* ortholog of FicD/HYPE was shown to AMPylate cytosolic proteins *in vivo* to modulate the immune response [41], which is consistent with its cytosolic activity in human cells [39]. Another *in vivo* study showed that the deletion of Drosophila Fic results in blindness in flies [42].

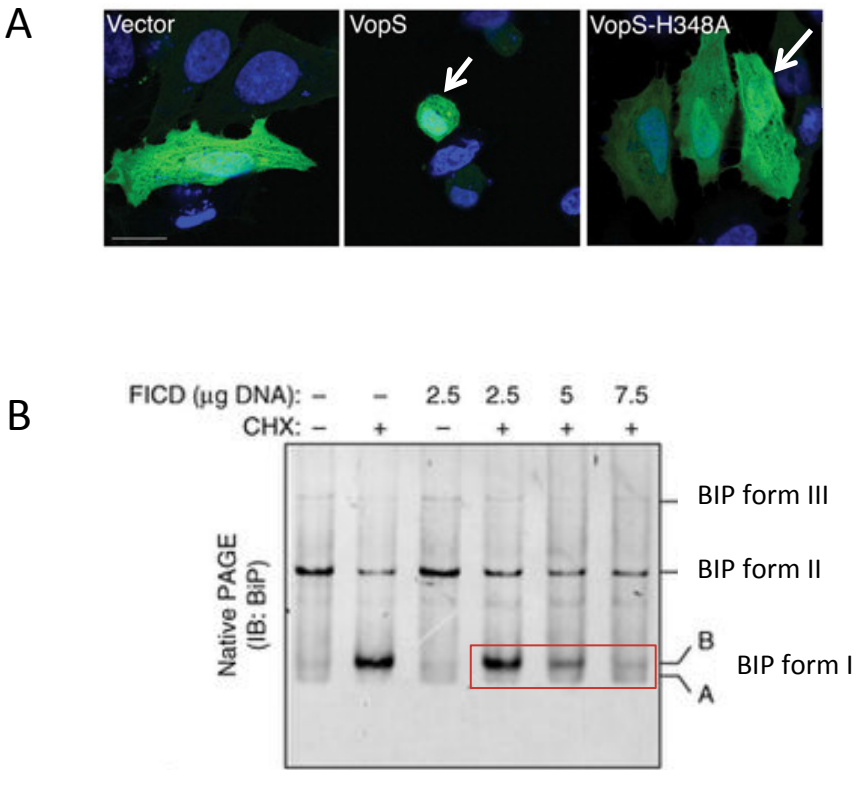

Figure 4: *In cellulo* analysis of FIC proteins. A) Ectopic expression of VopS in human cells results in the collapse of the actin cytoskeleton, suggesting that VopS inactivates Rho family small GTPases (reproduced from [10]). Hela cells were transfected with an empty vector or with a recombinant vector driving heterologous expression of the bacterial VopS protein under its active (wt) or inactive (VopS H348A) forms and then observed by confocal microscopy. Co-transfection with a vector expressing SFFV-eGFP fusion protein allows detection of transfected cells. Nuclei were identified by Hoechs stain. Scale bar, 10µm. The abnormal rounded shape specifically observed upon active VopS expression is typical of actin cytoskeleton disorganization. Reprinted with permission from [10]. B) Cellular effect of FICD overexpression on BIP deAMPylation. CHO-K1 cells, untransfected or transfected with increasing amounts of FICD expression vector, are exposed to cycloheximide (CHX) to promote BIP AMPylation. Proteins in lysates are then separated by native polyacrylamide gel electrophoresis and detected by anti FICD western blot. I, II and III corresponds to the different oligomerization states of BIP. The monomeric form (III) can be subdivided in unmodified (A) and AMPylated (B) forms. Increasing expression of FICD induces a correlative decrease in BIP AMPylation, consistent with FICD acting as a deAMPylating enzyme. Reprinted with permission from [23].

Concluding remarks

Research on FIC proteins is still in its youth, and original strategies to decipher their biochemical activities, regulations and functions in bacteria, infections and animals continues to reveal new surprises. New chemical tools are currently being devised to identify the target landscape of FIC proteins. For example, AMPylation-specific antibodies [43, 44], chemical reporters of AMPylation [41, 45] or of phosphocholination [46] that bind covalently to modified protein targets using click chemistry, or labeling with stable isosope-labeled ATP [47], provide tools that can be used in coordination to mass spectrometries to determine the PTM profiles in cells [48, 49]. Such approaches and their cross-validation by functional and biochemical studies will be important for future studies. Various experimental and computational methods have allowed important progresses and should continue to fertilize each other's finding. Likewise, discoveries in the bacterial and animal kingdoms should continue to contribute jointly to a more global understanding of the functional landscape of this fascinating family. Ultimately, this knowledge may guide the discovery of novel therapeutic strategies in infections and proteostasis-related diseases.

Acknowledgements.

This work was supported by grants from the Fondation pour la Recherche Médicale and from the Agence Nationale pour la Recherche to J.C. and by a grant from the DIM MALINF to S.V.

Table 1: Crystallographic FIC structures available in the Protein Data Bank. Secreted toxins are in pink; toxin/antitoxin modules are in green; bacterial single-domain FIC proteins with regulatory glutamate are in blue; other bacterial FIC proteins with regulatory glutamate are in khaki; animal FIC are in orange; other proteins with FIC domains are in white.

Name	Function	Bound protein	Ligand in the active site	Construct	PDB accession code	Ref.
Histophilus somnii **IbpA**	*AMPylation of Rho GTPases*	/	SO_4^{2-} – Zn2	FIC domain 2	3N3U	[26]
		CDC42	Tyr-AMP – Mg^{2+}	FIC domain 2 mutant for the catalytic histidine (H3717A)	4ITR	
Vibrio parahaemolyticus **VopS**	*AMPylation of Rho GTPases*	/	/	FIC domain	3LET	[10]
Legionella pneumophila **AnkX**	*Phosphocholination of Rab1 and Rab35 GTPase.*	/	SO_4^{2-} – Mg^{2+}	FIC domain	4BEP	[29]
		/	CMP		4BER	
		/	CMP – PC		4BES	
		/	CDP-choline	FIC domain Mutant for the catalytic histidine (H229A)	4BET	
Bartonella schoenbuchensis **VbhT**	*TA module AMPylation of E. coli GyrB and ParE*	Antitoxin VbhA	ATP – Mg^{2+}	FIC domain mutant for regulatory glutamate (E24G)	3ZCB	[33]
		Antitoxin VbhA	ATP	FIC domain	3ZC7	
		Antitoxin VbhA	/		3SHG	[24]
Escherichia coli **EcFICT**	*TA module AMPylation of E. coli GyrB and ParE*	Antitoxin EcFicA	Cl^-	Bacterial filamentation mutant (G55R)	5JFF	[12]
			/	WT	5JFZ	
Bacteriophage P1 **Doc**	*TA module Phosphorylation of Ef-Tu elongation factor*	Antitoxin Phd	/	WT	3K33	[50]
		Antitoxin Phd	Cl^-	Mutant for the catalytic phenylalanine (F68S)	3KH2	[31]
		Antitoxin Phd Cter	/	Mutant for the catalytic histidine (H66Y)	3DD7	[25]
		/	/		3DD9	[51]
Bartonella rochalimae **Bep1**	*TA module*	Antitoxin BiaA	SO_4^{2-}	FIC domain	5EU0	Not published
Neisseria meningitidis **NmFIC**	*AMPylation of E. coli GyrB*	/	/	WT	2G03	Structural genomics
			ADP		3S6A	[24]
			AMPPNP – Mg^{2+}	Deletion of C-terminal helix	3SE5	
			AMPPNP		3SN9	
			AMPPNP – Mg^{2+}	Mutant for regulatory glutamate (E186G)	3ZLM	[33]
			/	Mutant for interface residue (E102R)	5CGL	[34]
			/	Mutant for interface residue (E156G)	5CKL	
			Cl^-	Mutant for interface residues (E156R, Y183F)	5CMT	
Helicobacter pylori **HpFIC**	*Unknown*	/	Zn^{2+}	/	2F6S	Structural genomics
Enterococcus faecalis **EfFIC**	*Unknown*	/	/	WT	5NUW	Veyron et al in preparation
			/		5NV5	
			AMP – Ca^{2+}		6EP0	
			ADP		6EP5	
			ADP – Ca^{2+}		6EP2	

			/ SO_4^{2-} ADP	Mutant for catalytic histidine (H111A)	5NWF 5NVQ	
Bacteroides thetaiotaomicron **BtFIC**	*Unknown*	/	/	FIC domain	3CUC	Structural genomics
Shewanella oneidensis **SoFIC**	*Unknown*	/ / /	/ AMPPNP – Mg^{2+} AMPPNP – Mg^{2+}	WT Mutant for regulatory glutamate(E73G)	3EQX 3ZCN 3ZEC	[33]
Clostridium difficile **CdFIC**	*Unknown*	/ / /	/ ATP – Mg^{2+}	WT Mutant for regulatory glutamate and serine (S31A, E35A)	4X2E 4X2C 4X2D	[32]
Homo sapiens **FICD**	*AMPylation and de-AMPylation of endoplasmic reticulum chaperone BIP*	/ / / / /	/ ADP – Mg^{2+} ADP – Mg^{2+} ADP – Mg^{2+} ADP – Mg^{2+}	FIC domain FIC domain mutant for the regulatory glutamate (E234G) FIC domain WT but regulatory glutamate not visible FIC domain FIC domain	4U04 4U0S 4U07 4U0U 4U0Z	[52]
Caenorhabditis elegans **CeFIC-1**	*AMPylation cytosolic and endoplasmic reticulum HSP40 and HSP70*	/ /	SO_4^2 SO_4^2	FIC domain FIC domain mutant for the regulatory glutamate (E274G)	5JJ6 5JJ7	Not published [41]
Bartonella Quintana JK 31 **Bep**	*Unknown*	/	I^-	WT	4LU4	Structural genomics
Bartonella quintana strain Toulouse **Bep**	*Unknown*	/	ADP – Mg^{2+}	FIC domain	4N67	Structural genomics
Bartonella henselae **BepA**	*Virulence effector*	/ / /	$S0_4^{2-}$ Cl^- Ppi – Mg^{2+}	FIC domain FIC domain FIC domain	2VZA 2VY3 2JK8	[53]
Bartonella clarridgeiae **Bep5**	*Unknown*	/	/	FIC domain	4XI8	Structural genomics
Bartonella sp. 1-1C **Bep8**	*Unknown*	/	/	FIC domain	4PY3	Structural genomics
Desulfovibrio alaskensis **Dde_2494**	*Unknown*	/	Unknown ligand	WT	4RGL	Structural genomics
Pseudomonas syringae **AvrB**	*Unknown*	/ Peptide target RIN4 /	/ / ADP	WT WT WT	1NH1 2NUD 2NUN	[54] [55]

References

1. Garcia-Pino, A., N. Zenkin, and R. Loris, *The many faces of Fic: structural and functional aspects of Fic enzymes.* Trends Biochem Sci, 2014. **39**(3): p. 121-9.
2. Roy, C.R. and J. Cherfils, *Structure and function of Fic proteins.* Nat Rev Microbiol, 2015. **13**(10): p. 631-40.
3. Harms, A., F.V. Stanger, and C. Dehio, *Biological Diversity and Molecular Plasticity of FIC Domain Proteins.* Annu Rev Microbiol, 2016. **70**: p. 341-60.
4. Casey, A.K. and K. Orth, *Enzymes Involved in AMPylation and deAMPylation.* Chem Rev, 2017.
5. Truttmann, M.C. and H.L. Ploegh, *rAMPing Up Stress Signaling: Protein AMPylation in Metazoans.* Trends Cell Biol, 2017. **27**(8): p. 608-620.
6. Kinch, L.N., et al., *Fido, a novel AMPylation domain common to fic, doc, and AvrB.* PLoS One, 2009. **4**(6): p. e5818.
7. Khater, S. and D. Mohanty, *In silico identification of AMPylating enzymes and study of their divergent evolution.* Sci Rep, 2015. **5**: p. 10804.
8. Kawamukai, M., et al., *Cloning of the fic-1 gene involved in cell filamentation induced by cyclic AMP and construction of a delta fic Escherichia coli strain.* J Bacteriol, 1988. **170**(9): p. 3864-9.
9. Kawamukai, M., et al., *Nucleotide sequences of fic and fic-1 genes involved in cell filamentation induced by cyclic AMP in Escherichia coli.* J Bacteriol, 1989. **171**(8): p. 4525-9.
10. Yarbrough, M.L., et al., *AMPylation of Rho GTPases by Vibrio VopS disrupts effector binding and downstream signaling.* Science, 2009. **323**(5911): p. 269-72.
11. Worby, C.A., et al., *The fic domain: regulation of cell signaling by adenylylation.* Mol Cell, 2009. **34**(1): p. 93-103.
12. Stanger, F.V., et al., *Crystal Structure of the Escherichia coli Fic Toxin-Like Protein in Complex with Its Cognate Antitoxin.* PLoS One, 2016. **11**(9): p. e0163654.
13. Lu, C., et al., *Identification of Fic-1 as an enzyme that inhibits bacterial DNA replication by AMPylating GyrB, promoting filament formation.* Sci Signal, 2016. **9**(412): p. ra11.
14. Harms, A., et al., *Adenylylation of Gyrase and Topo IV by FicT Toxins Disrupts Bacterial DNA Topology.* Cell Rep, 2015. **12**(9): p. 1497-507.
15. Roy, C.R. and S. Mukherjee, *Bacterial FIC Proteins AMP Up Infection.* Sci Signal, 2009. **2**(62): p. pe14.
16. Mukherjee, S., et al., *Modulation of Rab GTPase function by a protein phosphocholine transferase.* Nature, 2011. **477**(7362): p. 103-6.
17. Castro-Roa, D., et al., *The Fic protein Doc uses an inverted substrate to phosphorylate and inactivate EF-Tu.* Nat Chem Biol, 2013. **9**(12): p. 811-7.
18. Cruz, J.W., et al., *Doc toxin is a kinase that inactivates elongation factor Tu.* J Biol Chem, 2014. **289**(11): p. 7788-98.
19. Feng, F., et al., *A Xanthomonas uridine 5'-monophosphate transferase inhibits plant immune kinases.* Nature, 2012. **485**(7396): p. 114-8.
20. Sanyal, A., et al., *A Novel Link between Fic (Filamentation Induced by cAMP)-mediated Adenylylation/AMPylation and the Unfolded Protein Response.* J Biol Chem, 2015. **290**(13): p. 8482-99.
21. Preissler, S., et al., *AMPylation matches BiP activity to client protein load in the endoplasmic reticulum.* eLife, 2015. **4**: p. e12621.

22. Ham, H., et al., *Unfolded Protein Response-regulated Drosophila Fic (dFic) Protein Reversibly AMPylates BiP Chaperone during Endoplasmic Reticulum Homeostasis.* J Biol Chem, 2014. **289**(52): p. 36059-69.
23. Preissler, S., et al., *FICD acts bifunctionally to AMPylate and de-AMPylate the endoplasmic reticulum chaperone BiP.* Nature structural & molecular biology, 2017. **24**(1): p. 23-29.
24. Engel, P., et al., *Adenylylation control by intra- or intermolecular active-site obstruction in Fic proteins.* Nature, 2012. **482**(7383): p. 107-10.
25. Garcia-Pino, A., et al., *Doc of prophage P1 is inhibited by its antitoxin partner Phd through fold complementation.* J Biol Chem, 2008. **283**(45): p. 30821-7.
26. Xiao, J., et al., *Structural basis of Fic-mediated adenylylation.* Nat Struct Mol Biol, 2010. **17**(8): p. 1004-10.
27. Luong, P., et al., *Kinetic and structural insights into the mechanism of AMPylation by VopS Fic domain.* J Biol Chem, 2010. **285**(26): p. 20155-63.
28. Allgood, S.C., et al., *Legionella Effector AnkX Disrupts Host Cell Endocytic Recycling in a Phosphocholination-Dependent Manner.* Front Cell Infect Microbiol, 2017. **7**: p. 397.
29. Campanacci, V., et al., *Structure of the Legionella effector AnkX reveals the mechanism of phosphocholine transfer by the FIC domain.* EMBO J, 2013. **32**(10): p. 1469-77.
30. Cheng, T., et al., *Structure-Based Virtual Screening for Drug Discovery: a Problem-Centric Review.* AAPS J., 2012. **14**: p. 133-141.
31. Arbing, M.A., et al., *Crystal structures of Phd-Doc, HigA, and YeeU establish multiple evolutionary links between microbial growth-regulating toxin-antitoxin systems.* Structure, 2010. **18**(8): p. 996-1010.
32. Dedic, E., et al., *A Novel Fic (Filamentation Induced by cAMP) Protein from Clostridium difficile Reveals an Inhibitory Motif-independent Adenylylation/AMPylation Mechanism.* J Biol Chem, 2016. **291**(25): p. 13286-300.
33. Goepfert, A., et al., *Conserved inhibitory mechanism and competent ATP binding mode for adenylyltransferases with fic fold.* PLoS One, 2013. **8**(5): p. e64901.
34. Stanger, F.V., et al., *Intrinsic regulation of FIC-domain AMP-transferases by oligomerization and automodification.* Proc Natl Acad Sci U S A, 2016. **113**(5): p. E529-37.
35. Mattoo, S., et al., *Comparative analysis of Histophilus somni immunoglobulin-binding protein A (IbpA) with other fic domain-containing enzymes reveals differences in substrate and nucleotide specificities.* J Biol Chem, 2011. **286**(37): p. 32834-42.
36. Goody, P.R., et al., *Reversible phosphocholination of Rab proteins by Legionella pneumophila effector proteins.* EMBO J, 2012. **31**(7): p. 1774-84.
37. Mishra, S., et al., *Cloning, expression, purification, and biochemical characterisation of the FIC motif containing protein of Mycobacterium tuberculosis.* Protein Expr Purif, 2012. **86**(1): p. 58-67.
38. Gavriljuk, K., et al., *Unraveling the Phosphocholination Mechanism of the Legionella pneumophila Enzyme AnkX.* Biochemistry, 2016. **55**(31): p. 4375-85.
39. Truttmann, M.C., et al., *Unrestrained AMPylation targets cytosolic chaperones and activates the heat shock response.* Proc Natl Acad Sci U S A, 2017. **114**(2): p. E152-E160.
40. Helaine, S., et al., *Internalization of Salmonella by macrophages induces formation of nonreplicating persisters.* Science, 2014. **343**(6167): p. 204-8.

41. Truttmann, M.C., et al., *The Caenorhabditis elegans Protein FIC-1 Is an AMPylase That Covalently Modifies Heat-Shock 70 Family Proteins, Translation Elongation Factors and Histones.* PLoS Genet, 2016. **12**(5): p. e1006023.
42. Rahman, M., et al., *Visual neurotransmission in Drosophila requires expression of Fic in glial capitate projections.* Nat Neurosci, 2012. **15**(6): p. 871-5.
43. Smit, C., et al., *Efficient synthesis and applications of peptides containing adenylylated tyrosine residues.* Angew Chem Int Ed Engl, 2011. **50**(39): p. 9200-4.
44. Hao, Y.H., et al., *Characterization of a rabbit polyclonal antibody against threonine-AMPylation.* J Biotechnol, 2011. **151**(3): p. 251-4.
45. Grammel, M., et al., *A chemical reporter for protein AMPylation.* J Am Chem Soc, 2011. **133**(43): p. 17103-5.
46. Heller, K., et al., *Covalent Protein Labeling by Enzymatic Phosphocholination.* Angew Chem Int Ed Engl, 2015. **54**(35): p. 10327-30.
47. Pieles, K., et al., *An experimental strategy for the identification of AMPylation targets from complex protein samples.* Proteomics, 2014. **14**(9): p. 1048-52.
48. Yu, X., et al., *Click chemistry-based detection of global pathogen-host AMPylation on self-assembled human protein microarrays.* Mol Cell Proteomics, 2014.
49. Broncel, M., et al., *Global Profiling of Huntingtin-associated protein E (HYPE)-Mediated AMPylation through a Chemical Proteomic Approach.* Molecular & cellular proteomics : MCP, 2016. **15**(2): p. 715-25.
50. Garcia-Pino, A., et al., *Allostery and intrinsic disorder mediate transcription regulation by conditional cooperativity.* Cell, 2010. **142**(1): p. 101-11.
51. Garcia-Pino, A., et al., *Crystallization of Doc and the Phd-Doc toxin-antitoxin complex.* Acta Crystallogr Sect F Struct Biol Cryst Commun, 2008. **64**(Pt 11): p. 1034-8.
52. Bunney, T.D., et al., *Crystal structure of the human, FIC-domain containing protein HYPE and implications for its functions.* Structure, 2014. **22**(12): p. 1831-43.
53. Palanivelu, D.V., et al., *Fic domain-catalyzed adenylylation: insight provided by the structural analysis of the type IV secretion system effector BepA.* Protein Sci, 2011. **20**(3): p. 492-9.
54. Lee, C.C., et al., *Crystal structure of the type III effector AvrB from Pseudomonas syringae.* Structure, 2004. **12**(3): p. 487-94.
55. Desveaux, D., et al., *Type III effector activation via nucleotide binding, phosphorylation, and host target interaction.* PLoS Pathog, 2007. **3**(3): p. e48.

II. Régulation d'une nouvelle protéine FIC bactérienne par un changement d'ion métallique

A. Introduction

Dans le cadre de l'étude des protéines FIC à glutamate régulateur, nous avons identifié par recherche bio-informatique fondée sur l'analyse des séquences protéiques, une nouvelle protéine de la bactérie *Enterococcus faecalis* que nous avons nommée EfFIC. Sa séquence, très proche de nombreuses autres petites protéines FIC, comporterait un site de fixation putatif de l'ATP et supporterait une activité d'AMPylation. L'intérêt que nous avons porté à cette nouvelle protéine FIC est renforcé par la dualité d'*E. faecalis*, bactérie commensale Gram positif qui a la particularité d'être la première à coloniser le système digestif humain tout en étant responsable de 10% des infections nosocomiales associées à une résistante multiple aux antibiotiques.

Au cours de ma thèse, j'ai mené une étude biochimique et structurale de cette nouvelle protéine. Pour cela, j'ai fait synthétiser le gène codant EfFIC, puis produit dans *E. coli* et purifié EfFIC sauvage ainsi que trois formes mutées. Les mutations sélectionnées touchent des résidus qui jouent un rôle clé dans les autres protéines FIC caractérisées, à savoir l'histidine catalytique (H111), le glutamate catalytique (E115) et le glutamate régulateur (E190).

Avec ces protéines recombinantes, j'ai tout d'abord mené une étude structurale par cristallographie en résolvant les structures des formes sauvage et mutée dans l'histidine catalytique (H111A). J'ai également résolu la structure de ces protéines en complexe avec l'ADP d'une part et le phosphate inorganique d'autre part. Les différentes structures montrent qu'EfFIC arbore la structure classique conservée des petites protéines FIC, comportant notamment le glutamate régulateur à la position attendue dans le site actif. Ces résultats montrent que EfFIC peut lier l'ADP dans une position catalytique comparée aux structures connues de FIC, ce qui est conforme avec l'activité d'AMPylation prédite. De plus, les différentes formes d'EfFIC cristallisent sous forme de tétramères, à l'exception du complexe avec l'ADP qui semble former un hexamère.

En collaboration avec l'équipe de Carmen Buchrieser à l'Institut Pasteur, j'ai ensuite testé l'activité d'AMPylation d'EfFIC. Ne pouvant à ce stade formuler d'hypothèses quant au substrat de l'enzyme, j'ai alors exploité le fait que des réactions d'auto-modification ont été décrites pour plusieurs protéines FIC de la même famille. J'ai en effet pu observer une activité d'auto-AMPylation d'EfFIC en présence de [α-32P] ATP et d'ion magnésium. J'ai également montré que la mutation

du glutamate régulateur (E190A) augmente significativement l'efficacité catalytique de l'enzyme. Ces résultats montrent la capacité d'EfFIC à catalyser une réaction d'AMPylation en utilisant l'ATP comme substrat et le magnésium comme cofacteur, et valident son utilisation comme modèle de FIC à activité d'AMPylation.

J'ai enfin résolu la structure d'EfFIC cristallisée en présence d'AMP et d'ion calcium, dans laquelle le nucléotide est en position similaire à celle observée pour le nucléotide dans la structure précédemment résolue de son homologue Ibpa en complexe avec son substrat Cdc42 AMPylé. Nous avons donc émis l'hypothèse que cette structure d'EfFIC était informative sur l'état initial de la réaction de dé-AMPylation, réaction nécessitant donc un ion calcium.

Par des expériences *in vitro* réalisées avec la protéine EfFIC sauvage et avec des formes mutantes, en l'absence d'ion métallique, ou en présence de magnésium ou de calcium, nous avons montré que si le magnésium est essentiel à l'activité d'AMPylation, le calcium et le glutamate dit régulateur sont nécessaires à la réaction de dé-AMPylation. Le remplacement du magnésium par le calcium change donc l'activité prédominante de la protéine d'AMPylation à dé-AMPylation. L'ensemble de ces observations nous a permis de proposer un mécanisme catalytique de dé-AMPylation.

Enfin, j'ai produit et purifié la protéine FICD, protéine FIC humaine de la même famille et nous avons montré que la bifonctionnalité de la protéine FICD humaine semble également régulée par cet « interrupteur ionique », ce qui nous permet de proposer des hypothèses quant à l'effet des variations de concentration calcique dans le réticulum endoplasmique sur l'activité de FICD.

A metal switch controls a dual AMPylation/de-AMPylation activity in FIC proteins

Simon Veyron[1], Giulia Oliva[2], Monica Rolando[2], Carmen Buchrieser[2],
Gérald Peyroche[1], Jacqueline Cherfils[1]

[1]Laboratoire de Biologie et Pharmacologie Appliquée, CNRS and Ecole normale supérieure Paris-Saclay, Cachan, France
[2] Biology of Intracellular Bacteria, CNRS and Institut Pasteur, Paris, France

Abstract

FIC enzymes are widespread in bacteria, where they form a diverse family comprised of the toxin component of toxin/antitoxin modules, toxins that are secreted into host cells by pathogens, and many proteins of unknown functions. All known FIC toxins carry out post-translational modifications (PTM) of substrate proteins by diverse phosphate-containing compounds using a diphosphate-containing cofactor such as ATP. An intriguing regulatory feature was described recently, which originated from the observation that the VbhA antitoxin inserts a glutamate into the active site of the VbhT toxin to impair productive binding of the ATP cofactor. A spacially equivalent glutamate was identified in the structures of other FIC protein subfamilies whose mutation potentiated the usage of ATP as a co-factor, which led to ascribing a general inhibitory role to this glutamate. In an unexpected new twist, an equivalent glutamate found in the sole animal FIC protein, FicD/HYPE, was recently shown to support both addition and removal of AMP to the BIP chaperone. However, the nature of the signal that releases auto-inhibition in bacterial FIC proteins or controls the alternation between the forward and reverse activities in human FicD has remained mysterious. In this study, we used a single-domain FIC protein from the bacterial pathogen *Enterococcus faecalis* (EfFIC) as a model to investigate regulation by this glutamate, using crystallography and analysis of its PTM activity in vitro. We discover that EfFIC is regulated by a metal switch, in which Mg^{2+} supports the forward AMPylation reaction and Ca^{2+} supports the reverse de-AMPylation activity. Furthermore, the same metal switch also operates in the human FicD. Our findings thus identify for the first time a tunable regulatory signal that can modulate the activity of the large group of FIC proteins with an inhibitory glutamate, which opens important perspectives for their functions in stress responses in bacteria and the unfolded protein response in animals.

Introduction

In less than a decade, FIC proteins have emerged as a superfamily of enzymes with versatile functions in bacteria and metazoans (reviewed in [1 , 2]). FIC proteins are characterized by a FIC motif, a conserved sequence with an invariant histidine that is critical for activity. The first FIC family member was discovered in E. coli by a mutation in a gene of unknown function that displayed filamentation induced by cAMP phenotype [3], which has since been identified as the toxin component of a toxin/antitoxin module [4]. The discovery that some FIC proteins from intracellular pathogens add an AMP moiety to host GTPases to divert their functions was pivotal to the realization that the probable generic function of FIC proteins is to carry out post-translational modifications of target proteins [5 , 6, 7]. This reaction, coined as adenylylation or AMPylation, is also catalyzed by other bacterial FIC proteins of unknown functions [8 , 9], by bacterial toxin/antitoxins [8 , 10] and by the only FIC protein found in metazoans, HYPE/FicD, which AMPylates the chaperone BIP in the unfolded protein response [11]. However PTM catalyzed by FIC proteins are not resctrited to AMPylation. For instance, Legionella AnkX uses CDP-choline to transfer phosphocholine onto a host GTPase [12 , 13] and Doc, the toxin component of the Doc/PhD toxin-antitoxin, uses ATP to phosphorylate EF-Tu [14]. All these reactions have in common that they involve the transfer of a phosphate-containing group from a disphosphate-containing compound onto Tyr, Ser or Tyr residues in the target protein, suggesting that this constitutes the core reaction of all FIC protein (reviewed in [1 , 2 , 15]).

As enzymes involved in important bacterial or cellular responses, it is logical that some, if not all, FIC proteins are regulated. The simplest case is that of toxin/antitoxin modules, in which the catalytic site of FIC toxin is obstructed by the antitoxin leading to strong inhibition that is releaved by dissociation of the antitoxin. This mechanism is described in Doc/PhD ([14] and in VbhA/VbhT [8] and the related FicT/FicA module from E.coli [10], where elements of the antitoxin wedge into the toxin active site and obstruct it. In VbhT/VbhA, obstruction of the VbhT active site is mediated by a glutamate from the VbhA antitoxin that impairs binding of the ATP co-factor [8]. Remarkably, numerous FIC proteins carry a structurally equivalent intramolecular glutamate, which is located in the N-terminal elements in FIC proteins such as HYPE [16], *Clostridum difficile* FIC [9] and *Shewanella oneidensis* FIC [17] or in a conserved C-terminal motif in FIC proteins examplified by the single-domain FIC proteins from *Neisseria meningitidis* [8] and *Helicobacter pylori* (PDB 2F6S). The intramolecular

glutamate has been proposed to impair the utilization of ATP as a donor for AMP, based on the observation that ATP could not be observed in a canonical conformation into the active site [8] and that its mutation to Ala or Gly enhanced the AMPylation activity in vitro and in cells in various FIC proteins [8 , 9 , 16 , 18 , 19]. A mechanism whereby this glutamate is displaced to allow productive binding of ATP has remained elusive. Single-domain FIC proteins have been proposed to be inhibited by oligomerization stabilized by ATP and activated by auto-modifications leading to displacement of the inhibitory glutamate [4]. In this framework, single-domain FIC proteins implement a self-timer fired by dilution.

Many questions remain however unanswered. For example, factors leading to a large dilution or a large variation of ATP concentration to activate single-domain FIC proteins have remained mysterious ; whether variations of the oligomerization mechanism operate in larger FIC proteins with an inhibitory glutamate is currently unknown. Furthermore, in recent new twists, alternative functions have been associated to this intriguing glutamate. A FIC protein from *Clostridium difficile* that carries a canonical inhibitory glutamate was recently shown to support significant auto-AMPylation activity [9]. In metazoan HYPE/FicD, which controls the reversible AMPylation of the BIP chaperone in the endoplasmic reticulum to match its activity to the load in unfolded proteins [11 , 20 , 21], the inhibitory glutamate was found to support de-AMPylation as the primary enzymatic activity in this protein [19].

These intringuing observations raise the issue of the nature of the signals that control opposite biochemical activities in FIC proteins with an inhibitory glutamate in their active site. In this study, we focused on a class III single-domain FIC protein from *Enterococcus faecalis* (EfFIC) that features an inhibitory glutamate in C-terminus to address this question. Enteroccoci are commensals of the gastrointestinal tract that become pathogenic outside of the gut and cause difficult-to-treat infections in the hospital due to acquisition and transmission of antibiotic resistance [22 , 23]. By combining crystallographic and biochemical analysis, we discover that EfFIC is regulated by a metal switch, in which Mg^{2+} supports the forward AMPylation reaction and Ca^{2+} supports the reverse de-AMPylation activity. Furthermore, the same metal switch also operates in human FICD. Our findings thus identify for the first time a tunable regulatory signal that can modulate the activity of FIC proteins. These observations suggest that the presence of a regulatory glutamate in FIC proteins is the signature for their ability to alternate between AMPylation and de-AMPylation activities in response to variations in Ca^{2+} fluxes. We speculate from these observations that single-

domain FIC proteins may increase the fitness of bacterial populations in stress situations accompanied by increased Ca^{2+} levels, such as loss of the bacterial cell wall integrity, and that HYPE/FicD may be a molecular integrator between Ca^{2+} signaling and the BIP-mediated unfolded protein response in the ER.

Results.

Crystal structures of Enterococcus faecalis FIC

Enterococcus faecalis FIC belongs to class III FIC protein, which are comprised of a single FIC domain with an autoinhibitory glutamate in C-terminus. We determined crystal structures of unbound, phosphate-bound and ADP-bound wild-type EfFIC and of unbound, sulfate-bound and ADP-bound EfFIC carrying a mutation of the catalytic histidine into an alanine (H111A) (**Table 1 and Table S1**). These structures obtained in different space groups yield 44 independent copies of the molecule and various environments in the crystal. EfFIC resembles closely *Neisseria meningitidis* FIC [18] and *Helicobacter pylori* FIC (PDB entry 2F6S), with which it shares about 50% sequence identity (**Figure 1A**) . All individual monomers have a well defined glutamate (Glu190) that points into the active site opposite to the FIC motif, which has the same position as in structures of NmFIC, CdFIC and HYPE (**Figure 1B**). In most crystal forms, EfFIC assembles as a tetramer which blocks access to the β-hairpin predicted to comprise the binding site for target protein (**Figure 1C**), and it also forms a tetramer in solution as measured by SEC-MALLs (not shown). The organization of the EfFIC tetramer is related to the low activity NmFIC tetramer [4]. Our crystal structures thus indicate that EfFIC has canonical features of auto-inhibited FIC proteins.

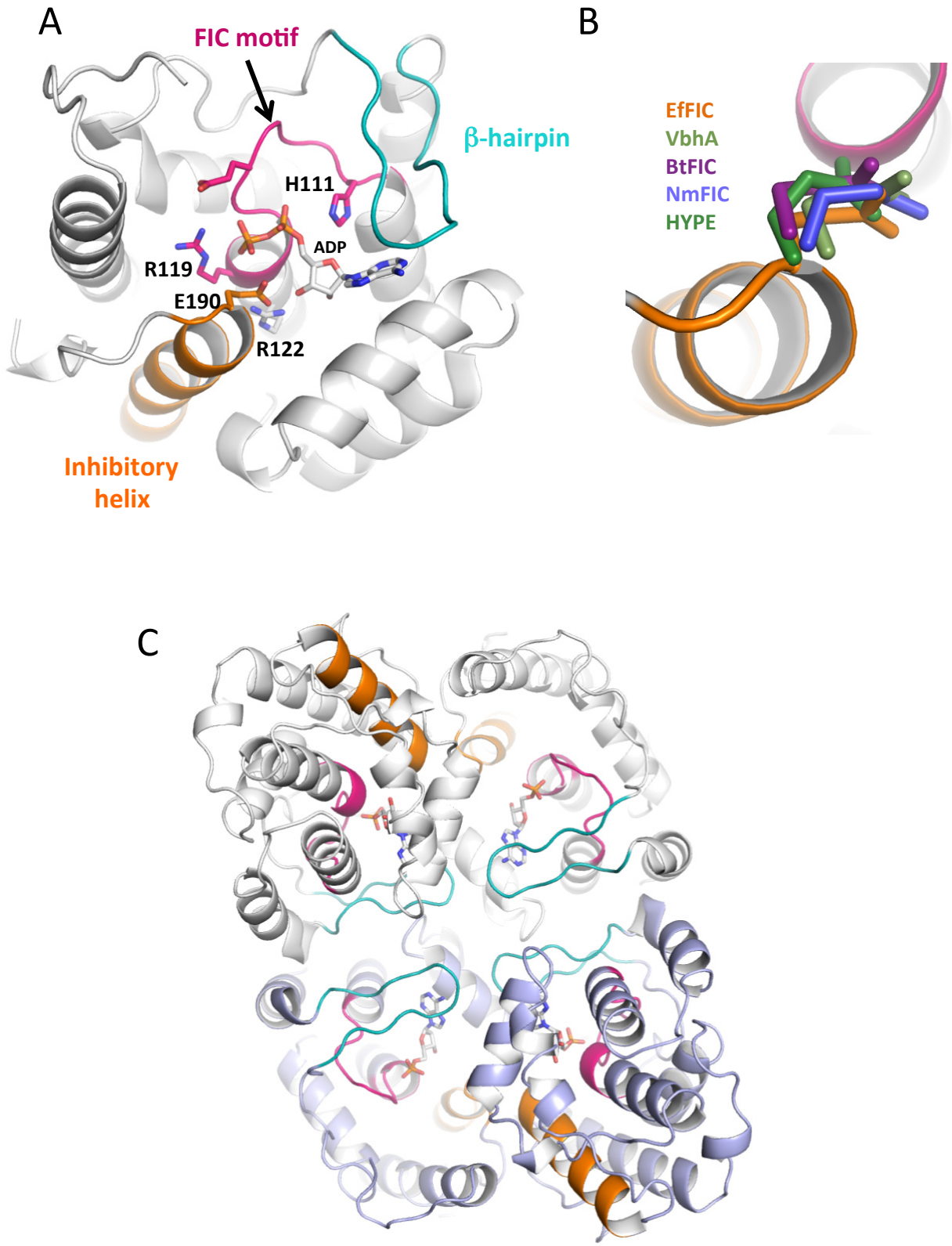

(legend next page)

Figure 1. The crystal structure of EfFIC.

A : Structure of the EfFIC monomer showing the FIC motif (pink), the inhibitory helix bearing the inhibitory glutamate (orange) and the β-hairpin predicted to bind protein substrates (cyan). ADP is shown in sticks.

B : Superposition of the inhibitory glutamate of EfFIC (orange) to the equivalent glutamate provided in trans by the Bartonella VbhA antitoxin (3SHG, khaki), found in the C-terminus of Neisseria NmFIC (2G03, blue) or in the N-terminus of Bacteroides BtFIC (3CUC, purple) and human HYPE (4U04, green).

C : The EfFIC crystallographic tetramer. In some structures, EfFIC forms a crystallographic dimer similar to the dimer shown in violet.

Form	Space group	Cell parameters *a*, *b*, *c* (Å)	Ligand	Resolution	PDB
WT	$P4_12_12$	65.13, 65.13, 248.06	Pi	2.29	5NUW
WT	I222	121.54, 131.00, 136.94	/	2.40	5NV5
WT	$P4_12_12$	64.98 64.98 246.24	AMP – Ca^{2+}	2.35	6EP0
WT	$P4_32_12$	125.35 125.35 362.8	ADP – Ca^{2+}	2.15	6EP2
WT	$P4_32_12$	87.84 87.84 364.94	ADP	1.93	6EP5
H118A	$P2_122_1$	76.67 77.11 103.15	/	2.60	5NWF
H118A	I222	121.93 131.16 136.71	SO_4^{2-}	2.20	5NVQ
H118A	$P2_12_12_1$	65.50 139.37 316.82	ADP	2.55	In progress

Table 1 – Summary of crystal structures of EfFIC determined in this study. All crystals have α, β and γ = 90°. Crystallographic statistics are given in Table S1.

Table S1: Crystallization conditions, data collection and refinement statistics

ADP binds to EfFIC in a manner that is competent for Mg^{2+}-regulated AMPylation

Well-defined electron density corresponding to ADP and the inhibitory glutamate was observed in several crystal structures co-crystallized with ADP or a non-hydrolyzable ATP analog (ATPγS) (**Figure 2A**). The presence of >15% ADP in commercial ATPγS samples makes it difficult to discriminate between the ligand being ADP or the γ-phosphate of ATPγS being disordered, and it is therefore refered to as ADP in subsequent analysis. To compare the position of the ADP phosphates with respect to catalytic FIC motif, we superposed our EfFIC-ADP structures to structures representative of the canonical position competent for PTM transfer, including the complex of AnkX carrying a mutation of the catalytic histidine with CDP-choline [13] and the complex of NmFIC carrying a mutation of the inhibitory glutamate with ATP and Mg^{2+} [8]. The α and β phosphates superpose well, indicating that ADP binds to EfFIC with its phosphates in a canonical position (**Figure 2B**). In contrast, the conformation of the α and β phosphates of ADP bound to EfFIC is distinct from that seen in ATP bound to wild type NmFIC-ATP (in which only the ADP moiety is visible) [8] or to CdFIC [9] (**Figure 2C**). In the former, the displacement from the canonical position was attributed to an unproductive conformation of the co-factor, while in the latter it was proposed to reflect an alternative AMPylation mechanism. The inhibitory glutamate in EfFIC binds strongly to this canonical conformation of ADP, thourgh interactions with the β-phosphate and an hydroxyl of the ribose of ADP and it is further held in place by a salt bridge with Arg122 (**Figure 2D**). Since this electrostatic network may in principle form in the presence of the ATP co-factor, we assessed whether wild-type EfFIC is intrinsically competent for AMPylation. We used auto-AMPylation as a convenient readout that has been used in previous studies of FIC proteins when their target is unknown [8 , 9]. As shown in **Figure 1E**, wild-type EfFIC has conspicuous auto-AMPylation activity which depends strictly on the presence of Mg^{2+} and this activity is potentiated by mutation of the glutamate. We conclude from this ensemble of experiments that Mg^{2+} is a strong regulator and the glutamate a partial inhibitor of the AMPylation actifivity of EfFIC.

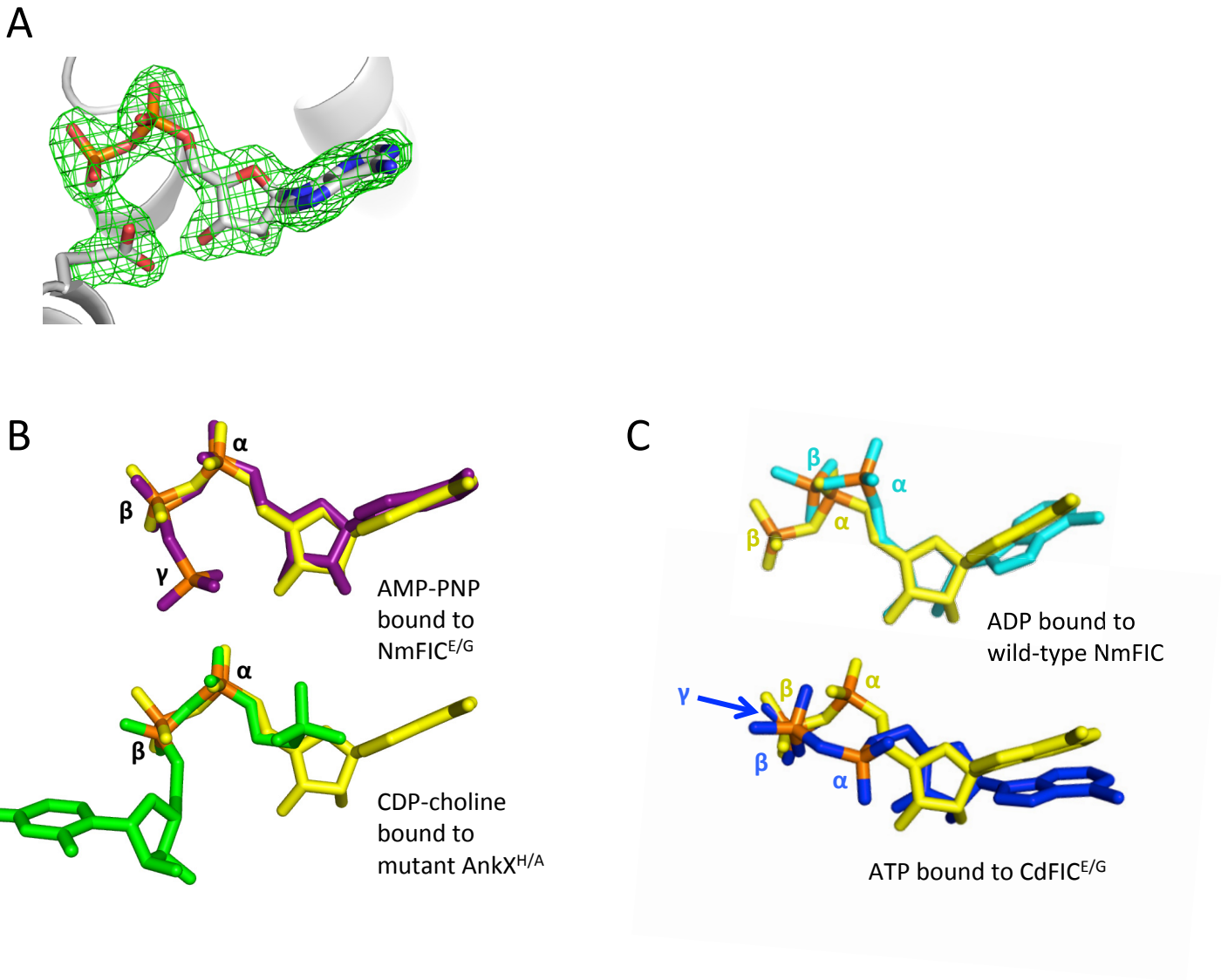

(legend next page)

Figure 2. Wild type EfFIC is competent for AMPylation.

A : Omit map showing the electron density of ADP and the inhibitory glutamate (Glu 190)

B : Superposition of ADP bound to EfFIC (in yellow) with the co-factors from NmFIC et AnkX bound in a canonical conformation as indicated

C : Superposition of ADP bound to EfFIC (in yellow) with co-factors from NmFIC and CdFIC bound in non-canonical conformations as indicated

D : Close-up view of interaction between ADP and the inhibitory glutamate in the active site of EfFIC.

E: Auto-AMPylation of wild-type EfFIC and the E190G mutant. AMPylation was measured by autoradiography after incubation with radioactive α-^{32}P-ATP.

Ca^{2+} converts EfFIC into a de-AMPylator.

We made the intriguing observation that in two crystal structures of nucleotide-bound EfFIC, strong electron density was present in the active site, which was attributed to calcium ions present to the exclusion of any other metal ion in the crystallization solution (**Table 1 and Table S1**). In the ADP-Ca^{2+} complex (**Figure 3A**), a single calcium ion was observed with a 7-coordination sphere with distance in the 2.3-2.8 Å range, in contact with the inhibitory glutamate, the α- and β-phosphates of ADP and 4 water molecules (**Figure 3B**). A calcium ion with a slightly different position was also observed in an AMP-bound EfFIC structure (**Figure 3C**), which interacted with the α-phosphate, E115 from the FIC motif, and with the inhibitory glutamate through a water molecule (**Figure 3D**). Ca^{2+} has electrochemical properties that distinguish it from Mg^{2+} that endows it with signaling capacities (reviewed in [24]). We therefore analyzed the activity of EfFIC in the presence of Ca^{2+}, using the auto-AMPylation reaction as a readout. Remarkably, Ca^{2+} supported a conspicuous de-AMPylation activity (**Figure 3E**), which was suppressed by mutation of the regulatory glutamate into a glycine (**Figure 3F**). We conclude from these experiments that EfFIC has a built-in de-AMPylating activity that depends on Ca^{2+} and the inhibitory glutamate and that alternation between AMPylation and de-AMPylation if controled by a Mg^{2+} /Ca^{2+} switch.

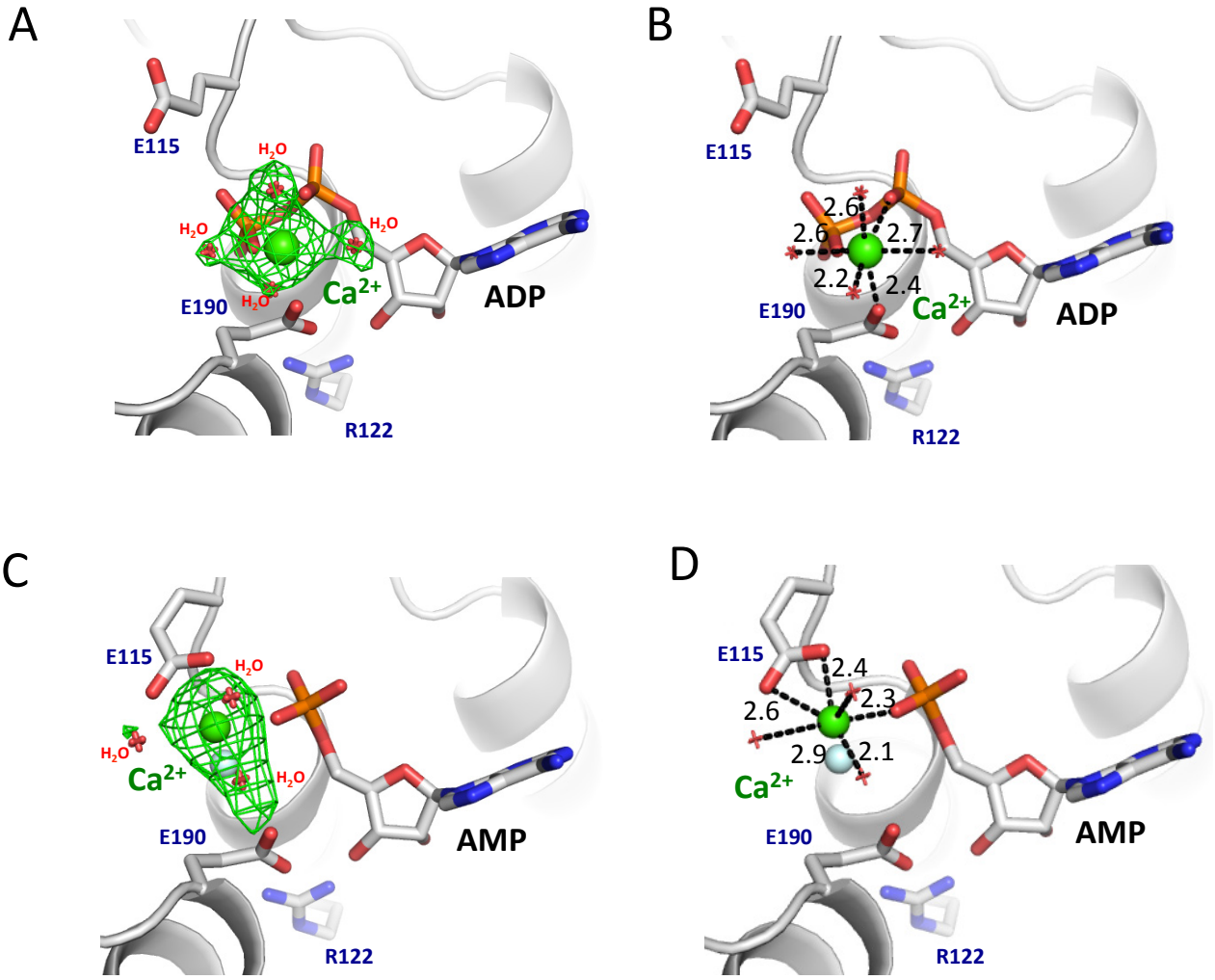

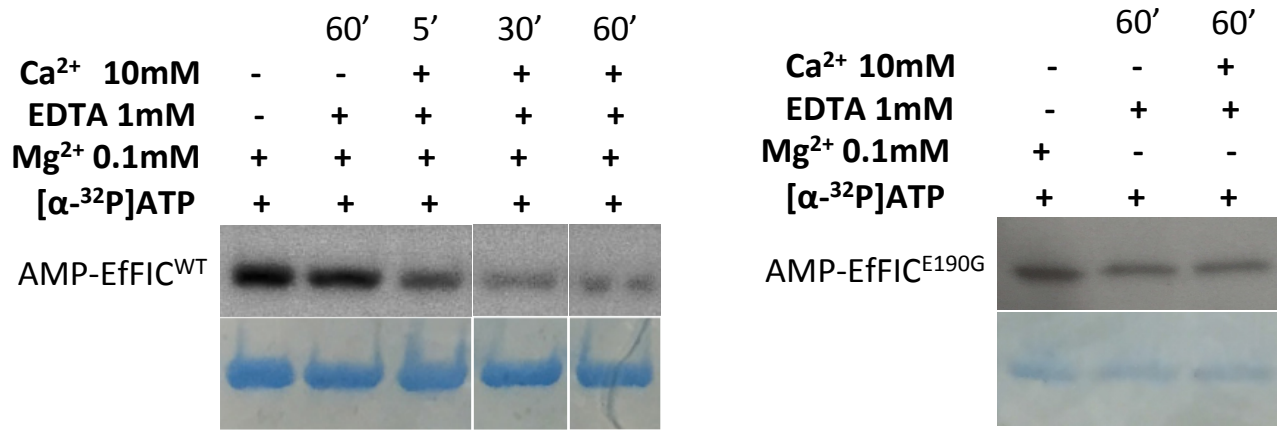

(legend next page)

Figure 3. Ca^{2+} switches EfFIC into a de-AMPylating enzyme.

A : Omit map showing the electron density of Ca^{2+} in the crystal structure of EfFIC-ADP-Ca^{2+}.

B : Close-up view of Ca^{2+} in the EfFIC-ADP-Ca^{2+} structure.

C : Omit map showing the electron density of Ca^{2+} in the crystal structure of EfFIC-AMP-Ca^{2+}.

D : Close-up view of Ca^{2+} in the EfFIC-AMP-Ca^{2+} structure.

E : Ca^{2+} switches EfFIC activity to de-AMPylation. Auto-AMPylation of EfFIC was first carried out in the presence of Mg^{2+} (lane 1), then Mg^{2+} was chelated by EDTA without Ca^{2+} (lane 2) or in the presence of Ca^{2+} (lanes 3-5). AMPylation was analyzed by autoradiography.

F : Mutation of the inhibitory glutamate impairs the Ca^{2+}-dependent de-AMPylation activity of EfFIC.

The de-AMPylation activity of human FicD/HYPE is also controled by a Mg^{2+}/Ca^{2+} switch

HYPE/FicD was recently described to function as a de-AMPylator to remove AMP from the endoplasmic reticulum chaperone BiP in vitro and in cells and this activity requires the inhibitory glutamate [19]. HYPE shares with EfFIC most residues in the active site including the regulatory glutamate [16]. We reasoned that the de-AMPylation activity of HYPE may therefore also be regulated by Ca^{2+}. As for EfFIC, we used the intrinsic auto-AMPylation activity of HYPE to prepare AMP-HYPE in the presence of Mg^{2+}, followed by replacement of Mg^{2+} by Ca^{2+}. As shown in **Figure 4**, Ca^{2+} supported conspicuous de-AMPylation of HYPE. Replacement of Ca^{2+} by Mg^{2+} thus also converts HYPE into a de-AMPylator, suggesting that the missing component to the activity of HYPE as a de-AMPylator in cells might be Ca^{2+}.

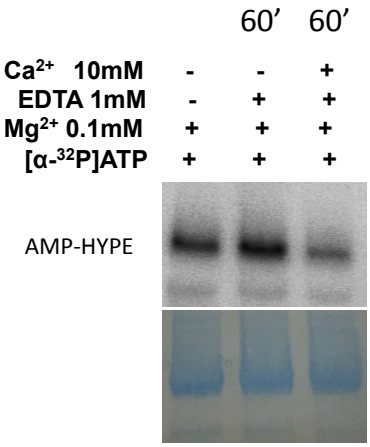

Figure 4. An Mg^{2+}/Ca^{2+} switch supports the de-AMPylation activity of HYPE/FicD
The reversible auto-AMPylation/ auto deAMPylation of human HYPE was analyzed by autoradiography.

Discussion

In this study, we determined the high resolution crystal structures of wild-type EfFIC and a catalytically inactive EfFIC mutant in unbound, phosphate-bound, AMP and ADP forms. The autoinhibitory glutamate is well defined in all structures, and is compatible with the binding of the α and β phosphates in a manner that is competent for the AMPylation reaction. Consistently, wild-type EfFIC displayed potent auto-AMPylation that was enhanced by mutation of the glutamate into glycine and was strictly dependent on the presence of Mg^{2+}. Unexpectedly, we observed the presence of a calcium ion in crystal structures of AMP-bound and ADP-bound EfFIC in the proximity of the inhibitory glutamate, which suggested that this metal may play a role in its biochemical activity. Remarkably, calcium stimulated de-AMPylation of EfFIC, establishing that EfFIC has a dual AMPylation/deAMPYlation activity controled by a metal switch mechanism. Finally, we extented this finding to human HYPE/FicD, whose activity also switched to de-AMPylation in the presence of Ca^{2+}.

Based on these structural and biochemical data, we propose a catalytic mechanism. It should be noted that EfFIC does not resemble the Legionella de-AMPylase SidD, which has a canonical phosphatase fold [25]or the de-AMPylation domain of E. coli glutamine synthase adenylyl transferase [26], hence is not expected to share catalytic features with these enzymes. Two key features of the active site of EfFIC can be depicted: i) a strong interaction of the nucleotide co-factor with the catalytic active site through multiple interactions of the

ribose and phosphate moieties and ii) several chemical elements in the vicinity of the expected position of the bond between AMP and the protein residue in an AMPymated substrate, which include the inhibitory glutamate E190, the catalytic histidine H111 and calcium. Comparison with previously described mechanisms of (phospho)ester bond hydrolysis suggests two putative mechanisms, depending on whether it is assisted by the co-factor (anchimeric reaction, **Figure 5A**) or not (conventional acido-basic catalysis**, Figure 5B**). Both mechanisms involve four steps: i) nucleophilic attack on the positively charged phosphorus, ii) P=O π electrons rearrangement leading to the production of a pentavalent intermediate harboring an additional negative charge, iii) stabilization of the intermediate by a positively charged environment and iv) facilitation of phosphor-ester bond cleavage through protonation of the leaving hydroxylate group. Therefore, the two mechanisms share two chemical requirements: i) a positively charged species, situated in the neighborhood of the phosphate group to increase the susceptibility of the phosphorus to nucleophilic attack and stabilize the developing negative charge in the intermediate ii) a proton donor, located close to the cleaved phosphor-ester bond to favor the production of the leaving group by giving up its proton.

A major difference between the two scenarii is that the nucleophilic attack is performed by the ribose 2' hydroxyl in the anchimeric mechanism, whereas it is achieved by an activated water molecule in conventional acido-basic catalysis. Consequently, the two mechanisms can be distinguished by two major features of the active site: i) anchimeric catalysis requires a proton attractor close to the ribose 2'OH, whereas the general acidic catalysis requires a proton attractor close to the substrate water molecule, itself located close to the leaving phosphate group; ii) the substrate-activated catalysis introduces an additional cycle between the phosphorus and the 2'OH of the AMP moiety, and therefore induces a large distortion of the substrate accompanied by a conformational change of the protein, while structural rearrangements are dispensable in the second mechanism.

Our structural data indicate that a large conformational change in the protein and the substrate needed for the anchimeric mechanism is unlikely. Furthermore, no proton acceptor is situated closed to the 2'OH in the structures, definitely ruling out this mechanism. In contrast, a careful analysis of the structures and the analysis of the catalytical properties of the mutant and calcium depleted enzymes leads to a scenario sustaining the second mechanism for de-AMPylation depicted in **Figure 5C**. In this mechanism, the inhibitory glutamate E190, whose

decorated by other structural elements. We propose that this glutamate plays a general regulatory role in supporting AMPylation/de-AMPylation alternation regulated by a metal switch in these FIC proteins; it cannot be excluded that their primary function is to function as de-AMPylators. Ca^{2+} has not been described as a regulatory metal in bacteria physiology, raising the intriguing issue of what could be the conditions leading to a sharp variation of Ca^{2+} levels in bacteria triggering de-AMPylation activity in FIC proteins. One such situation could be due to antibacterial peptides that disrupt the integrity of the bacterial wall. We note that the transition from low to high Ca^{2+} is important for some antimicrobial peptides themselves, some of which need high Ca^{2+} conditions encountered in the milieu to reach their lytic conformation. Because bacteria normally contain a low concentration of Ca^{2+}, increase of Ca^{2+}could be equated to a danger signal, warning the bacteria that it is under attack from another bacteria. Under this hypothesis, AMPylation/de-AMPylation may target antibacterial peptides, for which an arsenal of PTM has already been described. Of note, peptides are well suited to bind to FIC proteins by β-sheet extension. Whatever their substrate, this hypothesis would place the FIC proteins in mechanisms of stress and defense, which remains to be investigated.

Animal FicD/HYPE is the other group of FIC proteins with an inhibitory glutamate, and recent work has demonstrated that their primary function might be de-AMPylation of the endoplasmic reticulum chaperone BIP in response to an increase in the unfolded protein load [19]. Ca^{2+} homeostasis is critical to virtually all ER-supported functions (reviewed in [27]). We hypothesize that this activity of HYPE is also under the control of changes in Ca^{2+} concentration, and that HYPE could therefore function as an integrator of Ca^{2+} signals in the unfolded protein response.

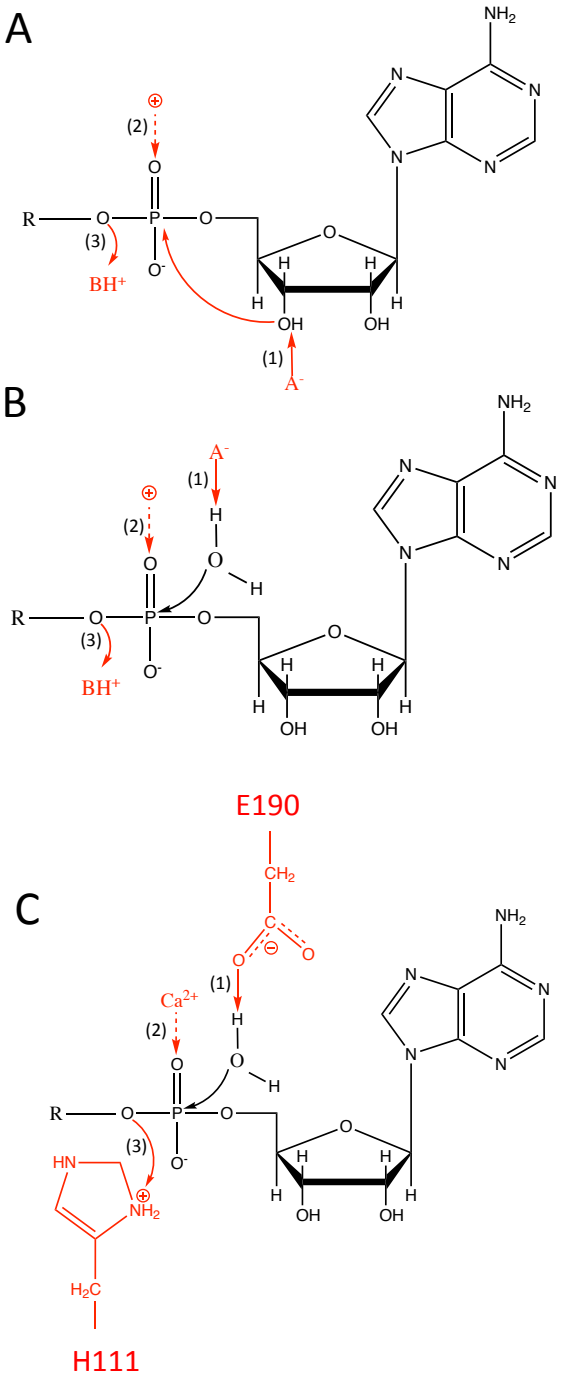

(legend next page)

Figure 5 : Proposed de-AMPylation catalytic mechanism.
A: Principle of anchimeric (substrate-assisted) catalysis. B: Principle of non-anchimeric (general acido-basic) catalysis. C: Application of the non-anchimeric catalysis model to the EfFIC deAMPylation reaction. (1) Proton attractor activating 2'OH (A) or a water molecule (B and C) (2) Positive charge increasing electrophily of the phosphorus and stabilizing the negative charge of the intermediate. (3) Proton donnor activating the leaving group. R : AMPylated protein

Material and Methods.

Protein cloning, expression and purification

The synthetic gene coding for full-length *Enterococcus faecalis* EfFIC with a 6-histidine tag at it N-terminus was ordered at GeneArt Gene Synthesis (ThermoFisher Scientific) and cloned into the pET22b(+). Mutations were performed with the QuickChange II mutagenesis kit (Agilent). The SUMO-FICD(45-459) construct was ordered on GeneArt Gene Synthesis (ThermoFisher Scientific) and cloned in pET151/D-TOPO (ThermoFisher Scientific). All constructs were verified by sequencing (GATC).
All EfFIC constructs were expressed in E. coli BL21 (DE3) pLysS in LB medium. Overexpression was induced overnight with 0.5 mM IPTG at 20°C. Bacterial pellets were lysed in lysis buffer (50 mM Tris pH 8, 150 mM NaCl, 5% glycerol 0.25 mg/mL lysosyme and a protease inhibitor cocktail) and flash frozen in liquid nitrogen. Bacterial pellet was then disrupted at 125 psi using a pressure cell homogenizer (FGP12800, Stanted). The cleared lysate supernatant was loaded on a Ni-NTA affinity chromatography column (HisTrap FF, GE Healthcare) and eluted with 250 mM imidazole. Purification was polished by gel filtration on a Superdex 200 16/600 column (GE Healthcare) equilibrated with storage buffer (50 mM Tris, 150 mM NaCl, pH 8). Human FICD was purified as EfFIC, except that the buffer contained 1mM DTT. In some experiments, the SUMO tag was removed using SUMO protease. SUMO-FICD was incubated with SUMO protease at 1/100 weight/weight ratio during 2 hours at room temperature. Cleaved fraction was separated from uncleaved fraction on affinity chromatography column and further purified by gel filtration equilibrated with storage buffer (50 mM Tris pH 8, 150 mM NaCl, 1mM DTT, 5% glycerol)

Crystallization and structure determination

A summary of the crystal structures determined in this study is in **Table 1**. Proteins were crystallized using a TTP Labtech's Mosquito LCP crystallization robot and different crystallization screens (Jena Bioscience and Quiagen). Conditions leading to crystals were subsequently optimized. Diffraction data sets were recorded at synchrotron SOLEIL and ESRF. Datasets were processed using XDS [28], xdsme (https://github.com/legrandp/xdsme) or autoProc [29]. Structures were solved by molecular replacement and refined with the Phenix suite [30] or Buster (Bricogne G., Blanc E., Brandl M., Flensburg C., Keller P., Paciorek W.,Roversi P, Sharff A., Smart O.S., Vonrhein C., Womack T.O. (2017). BUSTERversion 2.10.2. Cambridge, United Kingdom: Global Phasing Ltd.). Models were build using Coot [31]. Softwares used in this project were curated by SBGrid [32]. Crystallization conditions, data collection statistics and refinement statistics are given in **Table S1**.

AMPylation and de-AMPylation assays

Auto-AMPylation activities were assessed by autoradiography. 8 µg of purified proteins were mixed with 10 µCi [α-32P] ATP (Perkin Elmer) in a buffer containing 50mM Tris pH 7.4, 150 mM NaCl and 0.1 mM $MgCl_2$. Reactions were incubated for 1 h at 30 °C, supplemented with 5X of reducing SDS sample buffer, boiled for 5 min, and resolved by SDS-PAGE. De-AMPylation activites were initiated by allowing the AMPylation reaction as above for 1 h, followed by the addition of 1mM EDTA with or without the addition of 10mM $CaCl_2$. The initial reaction volume was 60 µl and at each point 15 µl of samples was removed from the reaction mixture and the de-AMPylation activity was monitored.

Acknowledgements.

This work was supported by grants from the Fondation pour la Recherche Médicale and from the Agence Nationale pour la Recherche to J.C. and by a grant from the DIM MALINF to S.V. We thank the scientific team at the PX1 and PX2 beamlines at the SOLEIL synchrotron (Gif-sur-Yvette, France) for making the beamline available to us. We thank the Plateforme de Biologie Moléculaire BMGIF (CNRS, Gif-sur-Yvette) for some clonings and mutations. We are grateful to Pascale Serror (INRA, Jouy-en-Josas, France) and Philippe Gläser (Institut Pasteur) for discussions and to the members of the Cherfils lab for help and shared expertise.

Table S1: Crystallization conditions, data collection and refinement statistics

	EfFIC WT	EfFIC WT	EfFIC WT-AMP-Ca
PDB accession code	6ER8	5NV5	6EP0
Data collection			
Space group	$P4_12_12$	I222	$P4_12_12$
Molecule/asu	2	4	2
a, *b*, *c* (Å)	65.13, 65.13, 248.06	121.54, 131.00, 136.94	64.98 64.98 246.24
α, β, γ (°)	90.00, 90.00, 90.00	90.00, 90.00, 90.00	90.00, 90.00, 90.00
Resolution (Å)	44.91-2.29 (2.38-2.29)	47.33-2.40 (2.49-2.40)	82.08-2.35 (2.48-2.35)
R_{merge}	0.312 (1.808)	0.087 (0.665)	0.139 (1.146)
I / σI	5.2 (1.4)	13.5 (2.2)	13.1 (2.3)
Completeness (%)	94.8 (91.7)	99.8 (97.6)	100.0 (100.0)
Multiplicity	4 (2.8)	5.6 (5.4)	16.7 (17.8)
Beamline	Proxima1	ID30A	ID29
MR model	2G03	EfFIC	EfFIC
Ligand	PO_4^{2-}	-	AMP-Ca
Refinement			
Resolution (Å)	2.29	2.40	2.35
No. reflections	23571	42957	22951
R_{work} / R_{free}	0.229/0.298	0.164/0.226	0.2018/0.264
No. atoms	3653	7316	3530
B-factors	35.47	44.03	61.1
R.m.s. deviations			
Bond lengths (Å)	0.008	0.010	0.010
Bond angles (°)	0.893	1.08	1.08

Table S1, continued

	EfFIC WT-ADP-Ca	EfFIC WT-ADP
PDB accession code	6EP2	6EP5
Data collection		
Space group	$P4_32_12$	$P4_32_12$
Molecule/asu	12	6
a, *b*, *c* (Å)	125.35 125.35 362.8	87.84 87.84 364.94
α, β, γ (°)	90.00 90.00 90.00	90.00 90.00 90.00
Resolution (Å)	118.45-2.15	47.3-1.93 (1.96-1.93)
R_{merge}	0.157	0.172 (2.806)
I / σI	10.5	9.8 (0.8)
Completeness (%)	99.6	99.9 (97.3)
Multiplicity	11.8	13.0 (12.6)
Beamline	Proxima1	ID30b
MR model	EfFIC	EfFIC
Ligand	ADP-Ca	ADP
Refinement		
Resolution (Å)	2.15	1.93
No. reflections	157231	108653
R_{work} / R_{free}	0.1869/0.2178	0.2003/0.2402
No. atoms	22152	11142
B-factors	41.95	33.71
R.m.s. deviations		
Bond lengths (Å)	0.005	0.007
Bond angles (°)	0.947	0.992

Table S1, continued

	EfFIC H118A	EfFIC H118A	EfFIC H118A-ADP
PDB accession code	5NWF	6ERB	In progress
Data collection			
Space group	$P2_122_1$	I222	$P2_12_12_1$
Molecule/asu	2	4	12
a, *b*, *c* (Å)	76.67 77.11 103.15	121.93 131.16 136.71	65.50 139.37 316.82
α, β, γ (°)	90.00, 90.00, 90.00	90.00, 90.00, 90.00	90.00, 90.00, 90.00
Resolution (Å)	103.15-2.60 (2.72-2.60)	47.32-2.20 (2.26-2.20)	47.73-2.55 (2.59-2.55)
R_{merge}	0.072 (0.499)	0.081 (1.321)	0.216 (1.151)
I / σI	15.5 (3.6)	18.5 (2.1)	8 (1.8)
Completeness (%)	99.1 (99.9)	100.0 (100.0)	99.6 (92.8)
Multiplicity	5.9 (6.1)	13.7 (14.2)	8.4 (7.0)
Beamline	Proxima2a	Proxima2a	Proxima2a
MR model	EfFIC	EfFIC	EfFIC
Ligand	-	SO_4^{2-}	ADP
Refinement			
Resolution (Å)	2.6	2.2	2.55
No. reflections	19240	55796	95908
R_{work} / R_{free}	0.191/0.250	0.2132/0.2488	0.2290/0.2760
No. atoms	3516	7095	20585
B-factors	62.79	54.64	5362
R.m.s. deviations			
Bond lengths (Å)	0.008	0.008	
Bond angles (°)	1.103	1.012	

References

1. Harms, A., F.V. Stanger, and C. Dehio, *Biological Diversity and Molecular Plasticity of FIC Domain Proteins.* Annu Rev Microbiol, 2016. **70**: p. 341-60.
2. Roy, C.R. and J. Cherfils, *Structure and function of Fic proteins.* Nat Rev Microbiol, 2015. **13**(10): p. 631-40.
3. Kawamukai, M., et al., *Nucleotide sequences of fic and fic-1 genes involved in cell filamentation induced by cyclic AMP in Escherichia coli.* J Bacteriol, 1989. **171**(8): p. 4525-9.
4. Stanger, F.V., et al., *Intrinsic regulation of FIC-domain AMP-transferases by oligomerization and automodification.* Proc Natl Acad Sci U S A, 2016. **113**(5): p. E529-37.
5. Yarbrough, M.L., et al., *AMPylation of Rho GTPases by Vibrio VopS disrupts effector binding and downstream signaling.* Science, 2009. **323**(5911): p. 269-72.
6. Worby, C.A., et al., *The fic domain: regulation of cell signaling by adenylylation.* Mol Cell, 2009. **34**(1): p. 93-103.
7. Xiao, J., et al., *Structural basis of Fic-mediated adenylylation.* Nat Struct Mol Biol, 2010. **17**(8): p. 1004-10.
8. Engel, P., et al., *Adenylylation control by intra- or intermolecular active-site obstruction in Fic proteins.* Nature, 2012. **482**(7383): p. 107-10.
9. Dedic, E., et al., *A Novel Fic (Filamentation Induced by cAMP) Protein from Clostridium difficile Reveals an Inhibitory Motif-independent Adenylylation/AMPylation Mechanism.* J Biol Chem, 2016. **291**(25): p. 13286-300.
10. Stanger, F.V., et al., *Crystal Structure of the Escherichia coli Fic Toxin-Like Protein in Complex with Its Cognate Antitoxin.* PLoS One, 2016. **11**(9): p. e0163654.
11. Sanyal, A., et al., *A novel link between Fic (filamentation induced by cAMP)-mediated adenylylation/AMPylation and the unfolded protein response.* J Biol Chem, 2015. **290**(13): p. 8482-99.
12. Mukherjee, S., et al., *Modulation of Rab GTPase function by a protein phosphocholine transferase.* Nature, 2011. **477**(7362): p. 103-6.
13. Campanacci, V., et al., *Structure of the Legionella effector AnkX reveals the mechanism of phosphocholine transfer by the FIC domain.* EMBO J, 2013. **32**(10): p. 1469-77.

14. Castro-Roa, D., et al., *The Fic protein Doc uses an inverted substrate to phosphorylate and inactivate EF-Tu.* Nat Chem Biol, 2013. **9**(12): p. 811-7.
15. Garcia-Pino, A., N. Zenkin, and R. Loris, *The many faces of Fic: structural and functional aspects of Fic enzymes.* Trends Biochem Sci, 2014. **39**(3): p. 121-9.
16. Bunney, T.D., et al., *Crystal structure of the human, FIC-domain containing protein HYPE and implications for its functions.* Structure, 2014. **22**(12): p. 1831-43.
17. Das, D., et al., *Crystal structure of the Fic (Filamentation induced by cAMP) family protein SO4266 (gi|24375750) from Shewanella oneidensis MR-1 at 1.6 A resolution.* Proteins, 2009. **75**(1): p. 264-71.
18. Goepfert, A., et al., *Conserved inhibitory mechanism and competent ATP binding mode for adenylyltransferases with fic fold.* PLoS One, 2013. **8**(5): p. e64901.
19. Preissler, S., et al., *FICD acts bifunctionally to AMPylate and de-AMPylate the endoplasmic reticulum chaperone BiP.* Nat Struct Mol Biol, 2017. **24**(1): p. 23-29.
20. Ham, H., et al., *Unfolded protein response-regulated Drosophila Fic (dFic) protein reversibly AMPylates BiP chaperone during endoplasmic reticulum homeostasis.* J Biol Chem, 2014. **289**(52): p. 36059-69.
21. Preissler, S., et al., *AMPylation matches BiP activity to client protein load in the endoplasmic reticulum.* Elife, 2015. **4**: p. e12621.
22. Hegstad, K., et al., *Mobile genetic elements and their contribution to the emergence of antimicrobial resistant Enterococcus faecalis and Enterococcus faecium.* Clin Microbiol Infect, 2010. **16**(6): p. 541-54.
23. Lebreton, F., et al., *Tracing the Enterococci from Paleozoic Origins to the Hospital.* Cell, 2017. **169**(5): p. 849-861 e13.
24. Carafoli, E. and J. Krebs, *Why Calcium? How Calcium Became the Best Communicator.* J Biol Chem, 2016. **291**(40): p. 20849-20857.
25. Chen, Y., et al., *Structural basis for Rab1 de-AMPylation by the Legionella pneumophila effector SidD.* PLoS Pathog, 2013. **9**(5): p. e1003382.
26. Xu, Y., et al., *Structure of the adenylylation domain of E. coli glutamine synthetase adenylyl transferase: evidence for gene duplication and evolution of a new active site.* J Mol Biol, 2010. **396**(3): p. 773-84.
27. Krebs, J., L.B. Agellon, and M. Michalak, *Ca(2+) homeostasis and endoplasmic reticulum (ER) stress: An integrated view of calcium signaling.* Biochem Biophys Res Commun, 2015. **460**(1): p. 114-21.

28. Kabsch, W., *Integration, scaling, space-group assignment and post-refinement.* Acta Crystallogr D Biol Crystallogr, 2010. **66**(Pt 2): p. 133-44.
29. Vonrhein, C., et al., *Data processing and analysis with the autoPROC toolbox.* Acta Crystallogr D Biol Crystallogr, 2011. **67**(Pt 4): p. 293-302.
30. Adams, P.D., et al., *PHENIX: a comprehensive Python-based system for macromolecular structure solution.* Acta Crystallogr D Biol Crystallogr, 2010. **66**(Pt 2): p. 213-21.
31. Emsley, P. and K. Cowtan, *Coot: model-building tools for molecular graphics.* Acta crystallographica. Section D, Biological crystallography, 2004. **60**(Pt 12 Pt 1): p. 2126-32.
32. Morin, A., et al., *Collaboration gets the most out of software.* Elife, 2013. **2**: p. e01456.

C. Résultats supplémentaires

1. Clonages et expressions supplémentaires

Objectifs :

Le glutamate catalytique (E115) est un résidu conservé chez toutes les protéines FIC. Il a été montré que ce résidu est responsable de la coordination de l'ion magnésium nécessaire à la réaction d'AMPylation et nous avons observé dans nos structures que ce résultat semble également nécessaire à la réaction de dé-AMPylation chez EfFIC. Muter ce résidu est donc apparu intéressant pour mener une étude biochimique de l'activité de cette protéine ; nous avons choisi de lui substituer une alanine.

Principe méthodologique :

J'ai utilisé le kit QuickChange II (décrit dans l'article) pour introduire cette mutation. J'ai pour cela déterminé la séquence de 2 amorces conduisant à la mutation ponctuelle voulue (Figure 1A) que j'ai fait synthétiser par la société Eurogenetec. La construction a finalement été vérifiée par séquençage complet du gène.

Résultat :

J'ai obtenu le gène modifié puis ai produit et purifié la protéine recombinante après expression chez *E. coli* (Figure 1B). Les protocoles d'expression et de purification utilisés sont identiques à ceux décrits dans l'article.

A

Primers used for mutation E115A (GAA =>GCA)
Forward
5' CGCACATCCGTTTCGT**GCA**GGTAATGGTCGTGCAACCC 3'
Reverse
5' GGGTTGCACGACCATTACC**TGC**ACGAAACGGATGTGCG 3'

B

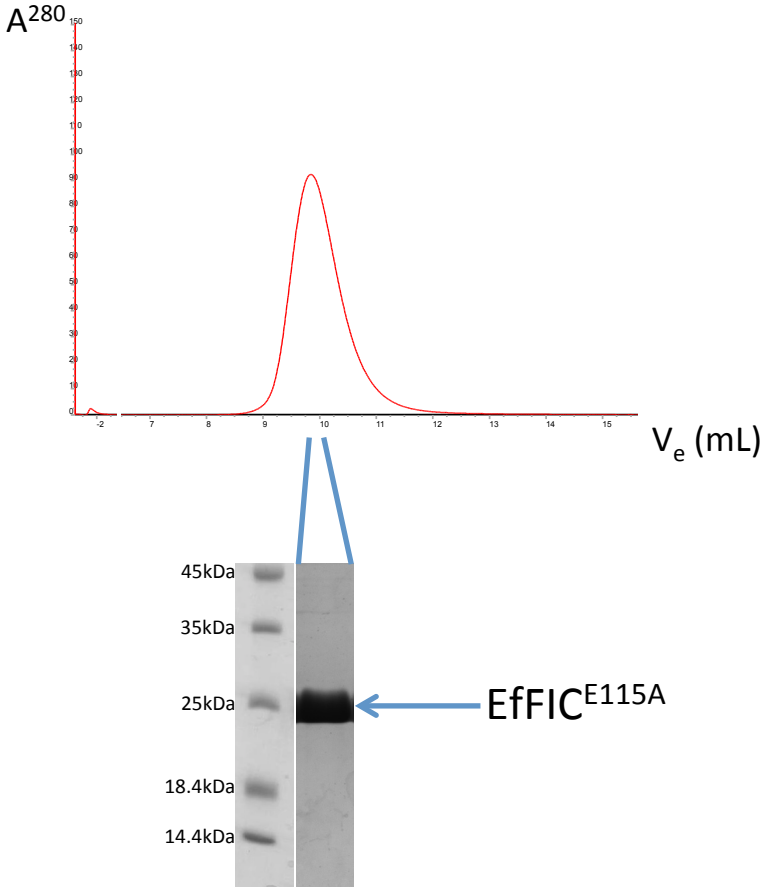

Figure 1: Purification d'EFIC^{E115A}

A : Séquence des oligonucléotides utilisés pour la mutagenèse dirigée.

B : Analyse de la protéine purifiée par chromatographie sur Superdex 75 10/300. Le panneau supérieur présente le chromatogramme obtenu par enregistrement de l'absorbance à 280 nm. Le panneau inférieur présente l'analyse de la fraction correspondant au volume d'élution 10mL par SDS-PAGE suivie de coloration au bleu de Coomassie.

2. Analyse *in vitro* de la fixation de l'ATP, l'ADP et l'AMP par EfFIC

Objectif. Afin d'identifier et de caractériser des ligands d'EfFIC, la méthode du Thermofluor (aussi appelée TSA pour Thermal Shift Assay ou encore DSF pour Differential Scanning Fluorimery) a été mise en oeuvre avec la protéine EfFIC purifiée et un ensemble de composés comportant deux phosphates.

Principe méthodologique. L'échantillon à analyser est mis en présence d'un composé fluorescent (SYPRO Orange, Thermofisher) qui comporte une forte affinité pour les régions protéiques hydrophobes et dont la fixation induit une augmentation du rendement de fluorescence. Il est ensuite soumis à une augmentation graduelle de la température, qui s'accompagne d'une augmentation de la fluorescence consécutive à la dénaturation de la protéine étudiée, et permet le calcul de la température de fusion (Tm). Tout ligand dont la fixation modifie la thermo-stabilité de la protéine entraîne donc une modification du Tm qui peut être mesurée. Étant donnés le pas de la rampe de température et la reproductibilité de la méthode, on considère usuellement qu'une variation du Tm est significative lorsqu'elle est supérieure à 0.6 °C.

Nous avons étudié par cette méthode l'effet sur $EfFIC^{WT}$ des nucléotides, en présence ou en l'absence des ions métalliques Mg^{2+} et Ca^{2+} , puis avons effectué une comparaison avec $EfFIC^{E115A}$ et $EfFIC^{E190G}$ pour étudier l'influence des résidus mutés sur la liaison du substrat et du cofacteur.

Résultats :

- Analyse de la protéine sauvage

Comparaison AMP/ADP/ATP. La protéine EfFIC (10 µM) est stabilisée par l'AMP, l'ADP et l'ATP (10 mM, *cf.* ΔTm^{WT} Table 1, partie I). Ces expériences ont été les premières à suggérer que l'ATP était un ligand d'EfFIC, et donc potentiellement un substrat. Elles ont été importantes dans la mise en place de la démarche dans son ensemble et ont été réalisées avant que la réaction d'auto-AMPylation *in vitro* en présence d'ATP ne soit mise en évidence.

Effet des ions magnésium et calcium. L'addition d'ions Mg^{2+} ou Ca^{2+} (10 mM) semble avoir un effet différentiel sur la stabilisation d'EfFIC par les nucléotides : le complexe EfFIC-AMP ne semble pas être plus stabilisé en présence de Ca^{2+} ou de Mg^{2+}, alors que les complexes EfFIC-ADP et EfFIC-ATP semblent être plus stabilisés par ces ions ($\Delta Tm^{WT\ ion}$ Table 1, partie I).

- Analyse des protéines mutantes. J'ai analysé par la même méthode les protéines mutées dans les résidus dont nos données cristallographiques montrent qu'ils sont en interaction avec le substrat ou l'ion dans le site actif de la protéine ($EfFIC^{E190G}$ et $EfFIC^{E115A)}$.

Effet de la mutation du glutamate catalytique. En l'absence de cation métallique, la

mutation du glutamate E115 conduit à une plus grande stabilisation en présence d'AMP, d'ADP ou d'ATP (ΔTm^{E115A}-ΔTm^{WT} Table 1, partie II). De plus, l'ajout d'ion Mg^{2+} ne permet pas d'obtenir l'effet d'augmentation du Tm observé avec la protéine sauvage, suggérant que ce résidu est impliqué la fixation du Mg^{2+} ($\Delta Tm^{E115A\ ion}$-$\Delta Tm^{wt\ ion}$ Table 1, partie II).

Effet de la mutation du glutamate régulateur. La mutation du résidu E190 entraîne une plus forte stabilisation par l'ATP et, dans une moindre mesure, par l'ADP en comparaison avec la protéine sauvage. En revanche, l'effet de l'AMP est diminué (ΔTm^{E190G}-ΔTm^{WT} Table 1, partie II) et on peut remarquer que la température de fusion de cette protéine mutante est là même lorsqu'elle est en présence d'ADP et d'ATP, suggérant une même stabilisation par ces deux nucléotides. Si l'on admet que ces variations de Tm reflètent bien des variations d'affinité, ces données suggèrent que la présence du glutamate E190 diminue significativement l'affinité pour l'ATP, plus modérément celle pour l'ADP et au contraire augmente celle pour l'AMP.

Enfin, la présence de cations métalliques ne semble pas stabiliser ce mutant différemment de la protéine sauvage, sauf en présence d'ATP. En effet, le Tm de la protéine en présence d'ATP n'est pas augmentée lorsque l'on ajoute du Mg^{2+} ($\Delta Tm^{E190G\ ion}$, Table 1, partie II) contrairement à la protéine sauvage. Ces résultats pourraient suggérer que ce résidu est impliqué indirectement dans la fixation de cet ion.

Ces données doivent être interprétées avec prudence, car les concentrations nucléotidiques utilisées sont très élevées, et l'effet n'a pas pu être observé avec des concentrations significativement plus faibles en nucléotides ou en ions métalliques. Si les complexes ainsi mis en évidence ont des KD de l'ordre du mM, il est probable que ces expériences ne reflètent pas le véritable complexe enzyme-substrat (par exemple, parce que le deuxième substrat de l'enzyme est absent et que les fixations ne sont pas indépendantes).

En conclusion, EfFIC semble bien être stabilisée par les dérivés de l'adénosine ce qui est cohérent avec l'hypothèse d'une activité AMPylase. L'analyse des mutants suggère que le glutamate régulateur E190 fait obstacle à la fixation de l'ATP tout en étant impliqué dans la fixation de l'AMP. Le glutamate catalytique E115 semble, quant à lui, impliqué indirectement dans la liaison des nucléotides, *via* la fixation des cations divalents. L'ensemble de ces résultats est en bonne adéquation avec les résultats que nous avons obtenus par ailleurs.

	EfFIC^{WT}			EfFIC^{E115A}			EfFIC^{E190G}		
cation divalent ajouté	aucun	Ca^{2+} (10mM)	Mg^{2+} (10 mM)	aucun	Ca^{2+} (10mM)	Mg^{2+} (10 mM)	aucun	Ca^{2+} (10mM)	Mg^{2+} (10 mM)
	ΔTm^{WT}	ΔTm^{WT-Ca}	ΔTm^{WT-Mg}	ΔTm^{E115A}	$\Delta Tm^{E115A-Ca}$	$\Delta Tm^{E115A-Mg}$	ΔTm^{E190G}	$\Delta Tm^{E190G-Ca}$	$\Delta Tm^{E190G-Mg}$
Pi	**0,00**								
PPi	**0,00**								
GDP	**-2,00**								
GTP	**-1,50**								
CTP	**-1,00**								
AMP	**3,91**	**-0,27**	**-0,93**	**5,20**	**-0,60**	**-1,20**	**1,80**	**-0,20**	**-0,80**
ADP	**3,84**	**1,15**	**1,82**	**6,00**		**-0,80**	**5,80**		**2,00**
ATP	**0,58**	**0,80**	**1,20**	**3,60**		**-2,00**	**6,20**		**-0,40**
ATPgS	**0,91**	**1,80**	**1,93**						
NAD	**-0,50**								

	Comparaison EfFIC^{WT}/EfFIC^{E115A}			Comparaison EfFIC^{WT}/EfFIC^{E190G}		
cation divalent ajouté	aucun	Ca^{2+} (10mM)	Mg^{2+} (10 mM)	aucun	Ca^{2+} (10mM)	Mg^{2+} (10 mM)
	ΔTm^{E115A}- ΔTm^{WT}	$\Delta Tm^{E115A-Ca}$- ΔTm^{WT-Ca}	$\Delta Tm^{E115A-Mg}$- ΔTm^{WT-Mg}	ΔTm^{E190G}- ΔTm^{WT}	$\Delta Tm^{E190G-Ca}$- ΔTm^{WT-Ca}	$\Delta Tm^{E190G-Mg}$- ΔTm^{WT-Mg}
Pi						
PPi						
GDP						
GTP						
CTP						
AMP	**1,29**	**-0,33**	**-0,27**	**-2,11**	**0,07**	**0,13**
ADP	**2,16**		**-2,62**	**1,96**		**0,18**
ATP	**3,02**		**-3,20**	**5,62**		**-1,60**
ATPgS						
NAD						

Table 1 : Thermofluor

Les expériences ont été réalisées avec 3µM de protéines mélangées dans un tampon 50 mM Tris pH 8.0 , 150 mM NaCl, SYPRO Orange 2x et, lorsque indiqués, en présence de nucléotides et d'ions divalents aux concentrations indiquées. Les mesures sont réalisées sur une CFX Connect (BioRad) qui augmente graduellement la température de 30°C à 90°C par pas de 0.2°C et toutes les 30 secondes. La température de fusion est déterminée comme la valeur de la température qui annule la dérivée seconde de la courbe primaire (point d'inflexion).

3. Essai de mise au point d'une méthode de mesure de l'analyse cinétique de l'auto-AMPylation

Objectifs :

Mesurer une cinétique de l'activité d'EfFIC

1. Par une méthode chromatographique

Principe méthodologique. La présence d'une réaction d'auto-AMPylation se traduit d'une part par une consommation d'ATP et d'autre part par une modification chimique de la protéine. Une chromatographie échangeuse d'anions (de type Mono Q) peut en théorie être exploitée :

- pour séparer et quantifier le nucléotide triphosphate ;
- pour séparer et quantifier les formes non modifiée et modifiée de la protéine, la présence du groupement phosphate augmentant théoriquement l'affinité pour le support chromatographique, donc les conditions d'élution.

Résultats. Aucune des expériences réalisées dans nos conditions avec $EfFIC^{WT}$ (Figure 2A), $EfFIC^{E190G}$ (Figure 2B) et FICD (non montré) n'ont permis d'obtenir des chromatogrammes significativement différents selon que la protéine a été pré-incubée en l'absence ou en présence d'ATP.

2. <u>Par une méthode de dosage du phosphate inorganique</u>

Principe méthodologique. La présence d'une réaction d'auto-AMPylation se traduit par la production de phosphate-inorganique. Une méthode de dosage du Pi peut donc être théoriquement utilisée pour mesurer l'activité d'AMPylation. J'ai donc cherché à mettre à profit un test de mesure de la concentration du phosphate inorganique par spectroscopie de fluorescence créé par Martin Webb (Brune *et al*. Biochemistry 1998) et récemment mis au point au laboratoire par Christian Galicia.

Ce test consiste à faire une expérience en présence d'une protéine liant le phosphate

inorgnique (Pi) d'*E.coli* (PBP, phosphate binding protein) qui sera liée covalemment à un fluorophore, la coumarine. La fixation de ce phosphate libre par la protéine modifiée (MDCC-PBP) entrainera donc un changement conformationnel déplaçant le fluorophore et entrainant un changement de l'intensité de fluroscence. Le plasmide portant le gène codant la PBP mutée nous a été généreusement donné par Martin Webb et la modification avec la coumarine a été réalisée par Christian Galicia.

Résultats. La méthode de dosage a été validée par la mise en évidence de l'activité ATPasique de la chaperone BIP en présence d'ATP et d'ion magnésium mais aucune variation de la concentration en phosphate libre n'a été observée avec $EfFIC^{wt}$ ou $EfFIC^{E190G}$ (figure 2C). De même, aucune variation de la concentration en Pi n'a été observée avec ces protéines en présence d'ADP (figure 2D). Enfin, l'activité ATPasique de BIP ne varie pas si cette protéine a été incubée avec FICD, ce qui montre que l'on ne parvient pas à observer d'activité de modification de BIP apr FICD dans nos conditions.

Les protéines EfFIC ayant une activité d'AMPylation observable par les méthodes décrites dans l'article, il est donc probable que l'efficacité de la réaction d'auto-AMPylation soit trop faible pour se traduire par une production de phosphate inorganique en concentration suffisante pour être quantifiée par la méthode testée.

A

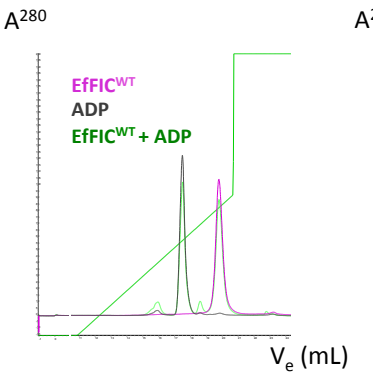

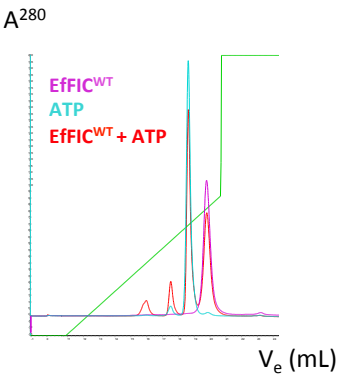

B

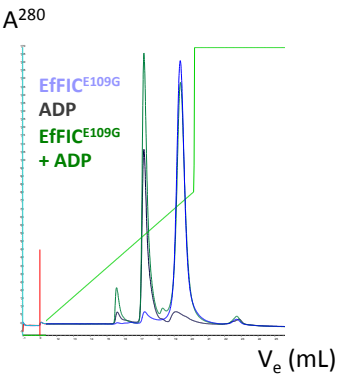

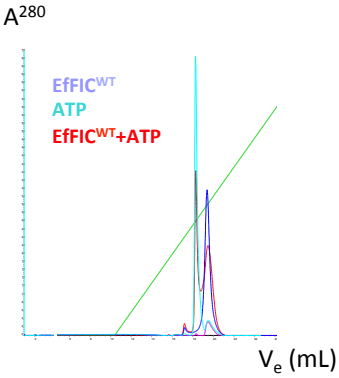

C

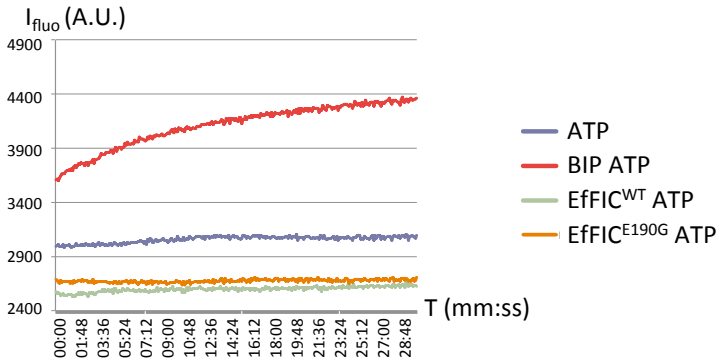

D

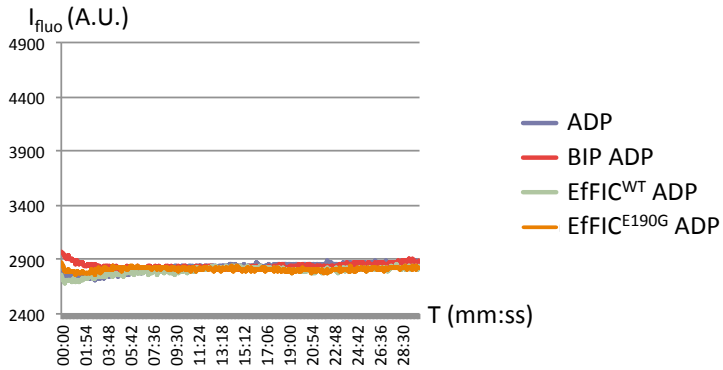

E

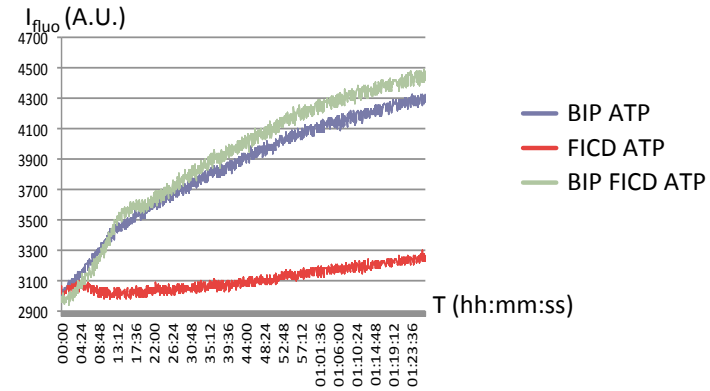

Université Paris-Saclay
Espace Technologique / Immeuble Discovery
Route de l'Orme aux Merisiers RD 128 / 91190 Saint-Aubin, France

Figure 2 :

Chromatographie sur MonoQ d'EfFIC^{WT} (A) et d'EfFIC^{E190G} (B) pré-incubées en présence d'ADP ou d'ATP. L'échantillon (200 µL) contenant 5mM de nucléotide ADP, 5mM de MgCl2 et 150µM de protéine, préincubé préalablement pendant 1h à 30°C, a été injecté sur une colonne échangeuse d'anions MonoQ 5/50 GL. La charge a été réalisée en présence d'un tampon sans NaCL et l'élution a été réalisée par un gradient de 0 mM à 500 mM de NaCl. L'échantillon et les tampons chromatographiques contenaient 50 mM de Tris-HCl à pH8.0.

C, D : Dosage du phosphate inorganique produit en présence d'EfFIC et d'ATP ou d'ADP. L'intensité de fluorescence du traceur MDCC-PBP (10 µM) a été mesurée à 25°C en tampon 50mM Tris pH8.0, 150mM NaCl et 10µM $MgCl_2$ sur un spectromètre Flexstation (Molecular Dynamics, excitation à 430 nm, émission à 465 nm) en présence de 5µM d'EfFIC^{WT}. Le temps t=0 correspond à l'ajout de 10µM d'ATP. Un contrôle positif est réalisé en présence de 5 µM de l'ATPase BIP.

E : Dosage du phosphate inorganique produit par l'activité ATPasique de BIP après incubation avec FICD.

Les expériences de dosage du Pi ont été réalisées à 25°C avec 100µM de MDCC-PBP, 2µM de protéine FIC, éventuellement 5µM de BIP et 10µM de nucléotide ADP ou ATP.

Les protéines FICD (5 µM) et BIP (5µM) ont été incubées pendant 45 minutes à 30°C en présence d'ATP (5 µM). L'analyse a ensuite été menée comme précédemment, après une nouvelle addition à t=0 d'ATP (5 µM).

4. Analyse de la structure quaternaire d'EfFIC

Objectifs :

Différents types de structures quaternaires ont été décrits pour les protéines FIC, et une étude suggère que des changements de structure quaternaire pourraient intervenir dans le contrôle de l'activité de la protéine NmFIC comme publié dans Stanger *et al.* PNAS 2015. Il s'agit donc d'analyser l'état d'oligomérisation d'EfFIC

1. Analyse des structures cristallines et confirmation par chromatographie

Principe méthodologique

L'analyse des structures cristallines résolues pendant ma thèse, et la corrélation avec les conditions de cristallisation, peut permettre de formuler des hypothèses qui sont ensuite testées par chromatographie d'exclusion stérique.

Résultat

J'ai observé deux états d'oligomérisation différents d'EfFIC dans les structures

cristallines : tétramèrique et hexamèrique (figure 3A) et l'analyse des conditions de cristallisation suggére que les formes à 6 sous-unités sont dues à la liaison avec l'ADP. Afin de confirmer cette hypothèse, EfFIC a été préincubée en présence d'ADP puis l'échantillon a été analysé par chromatographie d'exclusion stérique. Le même profil chromatographique, correspondant à un tétramère, a été observé avec et sans ADP (figure 3B).

2. Analyse en solution par SEC-MALS

Principe méthodologique :

Le SEC-MALS (Size Exclusion Chomatography - Multi-Angle Light Scattering) est une technique qui permet de déterminer avec précision le volume, et par déduction la masse, d'un objet en solution. L'échantillon est injecté sur colonne de chromatographie d'exclusion stérique couplée en sortie avec une mesure de la diffusion de la lumière laser, de l'index de réfraction et de l'absorbance UV.

Résultat

L'analyse réalisée sur la protéine EfFIC purifiée, en l'absence de ligand, dans le cadre d'une collaboration avec Bertrand Reynal et Sébastien Brule à l'Institut Pasteur (figure 3C) révèle une structure tétramérique.

L'ensemble de ces résultats indiquent la prévalence de la forme tétramérique en solution, et n'ont pas permis de déterminer si l'état hexamèrique est un état contraint par le cristal ou s'il s'agit d'un état biologique dont nous n'avons pas trouvé les conditions physico-chimiques propices à sa formation en solution.

A

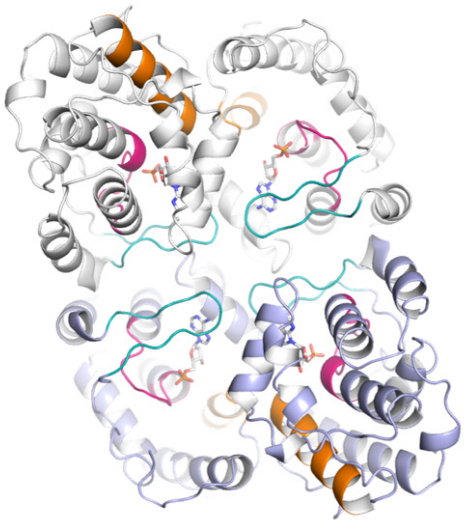

Tetramère

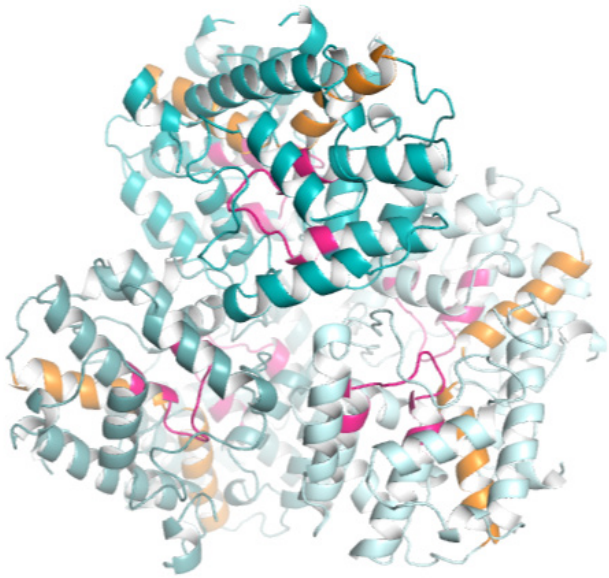

Hexamère

B

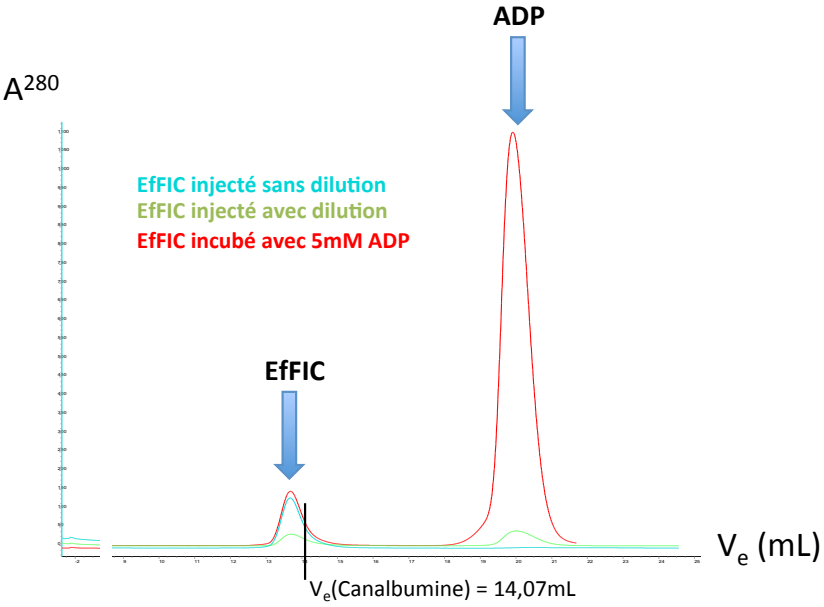

V_e(EfFIC) = 13,60mL

V_e(Canalbumine) = 14,07mL
MW(Canalbumine) = 75 000Da

C

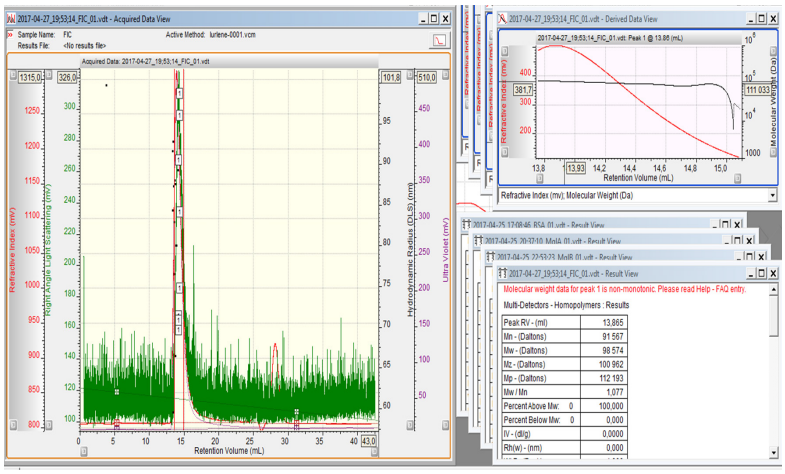

Masse moléculaire théorique d'un monomère de EfFIC= 24 598 Da

Masse moléculaire théorique d'un tétramère de EfFIC= 98 392 Da

Masse moléculaire mesurée de l'objet= 98 574 Da

Figure 3. Analyse par différentes approches de la structure quaternaire d'EfFIC

A : Tetramère et hexamère cristallins. Un dimère peut être retrouvé en 2 copies dans le tétramère et en 3 copies dans l'hexamère. Les deux protéines de chaque dimères sont représentées de la même couleur.

B : Analyse de la structure quaternaire d'EfFIC par chromatographie d'exclusion stérique. Les expériences ont été réalisées sur une colonne Superdex 200 10/300 équilibrée avec un tampon Tris-HCl 50mM pH8.0, NaCl 150mM par injection de la même quantité d'EfFIC (400µg) à une concentration finale de respectivement 170µM (violet) ou 35µM (rouge). La même expérience a été réalisée après incubation d'EfFIC pendant 30 minutes à 30°C en présence de 5 mM ADP (cyan). La comparaison du volume d'élution (Ve) de EfFIC et de la canalbumine montre que EfFIC est éluée à un volume qui correspondrait à un objet ayant une masse plus grande que 75 000Da.

C : SEC MALS

L'analyse a été effectuée sur un échantillon d'EfFIC à une concentration de 350µM en tampon 50mM Tris-HCl pH8.0, NaCl 150mM. La masse déduite correspond celle d'un tétramère.

III. Étude de la régulation de la toxine bactérienne AnkX par les membranes

A. Introduction

Cette partie porte sur un autre mécanisme de régulation de protéine FIC : la régulation par les membranes de l'effecteur de *Legionella pneumophila*, AnkX.

L. pneumophila est une bactérie Gram négative pathogène pour l'humain opportuniste. Lorsqu'elle est inhalée, la bactérie est phagocytée par les macrophages alvéolaires. Elle utilise alors un système de sécrétion de type 4 (T4SS) pour injecter plus de 300 effecteurs dans le cytoplasme du macrophage afin de détourner son trafic cellulaire et de se répliquer, ce qui est à l'origine de graves pneumopathies. Parmi ces effecteurs, se trouvent AnkX et Lem3 qui agissent sur des protéines du trafic cellulaire, les petites protéines G.

AnkX est une protéine prédite pour comporter 3 domaines distincts : un domaine catalytique FIC N-terminal, un domaine central composé de 8 à 12 motifs ankyrine répétés et un domaine C-terminal de structure et fonction inconnues. Il a été montré qu'AnkX catalyse la phosphocholination de ses cibles en transférant une molécule de phosphocholine (PC) à partir d'une molécule de cytidine diphospho-choline (CDP-choline ou CDC) et en présence d'un ion magnésium. Lem3, qui catalyse la réaction de dé-phosphocholination des cibles d'AnkX, est étudiée au laboratoire par Wenhua Zhang.

Il a été montré qu'AnkX peut modifier deux petites protéines G de la famille des Rab, Rab1 et Rab35, et que ces protéines sont nécessairement localisées à une membrane lorsqu'elles sont modifiées par l'effecteur bactérien. Cette dernière observation a orienté mon travail sur le rôle des membranes dans la régulation d'AnkX.

Bien que la structure d'une protéine AnkX tronquée comportant le domaine catalytique et les quatre premiers motifs ankyrine a été résolue par notre équipe préalablement à ma thèse, celle de la protéine entière est encore inconnue. J'ai donc également conduit une étude structurale dans le but de proposer un modèle de l'interaction d'AnkX avec les Rab et avec les membranes.

Afin de mener à bien ce projet, j'ai cloné, produit et purifié un ensemble de protéines recombinantes, notamment les formes de Rab1 et Rab35 comportant à leurs extrémités N-terminales une étiquette hexa-histidine (6his) permettant leur adressage aux membranes de liposomes contenant du nickel sans que cela requiert la présence de la modification lipidique post-traductionnelle naturelle, selon la méthode expliquée dans la partir IV de ce document.

Dans le but de mener une étude de l'interaction d'AnkX avec les membranes, j'ai synthétisé des liposomes de compositions définies. J'ai observé $AnkX^{FL}$ localisé à la surface de liposomes par cryo-microscopie électronique et montré que cette interaction laisse la partie N-terminale d'AnkX accessible au solvant. J'ai ensuite utilisé la technique de co-sédimentation pour confirmer l'interaction d'AnkX avec les membranes, et pour révéler le rôle clé de sa partie C-terminale dans cette interaction.

J'ai ensuite étudié la spécificité membranaire de la forme entière d'AnkX, en comparant l'interaction avec des membranes de différentes compositions lipidiques d'une part et avec des membranes de courbures différentes d'autre part. Les résultats de cette étude suggèrent que l'effecteur bactérien interagit plus facilement avec des liposomes contenant des lipides typiques de la membrane plasmique ou des lipides caractéristiques de l'endosome/lysosome.

J'ai montré que la forme entière d'AnkX est active en solution sur les protéines Rab1 et Rab35 mais également sur des peptides correspondant au segment de Rab1 comportant chacun le site putatif de modification. Cela m'a permis d'étudier l'influence des membranes sur l'activité d'AnkX en menant des expériences de phosphocholination de Rab1a et présence de liposomes contenant des lipides modifiés avec du nickel. Ces expériences ont montré que l'activité de l'effecteur bactérien est augmentée en présence de liposomes ce qui suggère qu'AnkX est régulée positivement par les membranes.

Enfin, j'ai mené une étude structurale afin de tenter de résoudre la structure tridimensionnelle de la protéine AnkX entière. Si mes essais de cristallisation de la protéine seule, en complexe avec différentes formes de Rab ou avec des peptides sont restés infructueux, j'ai tout de même obtenu un jeu de données de bonne qualité de la protéine par la technique de la diffraction de rayons X aux petits angles (SAXS). Ces données ont montré qu'AnkX a un profil SAXS caractéristique des protéines possédant 2 domaines globulaires reliés. La génération de modèles à partir de ces données par différentes approches suggère une conformation de la protéine en fer à cheval. Afin de confirmer ces hypothèses, j'ai modélisé en parallèle plusieurs structures 3D probables de cette toxine de Legionnela *via* les serveurs Robetta et iTasser. Les différents modèles obtenus présentent tous la même architecture en fer à cheval due au domaine central de motifs ankyrine répétés. Enfin, j'ai traduit ces modélisations en jeux de données théoriques de diffraction aux petits angles que j'ai comparés au jeu de données SAXS obtenu. L'ensemble de cette analyse me permet de proposer un modèle d'interaction d'AnkX avec Rab aux membranes.

Ces résultats feront l'objet d'une publication en cours d'écriture.

Legionella toxin AnkX interacts with membranes to phosphocholinate Rab GTPases

Simon Veyron[1], Wenhua Zhang[1], Sylvain Trepout[2], Gérald Peyroche[1], Jacqueline Cherfils[1]

[1]Laboratoire de Biologie et Pharmacologie Appliquée, CNRS and Ecole normale supérieure Paris-Saclay, Cachan, France

[2] Institut Curie and INSERM, Orsay, France

Abstract

Legionella pneumophila, the causative agent of the Legionnaire's diseases, escapes recognition by the immune system by invading pulmonary macrophages, where it avoids degradation by hiding in the Legionella-containing vacuole (LCV). Legionella uses a type IV secretion system to inject hundred of toxins collectively called effectors in the infected cell, some of them divert membrane traffic to support the maturation of the LCV. One of these toxins is AnkX, which modifies the endoplasmic reticulum Rab1 and endosomal Rab35 GTPases by post-translational addition of a phosphocholine, which impairs their displacement from the membrane by RabGDIs. AnkX is comprised of a FIC domain that binds Rab GTPases and carries out the catalytic reaction, followed by ankyrin repeats and a C-terminal domain of unknown functions. Here we investigated how the structure of AnkX supports its activity towards Rab GTPases on membranes by combining reconstitution in artificial membranes to hybrid structural analysis by SAXS and modeling. We find that AnkX binds to membranes by its C-terminus domain, and that its recruitment to membranes potentiates its phosphocholination of Rab GTPases. Binding of AnkX is highest to PI(4,5)P_2-containing membranes, where it activates Rab35 more efficiently than Rab1. Structural analysis of AnkX depicts a horseshoe-shaped conformation with the FIC and C-terminal domains located at opposite ends of the ankyrin repeats. Together, this suggests that AnkX recognizes the membrane and membrane-attached Rab simultaneously to define the sublocalization of its activity in infected cells.

Introduction

Membrane traffic is a frequent target of intracellular pathogens, which divert it to escape phagocytosis or to generate an intracellular compartment where they hide and replicate (reviewed in [1, 2]). Small GTPases of the Arf and Rab families, which regulate most aspects of intracellular traffic (reviewed in [3, 4]), are therefore frequent targets of bacterial pathogens (reviewed in [5]). Small GTPases are often likened to molecular switches, alternating between an inactive state bound to GDP and an active state bound to GTP, a cycle that is regulated by activating (guanine nucleotide exchange factors or GEFs) and inhibiting (GTPase activating proteins or GAPs) regulators (reviewed in [6]). This GDP/GTP cycle combines with a cytosol/membrane cycle regulated by GDIs, such that the active, GTP-bound GTPase is associated with membranes (reviewed in [6]). The opportunistic intracellular pathogen *Legionella pneumophila*, the causative agent of the Legionnaire's disease, injects a large number of effectors through its type IV secretion system to hide and replicate in the Legionella-containing vacuole (LCV) (reviewed in [7]), an unusual number of which feature eukaryotic-derived domains such as ankyrin repeats [8]. The LCV originates from the host phagosome, which is diverted from a lysosomal fate by effectors that modify its composition. Among these effectors, several of them have been shown to divert trafficking small GTPases, including the ArfGEF RalF which activates the Arf GTPase at the surface of the LCV [9], DrrA, which activates the Rab1 GTPase and modifies at by addition of AMP [10-12], and the AnkX toxin, which modifies Rab1 and Rab35 GTPases by a phosphocholine [13].

In this study, we focused on AnkX, a Legionella toxin originally discovered as an ankyrin repeats-containing effector that supports escape of the Legionella-containing phagosome from the lysosomal pathway [14]. Ankx was later found to carry a FIC domain that catalyzes the transfer of a phosphocholine group onto Rab GTPases, followed by tankyrin repeats and a C-terminal domain of unknown function [13]. FIC domains are widespread in bacteria, where they use di-phosphate-containing cofactors such as ATP for the post-translational modification (PTM) of target proteins by a mono-phosphate-containing moiety (reviewed in [15, 16, 17). Their catalytic domain has a conserved 3 dimensional structure, in which the catalytic activity is contained in a conserved sequence signature. In the case of AnkX, the co-factor was identified as being CDP-choline (CDC), whose binding to the catalytic site was observed in a construct comprising the FIC domain followed by a truncated ankyrin repeats domain {Campanacci, 2013 #99]. In vitro and in cells, AnkX phosphocholinates two Rab GTPases: Rab1, which is a major regulator at the Golgi (reviewed in [4]), and Rab35, which functions in endocytic recycling (reviewed in [18]). However, AMPylation but not phosphocholination was critical for the localization of Rab1 to the LCV [19], while AnkX disrupted host cell endocytic recycling [20] suggesting that Rab35 may be its physiological substrate.

AnkX modifies a serine of Rab1 and a threonine in Rab35 which are located in their switch 2 regions (a region of small GTPases that undergoes a conformational change upon binding to GTP; reviewed in Cherfils) and is involved in their interaction with RabGDI [21] and other regulators. Accordingly, phosphocholination was shown to impair their extraction from membranes by GDI and their activation by GEFs although the effect was milder on their effectors and GAPs were not affected [22-24]. These observations suggest that the substrates of AnkX are membrane-attached Rab GTPases. However, whether AnkX has structural determinants for the direct recognition of membranes which may contribute to the specificity and localization of its activity has remained poorly understood. In this study, we investigated how the structure of AnkX supports its activity towards Rab GTPases on membranes by combining reconstitution in artificial membranes to hybrid structural analysis by SAXS and modeling. Our data suggest that AnkX recognizes the membrane and membrane-attached Rab simultaneously to define the sublocalization of its activity in infected cells.

Results

AnkX binds to negatively charged membranes by its C-terminal domain

To analyze whether AnkX is able to interact directly with membranes, we first used cryo-electron microscopy to analyze the recruitment of purified recombinant full-length AnkX (**Figure 1A**) to liposomes. As shown in **Figure 1B**, the surface of liposomes containing PI(4,5)P_2 (lipid composition in **Table 1**) was conspicuously decorated by AnkX molecules, visualized either directly of by nanogold beads attached to its histidine tag. Next, we used liposome co-sedimentation to determine whether AnkX has a preference for specific phosphoinositides or for lipids with mono-unsaturated acyl chains (dioleoyl, DO) by measuring its recruitment to liposomes of different lipid compositions (**Table 1**). AnkX bound to all types of liposomes, but only PIP_2-containing liposomes supported its almost complete recruitment to liposomes; conversely, uncharged liposomes resulted in the lowest recruitment (**Figure 1C, 1D**). Finally, we investigated whether recruitment to liposomes is determined by the FIC domain, the C-terminal domain, or both, using purified AnkX constructs lacking either of these domains (see **Figure 1A**). We observed that the construct lacking the FIC domain bound to liposomes as strongly the full-length protein (**Figure 1E**). In contrast, a construct lacking the C-terminal domain was entirely found in the unbound fraction (**Figure 1E**). We conclude from these experiments that AnkX binds strongly to membranes independently of the presence of Rab GTPases with a preference for PIP2-containing membranes, and that this interaction is entirely encoded in its C-terminal domain.

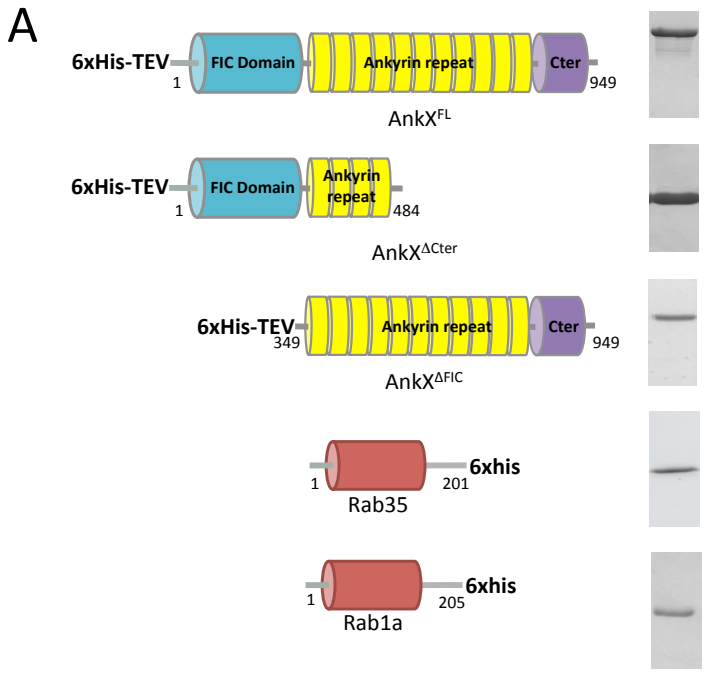

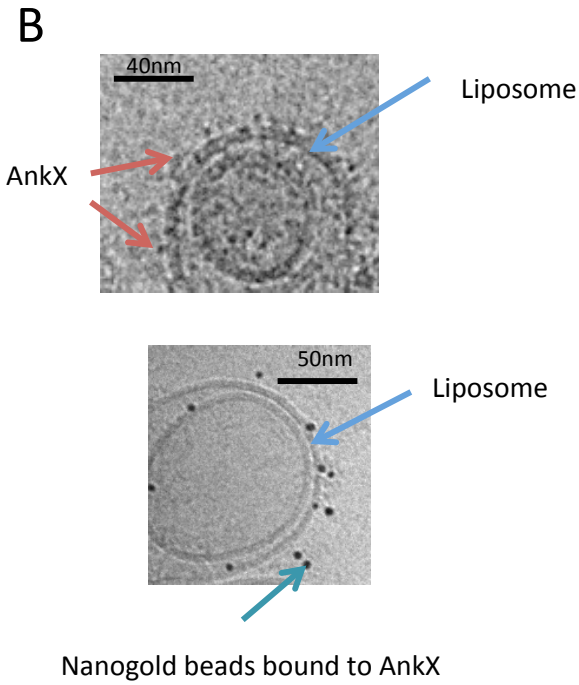

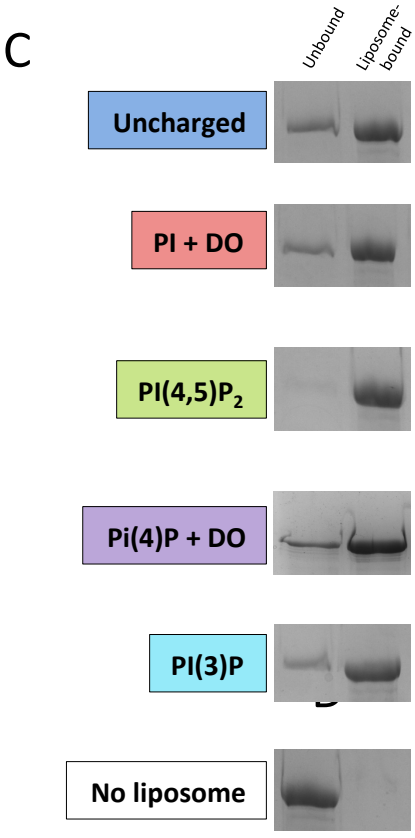

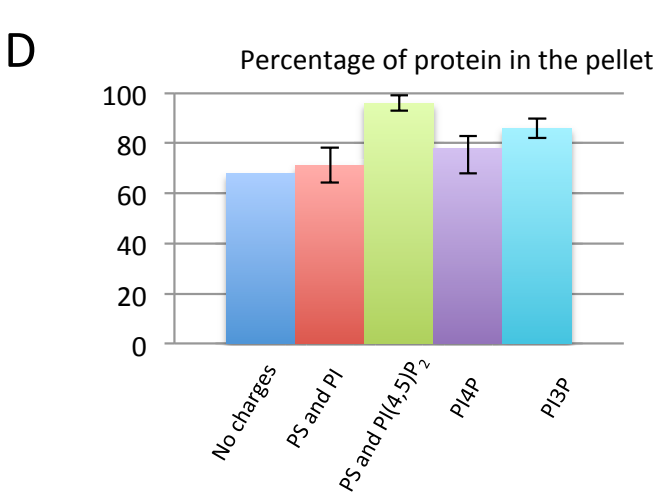

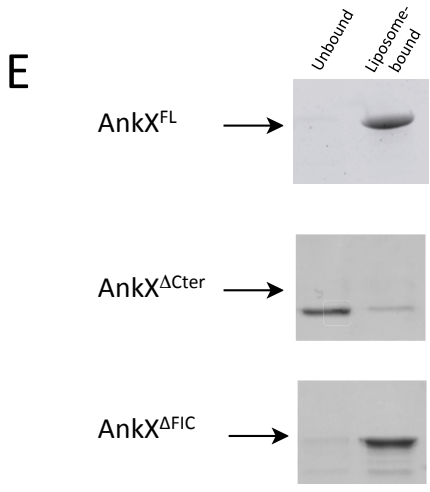

(legend next page)

Figure 1: Analysis of the interaction of AnkX with membranes.

A: SDS-PAGE analysis of Legionella AnkX and human Rab constructs used in this study

B: Cryo-electron microscopy analysis of the recruitment of AnkX to $PI(4,5)P_2$-containing liposomes. Arrows indicate the location of AnkX molecules at the surface of liposomes. The right panel shows Ni-NTA-nanogold labeled AnkX.

C: Co-sedimentation analysis of the recruitment of AnkX to liposomes of different composition as described in Table 1. The supernatant fraction contains unbound AnkX, the pellet contains liposome-bound AnkX.

D. Quantification of experiments shown in C. All experiments were done in triplicate.

E: AnkX interacts with membranes through its C-terminal domain. Binding of full-length AnkX, $AnkX^{\Delta FIC}$ and $AnkX^{\Delta Cter}$ to PIP_2-containing liposomes was analyzed by co-sedimentation

	PC (%)	DOPC (%)	PE (%)	DOPE (%)	PS (%)	PI (%)	PI(3)P (%)	PI(4)P (%)	$PI(4,5)P_2$ (%)	Cholesterol (%)	DOGS-NiNTA (%)
Uncharged	80		20								
PI + DO		70		20	5	5					
PI(3)P	70		20			5	5				
PI(4)P + DO	40	35	10	10				5			
PI(3)P	70		20			5	5				
$PI(4,5)P_2$	48		20		10				2	20	
$PI(4,5)P_2$ + NiNTA	46		20		10				2	20	2

Table 1 : Composition of liposomes used in this study

Phosphocholination of Rab GTPases by AnkX is potentiatted by membranes.

The above analysis shows that AnkX interacts with PIP_2-containing liposomes, suggesting that membranes may contribute to the efficiency of phosphocholination. We first controlled that full-length AnkX efficiently phosphocholinates a peptide derived from the switch 2 of Rab1. As shown in **Figure 2A**, a 13-residue peptide was efficiently phosphocholinated by AnkX, and this effect was strictly dependent on the residue previously identified by mass spectrometry [13]. These observations may indicate that the recognition of Rab GTPases by AnkX is mostly mediated by the switch 2 peptide. Next, we analyzed the kinetics of phosphocholination of full-length recombinant Rab1 and Rab35 in solution. Both Rab GTPases were efficiently phosphocholinated (**Figure 2B**). However, the kinetics were significantly faster for Rab35 than for Rab1, suggesting that Rab35 is a better substrate than Rab1, from which it differs by replacement of the phosphocholinated serine by a threonine. Because of its slowest kinetics that may facilitate the detection of a regulatory effect, we chose to focus on Rab1 to analyze the effect of membranes. We used a Rab1 construct that carries a His-tag in

C-terminus that allows its tethering to liposomes that contain Ni-NTA lipids in the absence of its natural post-translational lipidation [25], and we removed the His-tag from AnkX. As shown in **Figure 2C**, phosphocholination of membrane-tethered Rab1 by AnkX was conspicuously increased in the presence of membranes. These experiments demonstrate that the efficiency of AnkX is potentiated by membranes.

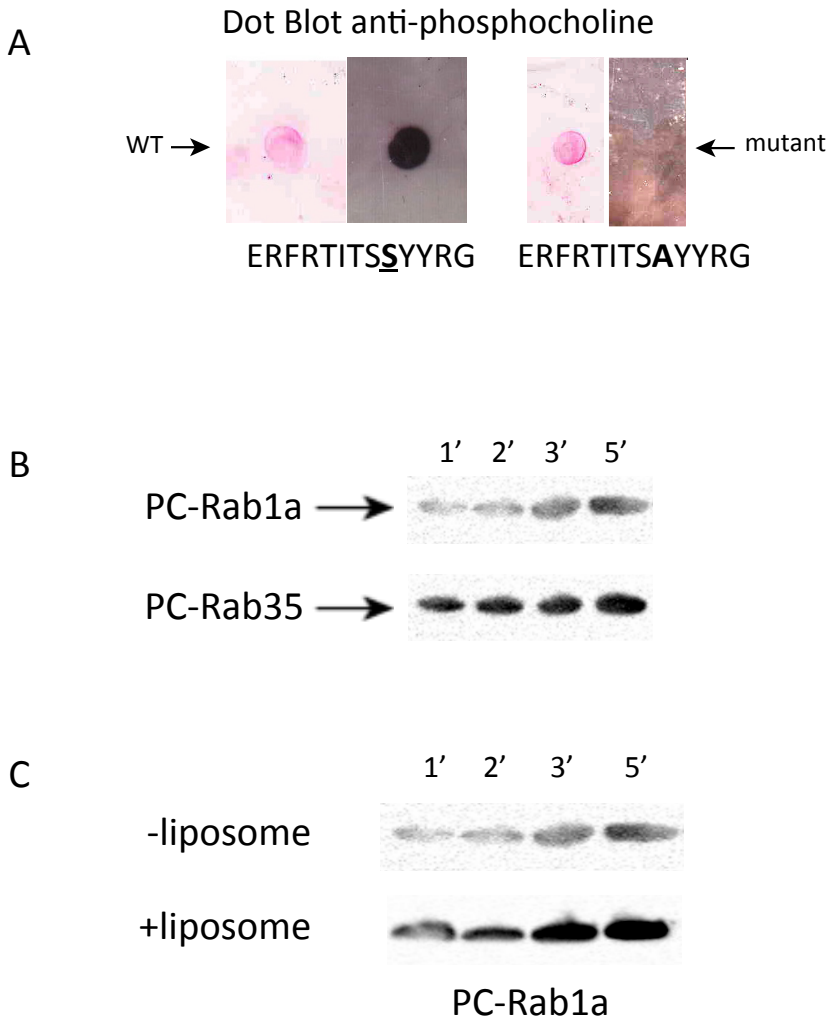

Figure 2. Phosphocholination of Rab GTPases by AnkX is potentiated by membranes

A: AnkX phosphocholinates a peptide derived from the switch 2 of human Rab1. Phosphocholination used a dot-blot format and was detected by Ponceau red and by Western blot using an anti-phosphocholine antibody. The mutant peptide lacks the phosphocholinated serine.

B: Kinetics of phosphocholination of human Rab1a and Rab35 by AnkX in solution. Phosphocholination was detected by Western blot using an anti-phosphocholine antibody.

C: The efficiency of AnkX is potentiated by membranes. Rab1a carrying a C-terminal 6xHis tag that mimics natural lipidation was tethered to $PI(4,5)P_2$ + Ni liposomes (**Table 1**). Kinetics of phosphocholination was detected by Western blot using an anti-phosphocholine antibody.

The solution structure of AnkX provides a framework for its phosphocholination of Rab GTPases on membranes.

The above experiments suggest that AnkX recognizes membranes both directly by its C-terminal domain, and indirectly through the interaction of its FIC domain to membrane-tethered Rab GTPases. We analyzed the structural basis of this dual recognition by structural analysis in solution using synnchrotron small angle x-ray scattering experiment coupled with size exclusion chromatography (SEC-SAXS). Statistics for data collection and analysis in **Table 2**. The analysis of the SAXS data is shown in **Figure 3**. AnkX eluted as a single peak, in which the radius of gyration (Rg) was stable across the frames (**Figure 3A**). The corresponding SAXS profile is shown in **Figure 3B.** The corresponding dimensionless Kratky plot is characteristic of well-folded protein (**Figure 3C**). The distance distribution function has a maximum distance of 144 Å, and displays a marked shoulder indicative of an anisotropic shape (**Figure 3D**). Ab initio modeling using the SAXS data alone suggested that AnkX has a horseshoe shape (not shown). AnkX is comprised of a FIC domain of known crystal structure in which 4 ankyrin repeats are present [26], central ankyrin repeats which are known to form rigid, curved scaffolds (reviewed in [27]) and a C-terminal domain rich in predicted alpha helices. Because high resolution structural information is already available for half the protein and the structure of ankyrin repeats is highly conservative, we modeled the structure of AnkX by fragment-based ab initio modeling guided by the SAXS data. Three-dimensional sequence-based models of AnkX were calculated using the Robetta and i-Tasser softwares, all of which described horseshoe shaped structures in which the FIC and C-terminal domains were placed at opposite ends of the ankyrin repeats. Each model was then fitted against the experimental SAXS data, and the model with the lowest χ^2 was further refined by rigid body modeling using SASREF, which resulted in a very low χ^2 (**Figure 3E).** This final model is compatible with the simultaneous binding of the C-terminal domain of AnkX to membranes and the FIC domain to membrane-tethered Rab (**Figure 3F**).

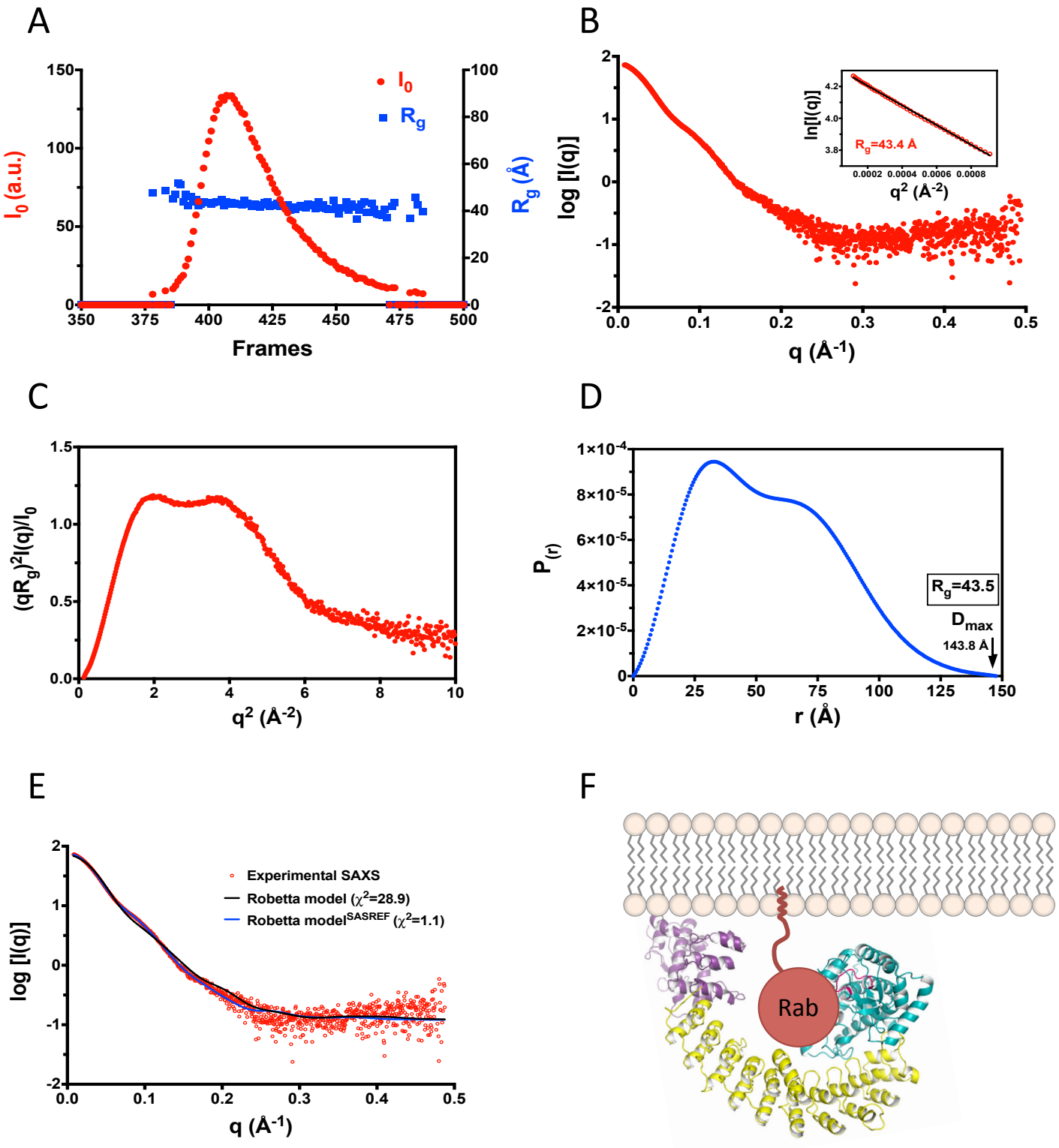

(legend next page)

Figure 3. Structural analysis of AnkX by SEC- SAXS.

A: The frame-resolved estimations of I(0) and Rg. Scattering data from 30 frames (396-425) was reduced and processed for structural analysis of AnkX. a.u., arbitrary unit.

B: The SAXS profile of AnkX. The insert shows the Guinier plot ($R_g q_{max}$=1.22).

C: The dimensionless Kratky plot analysis of AnkX.

D: The $P_{(r)}$ plot analysis gives a D_{max} estimate of 143.8Å.

E: The rigid fit between SAXS data and predicted models of AnkX. Robetta model, the predicted model by Robetta program; Robetta model^{SASREF}, rigid-body refinement of the Robetta model by SASREF, using three domains (1-375, 376-715 and 716-949).

F: A hybrid model of AnkX bound to membranes. The structure of AnkX was obtained by rigid-body refining the Robetta model with the best fit to the SAXS data using SASREF. The FIC domain is in cyan, the ankyrin repeats are in yellow, the membrane-binding C-terminal domain is in red. A tentative location of membrane-attached Rab is shown.

Discussion

In this study, we found that AnkX binds to PIP_2-containing membranes and that its membrane-binding determinants are located in its C-terminal domain of the protein. We showed that the efficiency of AnkX is modulated by both its Rab GTPase substrate, with Rab35 being a better substrate than Rab1, and by the presence of membranes binding to its C-terminus. Finally, we used hybrid structural analysis combining SAXS analysis in solution and fragment-based ab initio modeling to derive a model of membrane-bound AnkX which is compatible with its simultaneous interaction with the membrane by its C-terminus and with membrane-tethered Rab GTPase by its FIC domain, using the ankyrin repeats as a spacer.

These structural and biochemical determinants suggest that the activity of AnkX in the infected cell is driven by its concurrent recognition of its GTPase substrate and a specific membrane. Based on our in vitro observations, this points to Rab35 bound to peripheral or early endosomal membranes as its primary substrate. This is consistent with recent observations that AnkX co-localizes with Rab35 in transfected cells, and that it impairs host cell endocytic pathways where this GTPase functions [20]. An interesting question remaining is the role of the Legionella effector LidA/Lem3 in this context, which removes phosphocholine from Rab GTPases [28]. It is tempting to speculate that Lem3 should also recognize, and be potentiated by, membranes, in a manner that would allow it to function in a different context thank AnkX, for example to avoid accumulation of phosphocholinated Rab1 on the LCV. Future studies using purified recombinant proteins and artifical membranes should help in exploring how AnkX and Lem3 cooperate to divert Rab GTPases during Legionella infection.

Material and methods

Proteins

Full-length AnkX, AnkX$^{\Delta Ct}$ and AnkX$^{\Delta FIC}$ carrying a His-tag in N-terminus followed by a TEV protease cleavage site were purified essentially as described in [26], except that 5% glycerol was added which improved their stability. For removal of the His-tag, AnkX was incubated with 1/10 w/w of TEV protease overnight. The uncleaved fraction and the tag were removed with a HisTrap FF 5mL column (GE healthcare) and further purified by size exclusion chromatography on a Superdex Hiload 16/600. Removal of the His-tag was controlled by Western Blot using an anti-hexa-histidine antibody. Human Rab1a and Rab35 carrying a C-terminal 6-His tag were purified as described in [25]. Peptides were synthetized by Chinese Peptide Co. LTD.

Liposome assays.

Natural lipids or synthetic unsaturated lipids (Avanti Polar lipids) at the desired concentration were suspended in chloroform, mixed, dried with a rotavapor RII (BUTCHI) and resuspended in 50 mM Tris pH 8 buffer containing 120 mM NaCl for cryo-EM experiments or 220 mM sucrose for co-sedimentation experiments. Unilamellar liposomes were formed by five cycles of freezing in liquid nitrogen/thawing at 35°C. Liposomes were then flash-frozen and stored at -20°C. Sucrose-containing liposomes were unfrozen and extruded at 0.2µm with a hand extruder, diluted in 4 volumes of buffer (50 mM Tris pH 8, 120 mM NaCl), and centrifuged at 100000g for 20min at 25°C (Beckman rotor TLA 100.3). Liposome-containing pellet was then resuspended in IB* buffer (50 mM Tris pH 8, 120 mM NaCl, 1 mM DTT, 1mM $MgCl_2$). For co-sedimentation experiments, 2µM proteins and 1mM liposomes were incubated in IB* buffer during 10 min then centrifuged at 100000g for 20 min at 25°C and (Beckman rotor TLA 120.1). The supernatant was removed and mixed with 5xLeammli buffer and the pellet was resuspended in a IB* buffer and 5xLeammli buffer. The protein content was analyzed by SDS-PAGE and revealed with Instant Blue staining solution (Expedeon).

Cryo-electron microscopy

Liposomes containing PI(4,5)P_2 (**Table 1**) were diluted at 1.6 mg/mL and mixed with AnkX at 1.4 mg/mL in a 3:0.1 ratio in 10 mM HEPES pH 7.4 and 300 mM NaCl. In one experiment, AnkX was labelled with Ni-NTA-nanogold beads (5 nm; purchased from Nanoprobes) which were added just prior to sample freezing and used at a final concentration of 50 nM. For plunge freezing of samples, a 5 µl drop of sample was deposited onto 300 mesh holey carbon copper grids (Ted Pella). The excess of solution was manually blotted using a Whatman filter paper and the grid was plunge-frozen in liquid ethane using a Leica EM-CPC cryopreparation chamber. Data acquisition was performed on a 200 kV field emission gun JEOL 2200FS electron microscope equipped with a Gatan US1000 slow scan CCD camera and an in-column energy-filter essentially as described in [29].

Phosphocholination kinetics.

Peptide phosphocholination was performed with 10 µg of peptide and 5µg of $AnkX^{1-484}$ and revealed in dot blot format using an anti-phosphocholine antibody (TEPC15, Sigma). Kinetics in solution were measured using 8 µg of AnkX and 10µg of Rab GTPase in a reaction buffer (20 mM Hepes pH7.4, 50 mM NaCl, 1 mM DTT, 1 mM $MgCl_2$) in the presence or not of 1mM $PI(4,5)P_2$+ NiNTA liposomes (**Table 1**). The reaction was started by adding 5mM of CDP-choline then incubated at 30°C. At each time point, an aliquot was removed and the reaction was stopped by addition of Leammli buffer and heating at 95°C for 5 minutes. Phosphocholination was revealed by Western blot analysis using an anti-PC antibody. s

Modeling.

Fragment-based bb initio predictions of the 3D structure of AnkX were performed using the i-Tasser server (https://zhanglab.ccmb.med.umich.edu/I-TASSER/) [30] and the Robetta server (http://robetta.bakerlab.org/) [31].

SAXS sata collection, analysis and modeling.

SAXS data was acquired using an HPLC-coupled SAXS instrument at ESRF beamline BM29. 400 ug purified AnkX protein in 60 uL was injected onto the BIO-SEC3 column (300 Å, Agilent Inc.) on the HPLC system (Shimadzu, Japan) that is connected to the SAXS data collection instrument. The flow was 0.25 mL/min at 18 °C and 700 frames were collected with an exposure time of 1.0 s per frame. Data reduction and integration to absolute units, frame averaging, and subtraction were done using the EDNA pipeline moduled in ISPyBB software [32]. Frames corresponding to the high-intensity fractions of the peak and having constant R_g within were averaged for structural analysis.

All the data analyses and modeling were performed with the ATSAS package [33]. Statistics are summarized in **Table 2**. Radii of gyration (R_g) were evaluated by Guinier Wizard using the data within the range of Guinier approximation $sR_g<1.2$ and by Distance Distribution Wizard, both of which are modules of the PRIMUS program. The maximum distance D_{max} was estimated with PRIMUS and refined by trial and error with GNOM. The dimensionless Kratky plot, which measures the foldedness of a protein, was calculated by plotting $(qR_g)^2I_{(q)}/I_{(0)}$ against qR_g. The distance distribution functions $P_{(r)}$ were calculated with GNOM. The rigid fit between scattering amplitudes calculated for the predicted Robetta and i-Tasser models and the experimental SAXS profiles were carried out with CRYSOL using q = 0.49. The SASREF program was used for rigid-body refinement of the model with the lowest Chi2, allowing the ankyrin and C-terminal domains to rotate with respect to the FIC domain under the constraint of SAXS data (q=0.49) using SASREF. The refined model

with the best Chi^2 with respect to the experimental SAXS data was selected as full-length AnkX model.

Acknowledgements.

This work was supported by grants from the Fondation pour la Recherche Médicale and from the Agence Nationale pour la Recherche to J.C. and by a grant from the DIM MALINF to S.V. We thank the scientific team at the SAXS beamline BM29 at the ESRF synchrotron (Grenoble, France) for making the beamline available to us, and Dr Sergio Marco (Institut Curie Orsay, France) for making the cryo-EM facility of the Institut Curie available to us. We are grateful to Valérie Campanacci (CNRS, Gif-sur-Yvette, France) and to the members of the Cherfils lab for help and shared expertise.

Table 2 : HPLC-Coupled SAXS Data Acquisition, Analysis and Modeling

HPLC(SEC Column)		Bio-SEC3 (Agilent)		
SAXS Instrument		European Synchrotron Radiation Facility (ESRF) Beamline BM29		
Beam Geometry		Pinhole		
Wavelength (Å)		0.9919		
q Range (Å $^{-1}$)		0.0033-0.495		
Exposure Time (s)		1.0 per frame		
Temperature (K)		295		
Structural Parameters		**AnkX**		
Guinier Fit	$I_{(0)}$ **(cm^{-1})**	76.24±7.7e-2		
	R_g (Å)	43.1±1.1e-2		
$P_{(r)}$	$I_{(0)}$ **(cm^{-1})**	75.65		
	R_g (Å)	43.4		
	***V*p (Å^3)**	144.6e+3		
	D_{max} (Å)	143.8		
Molar Mass Determination (kD)				
Theoretic	**Estimated by Porod V[1]**		**By SAXS MOW2[2]**	**By DAMMIN model[3]**
107.2	99.3		119.0	93.0
Model Fit between SAXS Data and Robetta Model (q=0.49)				
CRYSOL (χ^2)	**SASREF Modeling (χ^2)**			
28.9	1.1			
***ab initio* Modeling (q=0.31)**				
DAMMIN (χ^2)	**GASBOR (χ^2)**			
1.0	2.4			

[1], M=*V*p/1.45; [2], SAXS MOW2 server (http://saxs.ifsc.usp.br); [3], M=Volume/2

References

1. Cossart, P. and C.R. Roy, *Manipulation of host membrane machinery by bacterial pathogens.* Curr Opin Cell Biol, 2010. **22**(4): p. 547-54.
2. Escoll, P., S. Mondino, M. Rolando, and C. Buchrieser, *Targeting of host organelles by pathogenic bacteria: a sophisticated subversion strategy.* Nat Rev Microbiol, 2016. **14**(1): p. 5-19.
3. Donaldson, J.G. and C.L. Jackson, *ARF family G proteins and their regulators: roles in membrane transport, development and disease.* Nat Rev Mol Cell Biol, 2011. **12**(6): p. 362-75.
4. Hutagalung, A.H. and P.J. Novick, *Role of Rab GTPases in membrane traffic and cell physiology.* Physiol Rev, 2011. **91**(1): p. 119-49.
5. Aktories, K., *Bacterial protein toxins that modify host regulatory GTPases.* Nat Rev Microbiol, 2011. **9**(7): p. 487-98.
6. Cherfils, J. and M. Zeghouf, *Regulation of small GTPases by GEFs, GAPs, and GDIs.* Physiol Rev, 2013. **93**(1): p. 269-309.
7. Isberg, R.R., T.J. O'Connor, and M. Heidtman, *The Legionella pneumophila replication vacuole: making a cosy niche inside host cells.* Nat Rev Microbiol, 2009. **7**(1): p. 13-24.
8. Cazalet, C., C. Rusniok, H. Bruggemann, N. Zidane, A. Magnier, L. Ma, M. Tichit, S. Jarraud, C. Bouchier, F. Vandenesch, F. Kunst, J. Etienne, P. Glaser, and C. Buchrieser, *Evidence in the Legionella pneumophila genome for exploitation of host cell functions and high genome plasticity.* Nat Genet, 2004. **36**(11): p. 1165-73.
9. Nagai, H., J.C. Kagan, X. Zhu, R.A. Kahn, and C.R. Roy, *A bacterial guanine nucleotide exchange factor activates ARF on Legionella phagosomes.* Science, 2002. **295**(5555): p. 679-82.
10. Machner, M.P. and R.R. Isberg, *A bifunctional bacterial protein links GDI displacement to Rab1 activation.* Science, 2007. **318**(5852): p. 974-7.
11. Zhu, Y., L. Hu, Y. Zhou, Q. Yao, L. Liu, and F. Shao, *Structural mechanism of host Rab1 activation by the bifunctional Legionella type IV effector SidM/DrrA.* Proc Natl Acad Sci U S A, 2010. **107**(10): p. 4699-704.

12. Muller, M.P., H. Peters, J. Blumer, W. Blankenfeldt, R.S. Goody, and A. Itzen, *The Legionella effector protein DrrA AMPylates the membrane traffic regulator Rab1b.* Science, 2010. **329**(5994): p. 946-9.
13. Mukherjee, S., X. Liu, K. Arasaki, J. McDonough, J.E. Galan, and C.R. Roy, *Modulation of Rab GTPase function by a protein phosphocholine transferase.* Nature, 2011. **477**(7362): p. 103-6.
14. Pan, X., A. Luhrmann, A. Satoh, M.A. Laskowski-Arce, and C.R. Roy, *Ankyrin repeat proteins comprise a diverse family of bacterial type IV effectors.* Science, 2008. **320**(5883): p. 1651-4.
15. Garcia-Pino, A., N. Zenkin, and R. Loris, *The many faces of Fic: structural and functional aspects of Fic enzymes.* Trends Biochem Sci, 2014. **39**(3): p. 121-9.
16. Roy, C.R. and J. Cherfils, *Structure and function of Fic proteins.* Nat Rev Microbiol, 2015. **13**(10): p. 631-40.
17. Harms, A., F.V. Stanger, and C. Dehio, *Biological Diversity and Molecular Plasticity of FIC Domain Proteins.* Annu Rev Microbiol, 2016. **70**: p. 341-60.
18. Klinkert, K. and A. Echard, *Rab35 GTPase: A Central Regulator of Phosphoinositides and F-actin in Endocytic Recycling and Beyond.* Traffic, 2016. **17**(10): p. 1063-77.
19. Hardiman, C.A. and C.R. Roy, *AMPylation is critical for Rab1 localization to vacuoles containing Legionella pneumophila.* MBio, 2014. **5**(1): p. e01035-13.
20. Allgood, S.C., B.P. Romero Duenas, R.R. Noll, C. Pike, S. Lein, and M.R. Neunuebel, *Legionella Effector AnkX Disrupts Host Cell Endocytic Recycling in a Phosphocholination-Dependent Manner.* Front Cell Infect Microbiol, 2017. **7**: p. 397.
21. Rak, A., O. Pylypenko, T. Durek, A. Watzke, S. Kushnir, L. Brunsveld, H. Waldmann, R.S. Goody, and K. Alexandrov, *Structure of Rab GDP-dissociation inhibitor in complex with prenylated YPT1 GTPase.* Science, 2003. **302**(5645): p. 646-50.
22. Goody, P.R., K. Heller, L.K. Oesterlin, M.P. Muller, A. Itzen, and R.S. Goody, *Reversible phosphocholination of Rab proteins by Legionella pneumophila effector proteins.* EMBO J, 2012. **31**(7): p. 1774-84.
23. Oesterlin, L.K., R.S. Goody, and A. Itzen, *Posttranslational modifications of Rab proteins cause effective displacement of GDP dissociation inhibitor.* Proc Natl Acad Sci U S A, 2012. **109**(15): p. 5621-6.

24. Gavriljuk, K., A. Itzen, R.S. Goody, K. Gerwert, and C. Kotting, *Membrane extraction of Rab proteins by GDP dissociation inhibitor characterized using attenuated total reflection infrared spectroscopy.* Proc Natl Acad Sci U S A, 2013. **110**(33): p. 13380-5.

25. Peurois, F., S. Veyron, Y. Ferrandez, I. Ladid, S. Benabdi, M. Zeghouf, G. Peyroche, and J. Cherfils, *Characterization of the activation of small GTPases by their GEFs on membranes using artificial membrane tethering.* Biochem J, 2017. **474**(7): p. 1259-1272.

26. Campanacci, V., S. Mukherjee, C.R. Roy, and J. Cherfils, *Structure of the Legionella effector AnkX reveals the mechanism of phosphocholine transfer by the FIC domain.* EMBO J, 2013. **32**(10): p. 1469-77.

27. Li, J., A. Mahajan, and M.D. Tsai, *Ankyrin repeat: a unique motif mediating protein-protein interactions.* Biochemistry, 2006. **45**(51): p. 15168-78.

28. Tan, Y., R.J. Arnold, and Z.Q. Luo, *Legionella pneumophila regulates the small GTPase Rab1 activity by reversible phosphorylcholination.* Proc Natl Acad Sci U S A, 2011. **108**(52): p. 21212-7.

29. Akendengue, L., S. Trepout, M. Grana, A. Voegele, C. Janke, B. Raynal, A. Chenal, S. Marco, and A.M. Wehenkel, *Bacterial kinesin light chain (Bklc) links the Btub cytoskeleton to membranes.* Sci Rep, 2017. **7**: p. 45668.

30. Yang, J., R. Yan, A. Roy, D. Xu, J. Poisson, and Y. Zhang, *The I-TASSER Suite: protein structure and function prediction.* Nat Methods, 2015. **12**(1): p. 7-8.

31. Ovchinnikov, S., H. Park, D.E. Kim, F. DiMaio, and D. Baker, *Protein structure prediction using Rosetta in CASP12.* Proteins, 2017.

32. De Maria Antolinos, A., P. Pernot, M.E. Brennich, J. Kieffer, M.W. Bowler, S. Delageniere, S. Ohlsson, S. Malbet Monaco, A. Ashton, D. Franke, D. Svergun, S. McSweeney, E. Gordon, and A. Round, *ISPyB for BioSAXS, the gateway to user autonomy in solution scattering experiments.* Acta Crystallogr D Biol Crystallogr, 2015. **71**(Pt 1): p. 76-85.

33. Franke, D., M.V. Petoukhov, P.V. Konarev, A. Panjkovich, A. Tuukkanen, H.D.T. Mertens, A.G. Kikhney, N.R. Hajizadeh, J.M. Franklin, C.M. Jeffries, and D.I. Svergun, *ATSAS 2.8: a comprehensive data analysis suite for small-angle scattering from macromolecular solutions.* J Appl Crystallogr, 2017. **50**(Pt 4): p. 1212-1225.

C. Résultats supplémentaires

I. Optimisation de l'expression et la purification des différentes formes d'AnkX

Objectifs :

Ma thèse prend place dans la continuité du travail entamé par Valérie Campanacci qui avait élaboré certains outils pour l'expression et la purification de différentes formes d'AnkX. Avant le début de ma thèse, les constructions $AnkX^{FL}$, $AnkX^{Nter}$ (appelé $AnkX^{\Delta Cter}$ dans l'article) et $AnkX^{\Delta FIC}$ avaient été réalisées et la forme $AnkX^{Nter}$ caractérisée par notre équipe. Aussi j'ai orienté mes travaux sur la forme d'AnkX entière et j'ai donc commencé par optimiser les conditions d'expression.

1. Amélioration des conditions de production

Étant donnés les problèmes de solubilité précédemment rencontrés, j'ai remplacé la souche de production Rosetta (DE3) pLysS par une souche BL21 (DE3) exprimant les chaperones dnaK-dnaJ-grpE ainsi que groES-groEL (BL21 pG-KJE8) ce qui a permis d'améliorer la pureté et la stabilité des formes d'AnkX précédemment construites.

2. Nouvelles constructions d'AnkX

J'ai construit de nouveaux vecteurs d'expression recombinants correspondant aux différents domaines d'AnkX, cloné et purifié les formes $AnkX^{\Delta Cter}$ (résidus 1 à 714) et $AnkX^{Cter}$ (résidus 728 à 949). J'ai également sous cloné les séquences codantes d'$AnkX^{FL}$ WT et $AnkX^{\Delta FIC}$ avec une étiquette 6his en C-terminal dans un vecteur d'expression Gateway n'ajoutant pas de séquence supplémentaire au gène d'intérêt, pDest14 et construit les formes 1-727 et 715-949 correspondant respectivement aux domaines FIC-ankyrine et au domaine C-terminal seul (Figure 1). Ces différentes constructions n'ont pas permis de purifier une protéine soluble et pure malgré le recours à de nombreuses conditions d'expression et de purification.

Enfin, j'ai construit les vecteurs d'expression et procédé à la purification de 2 formes tronquées de chaque Rab, dépourvues des boucles flottantes N-terminale et C-terminales, et comportant ou non une mutation du résidu modifié par AnkX ($Rab1a^{WT\ 6\text{-}178}$, $Rab1a^{S79A\ 6\text{-}178}$, $Rab35^{WT\ 5\text{-}176}$, $Rab1a^{T76A\ 5\text{-}176}$).

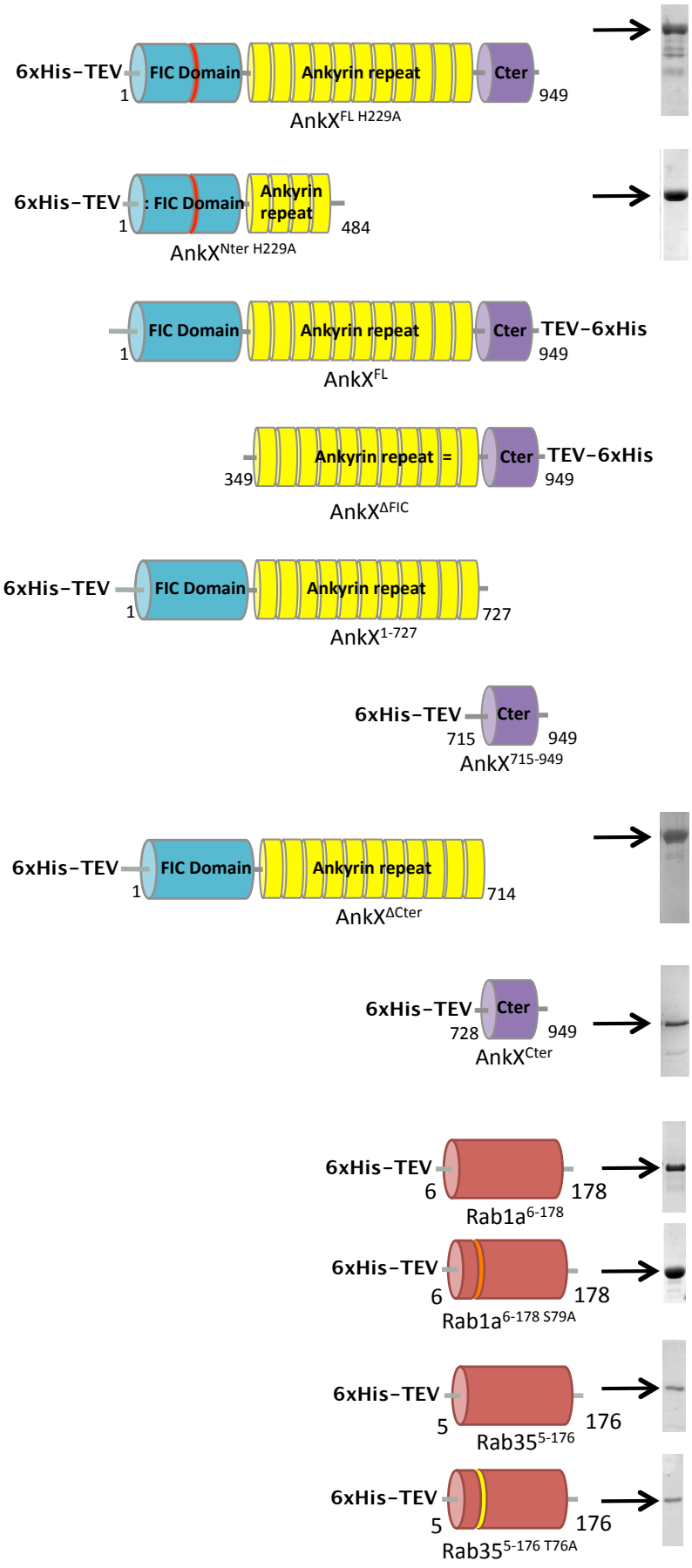

Université Paris-Saclay
Espace Technologique / Immeuble Discovery
Route de l'Orme aux Merisiers RD 128 / 91190 Saint-Aubin, France

Figure 1

Représentation schématique des différentes formes d'AnkX pour lesquelles des essais de production et de purification ont été menés. Lorsque la protéine a pu être purifiée, son analyse par SDS-PAGE suivie de coloration au bleu de Coomassie est montrée.

II. Recherche de conditions stabilisant le complexe AnkX/Rab

Objectifs :

Les essais de cristallisation d'AnkX-FL sont restés sans succès, ce qui pourrait résulter d'une trop grande flexibilité de la protéine. Comme il est connu que la structuration d'une protéine trop flexible qui accompagne son interaction avec un partenaire permet parfois d'obtenir un cristal du complexe, j'ai recherché les conditions expérimentales favorables à la formation d'un complexe stable d'AnkX avec sa cible.

1. En solution, par chromatographie d'exclusion stérique.

J'ai purifié 2 formes d'AnkX mutants pour l'histidine catalytique ($AnkX^{FL\ H229A}$ et $AnkX^{Nter\ H118A}$) dans le but de stabiliser la protéine pour mener une étude structurale.

Un complexe enzyme/substrat peut être stabilisé en empêchant le déroulement de la réaction catalysée par l'enzyme. Nous avons donc incubé $AnkX^{FL\ H229A}$ avec $Rab1a^{WT\ 6\text{-}178}$en présence de CDC et de $MgCl_2$. La formation de complexes a été analysée par chromatographie d'exclusion stérique. Si le complexe est stabilisé, on attend un pic d'absorption à 280nm correspondant à un poids moléculaire correspondant au complexe AnkX/Rab sur le chromatogramme.

Résultats :

Les pics correspondants à chacune des deux protéines non associées sont visibles, mais aucun complexe n'est observé (figure 2A). Ce résultat négatif peut résulter soit de l'absence de formation du complexe, soit de la dissociation du complexe, insuffisamment stable pour résister aux conditions de séparation utilisées.

2. En présence de membranes, par co-sédimentation

Les protéines Rab que nous utilisons étant dépourvues de modifications lipidiques, elles ne pourront pas interagir avec les membranes. Une association de Rab1 ou Rab35 avec les liposomes en présence d'AnkX indiquerait, de manière indirecte, la formation d'un complexe Rab-AnkX à la surface des liposomes.

Afin de favoriser l'obtention d'un complexe stable, l'expérience a été réalisée avec $AnkX^{FL\ H229A}$ entier ainsi qu'avec la forme $AnkX^{\Delta FIC}$ qui comporte les motifs ankyrines, motifs habituellement impliqués dans la reconnaissance protéine-protéine.

Résultats :

L'association aux liposomes a été analysée par la technique de co-sédimentation selon le protocole décrit dans l'article. Aucune co-sédimentation de Rab1a via AnkX n'a pu être observée (Figure 2B).

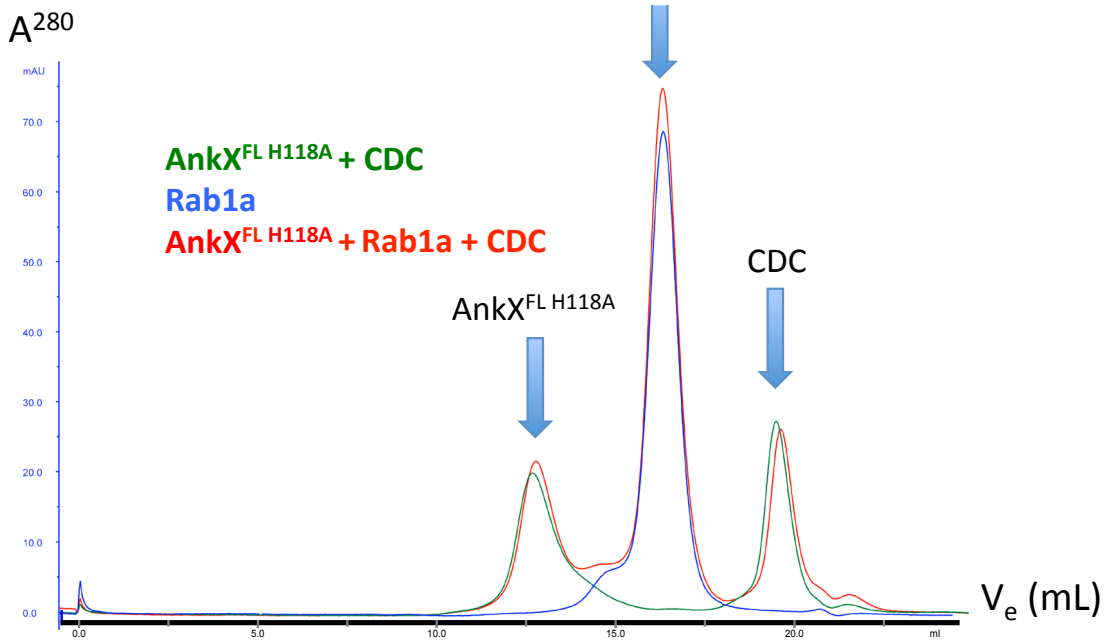

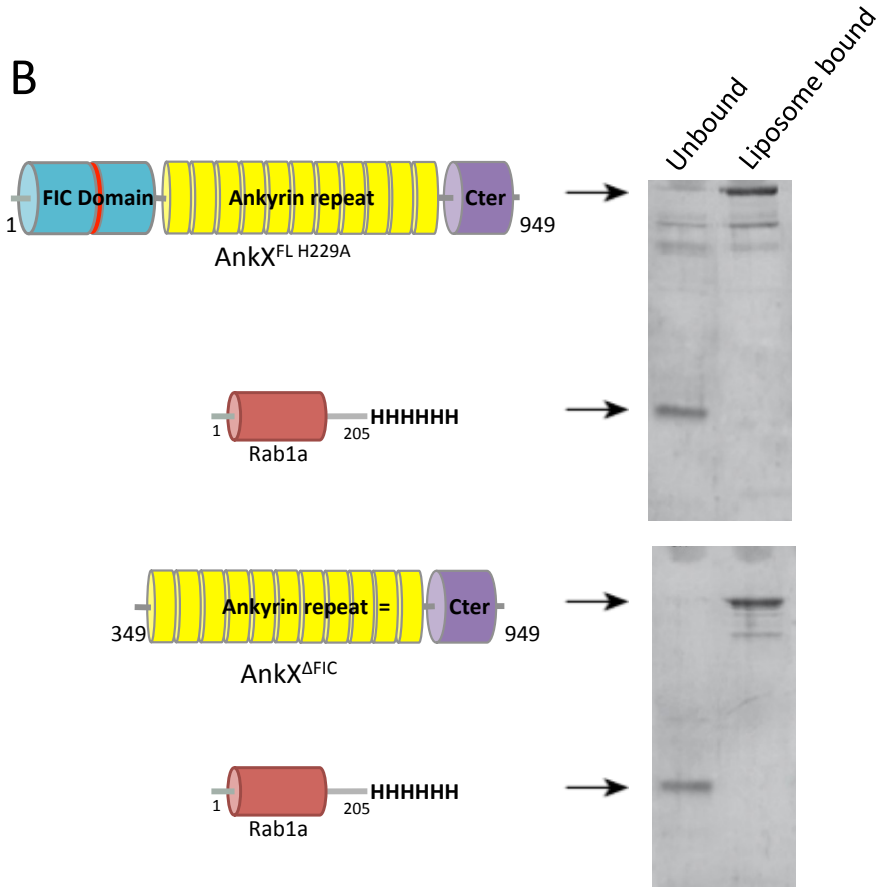

Figure 2 – Recherche de conditions d'obtention d'un complexe entre AnkX et Rab1a

A : Analyse des complexes par chromatographie d'exclusion stérique. $AnkX^{FL\ H118A}$ (10µM) et Rab1a (50µM) ont été incubés pendant 40min à 30°C dans un tampon de réaction HEPES 10mM pH 7.4, NaCl 150mM, DTT 1mM en présence de CDC (1mM) et de $MgCl_2$ (2mM). Les protéines ont ensuite été séparées par chromatographie d'exclusion stérique sur colonne Superdex 200 10/300.

B : Analyse des complexes par co-sédimentation avec des liposomes. L'expérience a été menée avec 1 µM de chaque protéine et des liposomes de type membrane plasmique (S-PM), en suivant le protocole de sédimentation décrit dans l'article.

III. Synthèse d'un composé fluorescent et mise au point d'une méthode d'analyse cinétique d'AnkX.

Objectifs :

Dans le but de développer une méthode d'étude cinétique de l'activité de phosphocholination d'AnkX, nous avons envisagé une approche par spectrométrie de fluorescence mettant à profit les caractéristiques de fluorescence d'un analogue du substrat CDC possédant un groupement N-Methylanthraniloyl (MANT) lié à l'oxygène 2' ou 3' du ribose. La réaction catalysée par AnkX, en convertissant la MANT-CDC en MANT-CMP, pourrait entraîner une variation mesurable de l'intensité de fluorescence.

Ce composé MANT-CDC n'étant pas disponible dans le commerce, j'ai réalisé ce travail de synthèse organique sous la supervision de Joanne Xie au sein de son équipe (du laboratoire PPSM, de l'ENS Paris-Saclay).

Synthèse organique d'un dérivé fluorescent de la CDC

Nous avons mis en place cette expérience en nous basant sur les travaux réalisés avec des adénosines et guanidines (Hiratsuka JBC 1982). J'ai mélangé 100µmol de CDP-choline (substrat) avec 10 équivalents de NMIA (N-methylisatoic anhydride, réactant) et 2 équivalents d'acétonitrile (solvant) à 35°C pendant 16h sous agitation puis ajout de 3 équivalents d'H_2O et 1.5 équivalent d'acétonitrile et procédé à une nouvelle incubation de 3h à 55°C.

Durant la synthèse, j'ai vérifié l'apparition du produit MANT-CDC par chromatographie sur couche mince (CCM ou TLC) sur plaque de silice, après avoir déterminé qu'un mélange Propanol-Ammoniaque-solution d'EDTA à 0.5g/L (ratio 6 :3 :1) comme solvant de migration était optimal (Figure 3A). Une fois la réaction achevée, j'ai séparé les

différents composés par chromatographie échangeuse de cations et ai vérifié la composition de ces fractions par CCM (Figure 3B). J'ai ensuite testé ces fractions en tant que substrats d'AnkX par test de phosphocholination en solution comme décrit dans l'article (Figure 3C) ; le résultat positif obtenu indique que le composé fluorescent synthétisé est donneur de phosphocholine dans la réaction catalysée par AnkX.

Utilisation du dérivé fluorescent pour des analyses cinétiques:

J'ai utilisé ce composé MANT-CDC pour effectuer des premiers tests d'activité d'AnkX en utilisant un spectrofluorimètre (Cary Eclipse, Varian) pour une longueur d'excitation de 360mm et d'émission de 440mm. Aucune variation de l'intensité de fluorescence n'a malheureusement été observée en présence d'AnkX et de Rab1a dans notre essai. De nouvelles expériences sont à prévoir afin de tester ce composé.

A

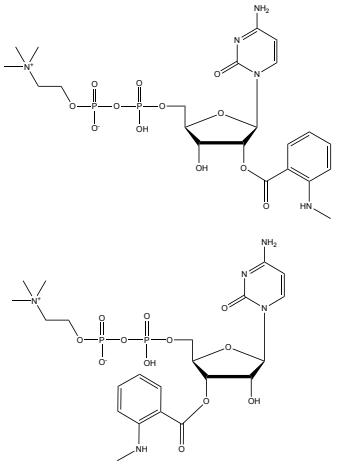

B

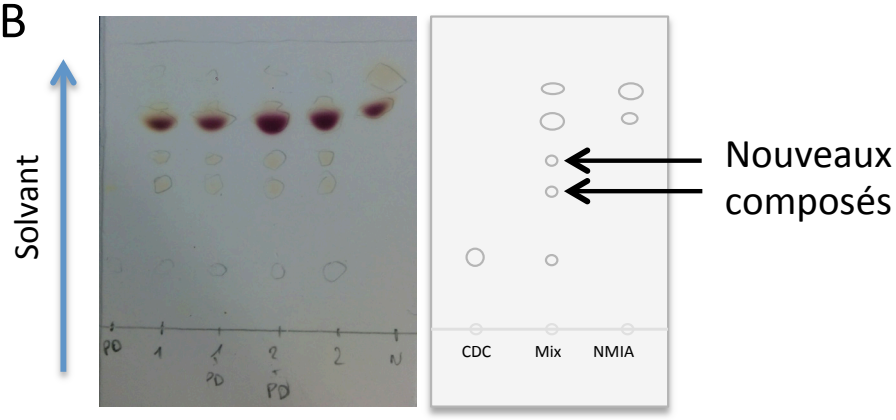
Solvant
CDC
Mix
NMIA
Nouveaux composés

C

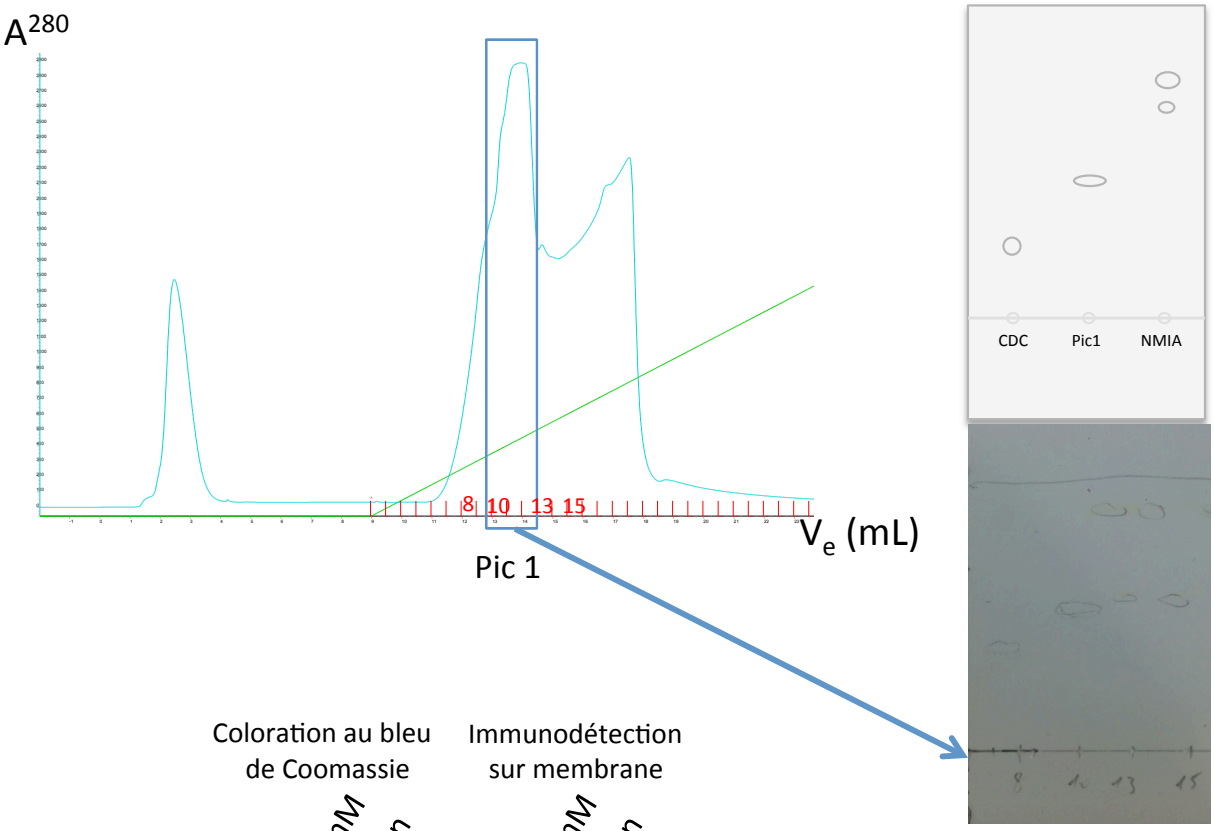
A280
8
10
13
15
Ve (mL)
Pic 1
CDC
Pic1
NMIA

D

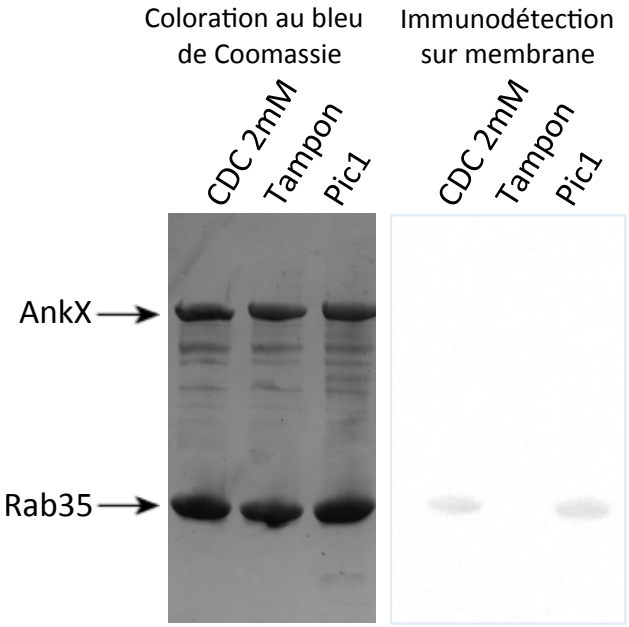
Coloration au bleu de Coomassie
Immunodétection sur membrane
CDC 2mM
Tampon
Pic1
CDC 2mM
Tampon
Pic1
AnkX
Rab35

Figure 3:

A : Schéma du composé MANT-CDC

Un mélange de 2'-N-Methylanthraniloyl et 3'-N-Methylanthraniloyl sera forcément obtenu.

B : Résultat obtenu par l'analyse en chromatographie sur couche mince de l'avancée de la réaction de synthèse de MANT-CDC. Comparaison de la composition du mélange réactionnel final avec celle des solutions de substrats (CDC et NMIA respectivement). La photographie du chromatogramme et sa représentation schématique sont données.

C : Séparation des différents composants par chromatographie échangeuse d'anions.

Les composés présents dans le mélange réactionnel final ont été séparés par chromatographie sur colonne échangeuse d'anions MonoQ 5/50GL. La composition du pic 1, analysée par CCM, révèle qu'il comporte la MANT-CDC et ne contient pas de quantité détectable de CDC non modifiée.

D : Activité d'auto-phosphocholination d'AnkX par le MANT-CDC nouvellement synthétisé.

La réaction de phosphocholination a été réalisée comme décrit dans l'article en substituant la CDC par 20µL de la fraction correspondant au pic 1 (*cf.* B). Le mélange réactionnel a ensuite été soumis à une électrophorèse en conditions dénaturantes et analysé par coloration en bleu de Coomassie et par immunodétection avec des anti-phosphocholine.

IV. Étude structurale.

Objectifs :

Il s'agissait d'obtenir des informations sur la structure à haute résolution de la forme entière d'AnkX qui est toujours inconnue, à partir d'AnkX seule ou en complexe avec une protéine Rab.

1. Microscopie électronique par coloration négative

Nous avons contacté Sergio Marco à l'Institut Curie afin d'établir une collaboration et obtenir une image de la protéine entière par microscopie électronique. Nous avons opté pour la technique de coloration négative avec un contrastant appelé « UranyLess ».

J'ai pu réaliser un unique essai mais l'analyse des images a révélé que la protéine était en majorité précipitée dans l'échantillon utilisé, ce qui a empêché leur interprétation.

2. Essais de cristallographie

J'ai criblé de nombreuses conditions dans l'objectif d'obtenir des cristaux de chacune des formes d'AnkX exprimées et purifiées, seules ou en complexe avec les différentes formes de Rab ou avec les peptides (décrits dans l'article).

Mes essais de cristallisation n'ont donné aucun cristal de protéine.

Dernièrement, nous sommes parvenus à obtenir des cristaux d'AnkX$^{C\text{-}ter}$ (domaine de

fonction et de structure inconnue, Figure 4). Ces cristaux faisant diffracter les rayons X à basse résolution et la protéine n'ayant pas d'homologue, une optimisation ainsi que la détermination d'une stratégie pour répondre à la question des phases est encore à mener.

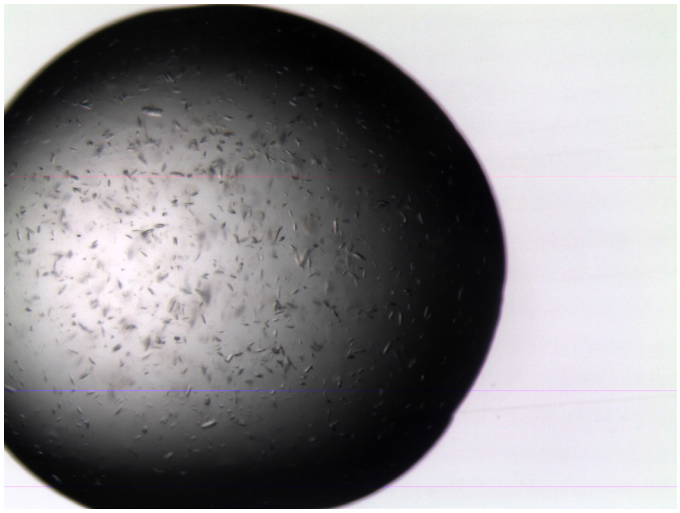

Figure 4:

Cristaux d'AnkXC-ter

Obtenus par cristallisation par diffusion de vapeur en goutte assise avec un crible commercial PEGII (Qiagen). La protéine est concentrée à 5mg/mL (170µM) dans un tampon 50mM Tris pH 8.0 150mM NaCl et mélangée aux conditions de précipitation 0.1M HEPES pH 7.5, 10% (w/v) PEG 4000, 5% (w/v) Isopropanol dans un ratio 1:1 (v/v). Les cristaux ont été amenés sur la ligne ID29 et ont montré une capacité à faire diffracter les rayons X vers 15Å.

IV. Mise en place d'un système d'étude des petites protéines G aux membranes

A. Introduction

Les petites protéines à activité GTPase sont des protéines ubiquitaires et des acteurs majeurs de la signalisation cellulaire. Ces protéines ont la particularité de pouvoir lier le GTP ou le GDP et d'avoir une activité de transduction du signal au sein de la cellule seulement en état liée au GTP. L'échange nucléotidique va donc avoir le rôle d'interrupteur moléculaire au sein de la cellule.

Les petite protéines G vont donc osciller entre un état actif, lié au GTP, et un état inactif, lié au GDP et cette oscillation sera gouvernée par deux protéines qui auront une spécificité au sein des petites GTPase : la Guanine exchange factor (GEF) va permettre l'échange du nucléotide GDP pour un GTP et la GTPase activating protein (GAP) qui va activer l'activité GTPasique de la petite protéine G, hydrolysant le GTP en GDP+Pi.

Au sein de la cellule, les petites protéines G actives, liées au GTP seront ancrées à la membrane par une modification lipidique post-traductionnelle portée par un de leur résidu. Sous forme liées au GDP, les petites protéines G seront en solution dans le cytoplasme, leur modification lipidique sera alors enfouie dans la petite GTPase ou dans une autre protéine.

Les membranes étant une composante essentielle à l'activité des petites protéines G *in vivo*, il est nécessaire de les prendre en compte lors d'études *in vitro*.

Afin de contourner la difficulté d'obtenir des petites protéines G modifiée et de palier aux difficultés inhérentes au travail avec des protéines portant une modification lipidique, notre équipe a mis au point une technique de permettant de mimer cette modification lipidique. Nous avons cloné et purifié plusieurs petites protéines G différentes portant une étiquette hexa-histidine à la place de leur modification lipidique naturelle puis nous avons synthétisés des liposomes comportant des lipides portant des ions nickel afin d'adresser ces petites protéines G aux membranes.

Enfin, nous avons caractérisé nos protéines en solution et en présence de membranes par activité d'échange nucléotidique en fluorescence.

Toute cette étude a fait l'objet d'un article publié en février 2017 chez Biochemical Journal, article dans lequel j'ai été responsable du clonage et de la purification des petites protéines G Rab1a et Rab35 ainsi que de la GEF de Rab35, DENND1B.

Biochemical Journal (2017) **474** 1259–1272
DOI: 10.1042/BCJ20170015

PORTLAND PRESS

Research Article

Characterization of the activation of small GTPases by their GEFs on membranes using artificial membrane tethering

François Peurois, Simon Veyron, Yann Ferrandez, Ilham Ladid, Sarah Benabdi, Mahel Zeghouf, Gérald Peyroche and Jacqueline Cherfils

Laboratoire de Biologie et Pharmacologie Appliquée, CNRS and Ecole Normale Supérieure Paris-Saclay, 61 Avenue du Président Wilson, Cachan 94235, France

Correspondence: Jacqueline Cherfils (jacqueline.cherfils@ens-paris-saclay.fr)

Active, GTP-bound small GTPases need to be attached to membranes by post-translational lipid modifications in order to process and propagate information in cells. However, generating and manipulating lipidated GTPases has remained difficult, which has limited our quantitative understanding of their activation by guanine nucleotide exchange factors (GEFs) and their termination by GTPase-activating proteins. Here, we replaced the lipid modification by a histidine tag in 11 full-length, human small GTPases belonging to the Arf, Rho and Rab families, which allowed to tether them to nickel–lipid-containing membranes and characterize the kinetics of their activation by GEFs. Remarkably, this strategy uncovered large effects of membranes on the efficiency and/or specificity in all systems studied. Notably, it recapitulated the release of autoinhibition of Arf1, Arf3, Arf4, Arf5 and Arf6 GTPases by membranes and revealed that all isoforms are efficiently activated by two GEFs with different regulatory regimes, ARNO and Brag2. It demonstrated that membranes stimulate the GEF activity of Trio toward RhoG by ∼30 fold and Rac1 by ∼10 fold, and uncovered a previously unknown broader specificity toward RhoA and Cdc42 that was undetectable in solution. Finally, it demonstrated that the exceptional affinity of the bacterial RabGEF DrrA for the phosphoinositide PI(4)P delimits the activation of Rab1 to the immediate vicinity of the membrane-bound GEF. Our study thus validates the histidine-tag strategy as a potent and simple means to mimic small GTPase lipidation, which opens a variety of applications to uncover regulations brought about by membranes.

Introduction

A vast majority of small GTPases couple their GDP/GTP structural cycle to cytosol/membrane alternation to function as versatile molecular switches in the cell (reviewed in ref. [1]). Membrane localization of their active, GTP-bound form is pivotal to their ability to propagate information, and this requires their post-translational modification by lipids (reviewed in ref. [2]). Ras, Rho and Rab family small GTPases are modified by isoprenoid lipids attached to their C-terminus and are maintained in a soluble form by GDIs, which shield the lipid from the solvent and dissociate from the GTPases prior to their activation by guanine nucleotide exchange factors (GEFs; reviewed in ref. [3]). Arf GTPases are modified by a myristate attached to their N-terminus, which is shielded by intramolecular interactions in their inactive state [4]. The myristoylated N-terminus is autoinhibitory in solution and is displaced by membranes, which primes Arf GTPases for subsequent activation by their GEFs (reviewed in ref. [5]). Accordingly, the functional cycle of small GTPases, including their activation by GEFs, their interaction with effectors and termination of their activity by GTPase-activating proteins (GAPs), mostly takes place at the membrane interface. Studies of the activation of myristoylated Arf

Received: 9 January 2017
Revised: 3 February 2017
Accepted: 13 February 2017

Accepted Manuscript online: 14 February 2017
Version of Record published: 23 March 2017

PORTLAND PRESS

Biochemical Journal (2017) **474** 1259–1272
DOI: 10.1042/BCJ20170015

GTPases by their GEFs reconstituted on artificial membranes revealed that membranes are a major determinant of the GEF reaction [6–10], underlying that actual efficiencies cannot be reliably recapitulated by solution assays.

Methods to generate and manipulate lipidated small GTPases have been devised, yet have remained tedious to implement. Because of their intramolecular GDI mechanism, myristoylated Arf GTPases can be obtained by co-expression with *N*-myristoyltransferase in bacteria [11–13] or by modification of purified proteins by recombinant *N*-myristoyltransferases [14], but the procedure is tedious and the yield is limited by inefficient cleavage of the N-terminal methionine in the bacteria [14], which has hampered their use as standard biochemical tools. All other small GTPases are modified by insoluble farnesyl or geranylgeranyl isoprenoids that require solubilization by cognate GDIs. Soluble isoprenylated GTPases–GDI complexes have been produced using eukaryotically expressed lipidated GTPases either by co-expression with their cognate GDI or by subsequent membrane extraction by bacterially expressed GDI [15–17]. This approach was used to highlight that membrane translocation of Rac favors its activation by the RacGEF Tiam [18]. Alternatively, Rab GTPases could be prenylated *in vitro* in complex with escort protein using immobilized geranylgeranyl transferase [19]. An elegant alternative has been the semisynthesis of lipidated GTPases, involving bacterial expression of truncated non-lipidated proteins and their covalent coupling to chemically synthesized lipidated peptides [20], which found various applications in investigating the biology of Ras and other GTPases on membranes (reviewed in ref. [21]).

However, the above approaches have remained difficult to implement, which has limited the quantitative characterization of their reactions on membranes, begging for alternatives based on soluble GTPases. Two main approaches have been devised: covalent cross-linking of a cysteine residue to liposomes containing maleimide-derivatized lipids and noncovalent tethering by a polyhistidine tag to liposomes containing Ni^{2+}-NTA lipids (Ni-lipids). Both strategies uncovered pivotal contributions of membranes to the regulation of small GTPases. Thiol-maleimide cross-linking of Ras to membranes showed that membranes induce a large enhancement of the exchange rate of the RasGEF SOS [22]. Likewise, reconstitution of His-tagged RhoA-GTP in liposomes enhanced activation of RhoA by PDZ-RhoGEF, highlighting a positive feedback effect that was undetectable in solution [23]. Membrane tethering by a histidine tag of yeast Ypt7 and Ypt21/32, both members of the Rab family, also uncovered a potent GEF activity of their respective GEFs, Mon/Ccz1 [24] and TRAPPII [25], which had remained uncertain in solution. These studies point to the considerable potential of artificially tethered GTPases as standard tools to monitor the activity of small GTPases on membranes in a quantitative manner; however, their use has remained limited and comparison with lipidated GTPases has not been done.

Here, we designed His-tagged versions of 11 members of the Arf, Rho and Rab GTPases and characterized their kinetics of activation by GEFs on Ni-lipid-containing artificial membranes. We first used Arf1 and Arf6 GTPases, for which extensive characterization of the lipidated proteins is available, to demonstrate that the His-tagged GTPases quantitatively recapitulate the contribution of membranes to their activation by GEFs. We then extented the approach to all five Arf isoforms, to four major representatives of the Rho GTPases family and to two Rab GTPases that are hijacked by bacterial effectors. In all cases, the approach uncovered important contributions of membranes to the specificity and efficiency of the reactions. We conclude that tethering small GTPases to membranes by a histidine tag provides a general and easy-to-implement means to investigate their activities on membranes, which should be of broad application for understanding how GEFs, GAPs and effectors work at the membrane interface.

Results

Reconstitution of membrane-dependent activation of Arf1 and Arf6 by histidine-tag tethering

The regulation, efficiency and specificity of Arf GTPases and their GEFs cannot be reliably assessed in solution, notably because of their autoinhibition by their N-terminal helix (reviewed in ref. [26]). To assess whether tethering small GTPases to membranes by a histidine tag recapitulates the properties of the lipidated proteins, we focused on Arf1, a major regulator of membrane traffic throughout the cell, and Arf6, which functions at the crossroads of traffic and cytoskeletal dynamics at the plasma membrane (reviewed in ref. [27]), because the kinetics of activation of their myristoylated forms have been extensively characterized. We fused Arf1 and Arf6 with a 6-histidine tag in the N-terminus followed by a 2-glycine linker (Table 1). Both proteins were expressed in *Escherichia coli* and purified to homogeneity (Figure 1A, left panel), and the presence of the N-terminal

Biochemical Journal (2017) **474** 1259–1272
DOI: 10.1042/BCJ20170015

PORTLAND PRESS

Table 1 Sequences of the N-terminal helix (Arf) and C-terminal extensions (Rho and Rab) of the His-tagged GTPase constructs used in the present study

The residue carrying the lipid post-translational modification is indicated in bold. The sequences of the tags are underlined.

GTPase	Natural lipid	Sequence
His-Arf1	Myristate	GHHHHHHGG **G**NIFANLFKGLFGKK EMRI …
His-Arf3	Myristate	GHHHHHHGG **G**NIFGNLLKSLIGKK EMRI …
His-Arf4	Myristate	GHHHHHHGG **G**LTISSLFSRLFGKK QMRI …
His-Arf5	Myristate	GHHHHHHGG **G**LTVSALFSRIFGKK QMRI …
His-Arf6	Myristate	GHHHHHHGG **G**KVLSKIFGNK EMRI …
RhoG-His	Geranylgeranyl	… AVRAVL NPTPIKRGRS**C**ILL HHHHHH
Rac1-His	Geranylgeranyl	… AIRAVL CPPPVKKRKRK**C**LLL HHHHHH
RhoA-His	Geranylgeranyl	… ATRAAL QARRGKKKSG**C**LVL HHHHHH
Cdc42-His	Geranylgeranyl	… AILAAL EPPEPTKKRK**C**KFL HHHHHH
Rab1-His	Geranylgeranyl	… EIKKR MGCPGATAGGAEKSNVKIQSTPVKQSGGG**CC** HHHHHH
Rab35-His	Geranylgeranyl	… AKKDN LAKQQQQQQNDVVKLTKNSKRKKR**CC** HHHHHH

6xHis-tag was confirmed by western blot (Figure 1A, right panel). His-Arf1 and His-Arf6 bound efficiently to liposomes containing a small percentage of Ni-lipids (5%) as shown by a stringent liposome flotation assay (Figure 1B), indicating that the location of the tag on a switch element is compatible with its binding to membranes.

Next, we determined the activation rates of His-Arf1 and His-Arf6 by ARNO, an ArfGEF of the cytohesin subfamily involved in signal transduction which consists of a Sec7 domain carrying the GEF activity and a pleckstrin homology (PH) domain that binds PI(4,5)P_2 (PIP_2) and PI(3,4,5)P_3 phosphoinositides [6,28]. Spontaneous and ARNO-stimulated nucleotide exchange kinetics were monitored by tryptophan fluorescence in solution and in the presence of liposomes containing Ni-lipids and PIP_2 (Figure 1C). We checked by dynamic light scattering (DLS) that no aggregation or physical alteration of liposomes occurred in the course of the reaction (Figure 1D). His-Arf1 and His-Arf6 were resistant to activation in solution, indicating that the replacement of the myristate by a 6xHis-tag preserves autoinhibition. The addition of liposomes resulted in slow spontaneous nucleotide exchange, probably reflecting the fact that membranes unlock the N-terminal helix to facilitate subsequent activation by GTP (reviewed in ref. [5]). Remarkably, nucleotide exchange in the presence of liposomes was strongly increased by catalytic amounts of ARNO (1:50 ratio), and this increase was suppressed by displacing the His-tagged GTPases from membranes by imidazole.

We then compared the efficiency of the activation of myristoylated and His-tagged Arf1 and Arf6 by determining k_{cat}/K_m on liposomes accurately using a range of ARNO concentrations. ARNO activated both His-Arf1 and His-Arf6 with high efficiencies, and these were in the same range as those of the myristoylated proteins (Figure 1E and Table 2). Altogether, these experiments show that the contribution of membranes to the efficiency of activation of myristoylated Arf GTPases by their GEFs is efficiently recapitulated by their attachment to membranes by a 6xHis anchor.

Family-wide analysis of the efficiency and specificity of ArfGEFs using His-tagged Arf GTPases

The Arf GTPase family consists of five members, of which the biochemistry and function of class I Arf3 and class II Arf4 and Arf5 have remained poorly understood. Notably, these isoforms have remained difficult to purify in their myristoylated form, which has limited the investigation of their activation by GEFs. All Arf isoforms share >60% identity with Arf1, the highest divergence being in their N-terminal helix. We designed His-tagged versions of human Arf3, Arf4 and Arf5 (Table 1), which were purified to homogeneity (Figure 1A, left panel) and assessed for the presence of the His-tag (Figure 1A, right panel) and binding to Ni-lipid-containing liposomes (Figure 1B). All three Arf isoforms were resistant to the activation by ARNO in solution, and their spontaneous nucleotide exchange in the presence of liposomes was very slow (Figure 2A).

PORTLAND PRESS

Biochemical Journal (2017) **474** 1259–1272
DOI: 10.1042/BCJ20170015

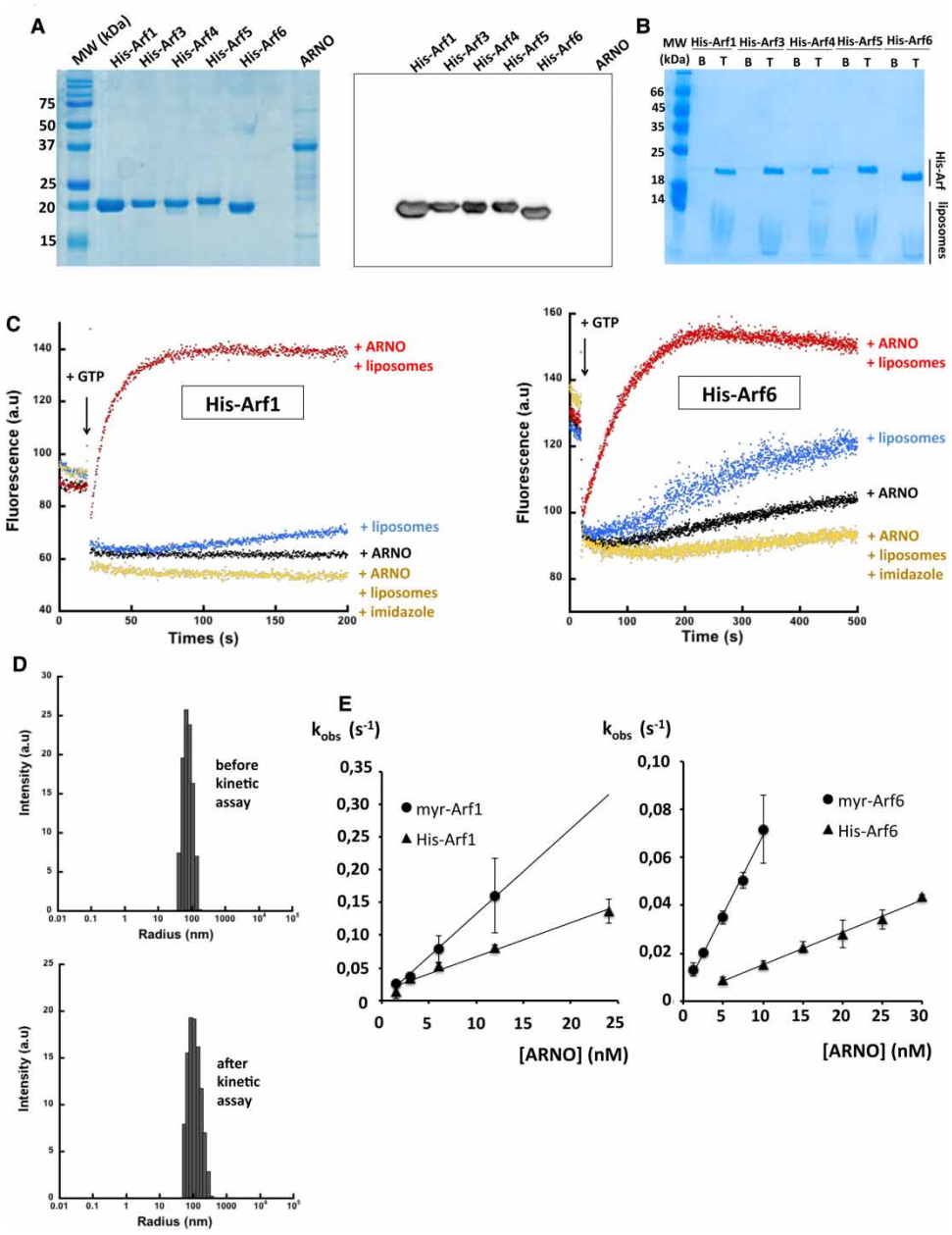

Figure 1. Comparison of His-tagged and myristoylated Arf1 and Arf6.

(**A**) Purity of the Arf GTPases and their GEF and the presence of the histidine tag were checked by SDS–PAGE (left) and anti-His-tag western blot (right). (**B**) Binding of His-Arf GTPases to Ni-liposomes was analyzed by liposome flotation. Proteins bound to liposomes are found in the top fraction (lanes 'T'); unbound proteins are in the bottom fraction (lanes 'B'). (**C**) Activation of liposome-bound His-Arf1 and His-Arf6 (500 nM) by ARNO (10 nM) was measured by tryptophan fluorescence kinetics; a.u., arbitrary unit. (**D**) Representative liposome size distribution measured by DLS, showing the absence of physical alterations. (**E**) Determination of k_{cat}/K_m of ARNO for His-tagged and myristoyled Arf1 and Arf6 in the presence of liposomes. All liposomes contained Ni-lipids, except for myrArf6 which has an uncleavable C-terminal His-tag that may interfere with the reaction.

In contrast, all isoforms were efficiently activated by ARNO in the presence of liposomes, revealing that ARNO does not display significant specificity within the Arf family (Figure 2A,B).

A unique feature of ARNO is that its Sec7 domain is autoinhibited by its PH domain and autoinhibition is released by interaction of the PH domain with Arf-GTP [6,28,29]. In contrast, BRAG2, which is involved in

Biochemical Journal (2017) **474** 1259–1272
DOI: 10.1042/BCJ20170015

PORTLAND PRESS

Table 2 k_{cat}/K_m values determined in the present study

GTPase/GEF	Liposomes	k_{cat}/K_m ($\times 10^5$ M^{-1} s^{-1})
myrArf1/ARNO	+	130.1
His-Arf1/ARNO	+	52.1
myrArf6/ARNO	+	65.6
His-Arf6/ARNO	+	13.5
RhoG-His/Trio	–	1.9
RhoG-His/Trio	+	59.1
Rac1-His/Trio	–	0.9
Rac1-His/Trio	+	8.2
Rab1-His/DrrA	–	8.5
Rab1-His/DrrA	+	3.4

endosomal signaling, is constitutively active and does not feature feedback regulation (reviewed in ref. [30]). To investigate the response of the His-tagged Arf isoforms to GEFs with different regulatory regimes, we measured their activation rates by BRAG2 on membranes (Figure 2C,D). As for ARNO, all Arf isoforms were efficiently activated by BRAG2, revealing that this GEF, originally described as being specific for Arf6 and later shown to activate Arf1, is in fact a potent activator for all members of the Arf family. Altogether, these results indicate that the His-tagged Arf isoforms recapitulated the mechanistic properties of the myristoylated GTPases, and uncover that the GEFs ARNO and BRAG2 activate all Arf isoforms.

His-tagged Rho family GTPases highlight activity enhancement and broader specificity of the GEF Trio on membranes

Small GTPases of the Rho/Rac/Cdc42 family regulate many aspects of actin cytoskeleton dynamics whereby they control cell shape and motility (reviewed in ref. [31]). They are modified by a geranylgeranyl lipid attached to a cysteine in their variable C-terminus, which binds strongly to membranes and renders them insoluble in the absence of a GDI (reviewed in ref. [32]). Unlike Arf GTPases, they do not have autoinhibitory elements and are readily activated in solution. However, because geranylgeranylated proteins are difficult to purify and manipulate, our understanding of the contribution of membranes to the regulation of these GTPases has remained fragmentary. We designed His-tagged versions of human Rac1, RhoA, Cdc42 and RhoG, in which six histidines were added immediately after the C-terminal residue (Table 1). All proteins were purified to homogeneity and assessed for the presence of the His-tag and for their ability to bind to Ni-lipid-containing liposomes (Figure 3A,B). To analyze their activation on membranes, we selected the N-terminal DH-PH tandem (DH1-PH1) of Trio, a RhoGEF with a prominent role in neuronal development, cell adhesion and G-protein-coupled receptor signaling (reviewed in ref. [33]). The DH1-PH1 domain has been reported to bind pure phospholipids detectably only in the presence of RhoG in a dot-blot assay, and this required its unlipidated C-terminus, yet phospholipid headgroups had no effect on its GEF efficiency in solution [34].

These intriguing features call for the analysis of Trio interactions and GEF activity in the presence of membranes and membrane-attached GTPases. First, we used a liposome flotation assay to characterize the recruitment of Trio to membranes. We find that Trio is poorly recruited to membranes on its own, but it is entirely bound to liposomes containing RhoG-His and this effect is lost upon dissociation of RhoG-His from liposomes by imidazole (Figure 3C). Next, we investigated the effect of membranes on the efficiency of Trio. His-tagged GTPases were loaded with mant-GDP and the kinetics of nucleotide exchange were monitored by the decrease in fluorescence following mant-GDP dissociation. In solution, Trio activated both RhoG-His and Rac1-His efficiently (Figure 3D) and was inactive toward RhoA-His and Cdc42-His (Figure 3E), which is consistent with previous studies using unlipidated GTPases [34–36]. Remarkably, membranes increased k_{cat}/K_m by 30-fold for RhoG-His and 8.5-fold for Rac1-His (Figure 3F and Table 2). This enhancing effect was lost when RhoG-His and Rac1-His were dissociated from liposomes by imidazole, indicating that it originates from the membrane association of the GTPase. We note that the effect of imidazole on Rac1-His is incomplete, possibly due to an interaction of its C-terminus with anionic phospholipids. Thus, the reconstitution of His-tagged RhoG and

PORTLAND PRESS

Biochemical Journal (2017) **474** 1259–1272
DOI: 10.1042/BCJ20170015

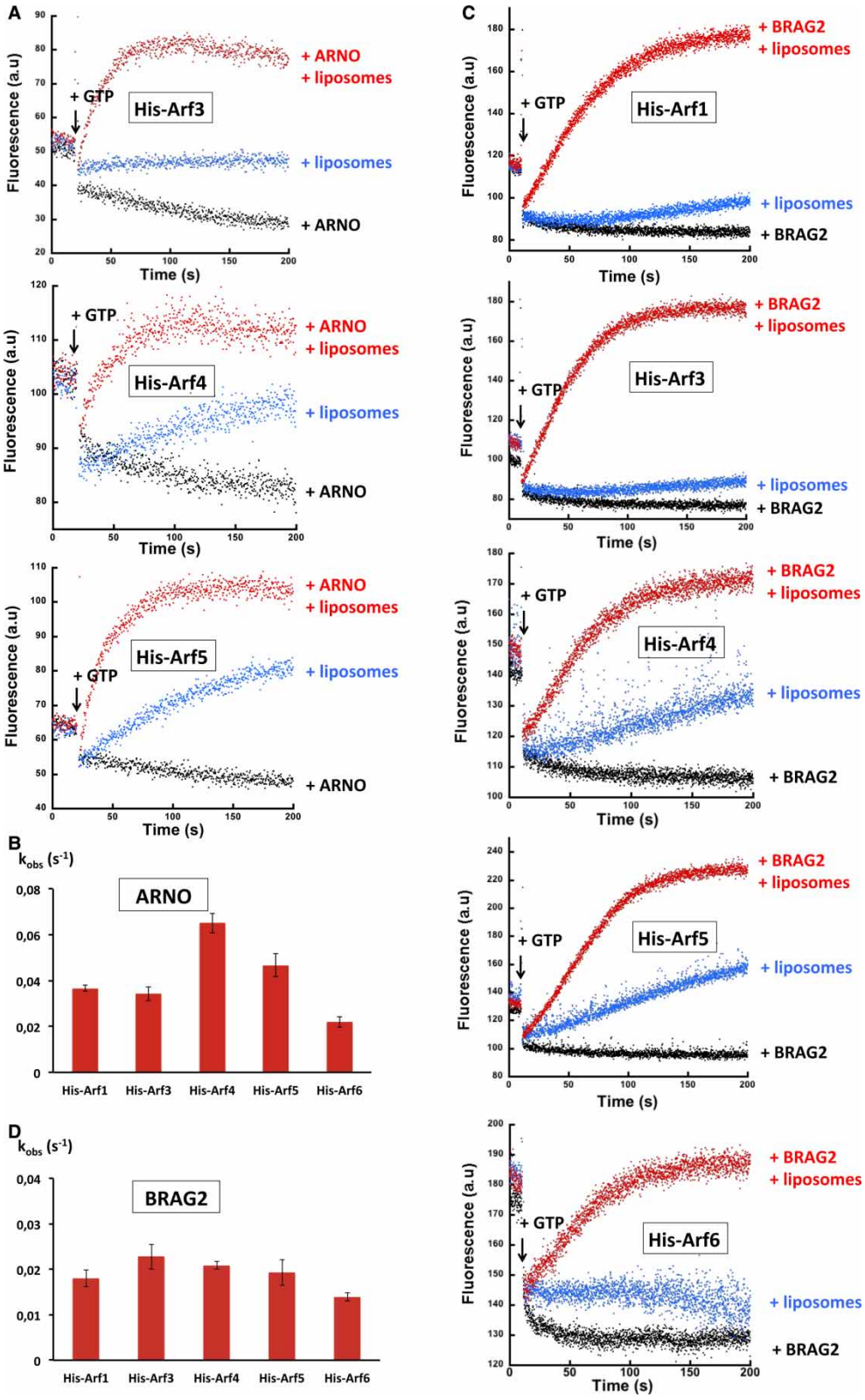

Figure 2. Family-wide analysis of the activation of His-Arf GTPases in the presence of Ni-liposomes. Part 1 of 2

(**A**) Activation of liposome-bound His-Arf GTPases (500 nM) by ARNO (10 nM) measured by tryptophan fluorescence kinetics. (**B**) Activation rates (k_{obs}) of His-Arf GTPases by ARNO on liposomes. (**C**) Activation kinetics of liposome-bound His-Arf

Biochemical Journal (2017) **474** 1259–1272
DOI: 10.1042/BCJ20170015

Figure 2. Family-wide analysis of the activation of His-Arf GTPases in the presence of Ni-liposomes. Part 2 of 2
GTPases (500 nM) by BRAG2 (10 nM) measured as in (**A**). (**D**) Activation rates (k_{obs}) of His-Arf GTPases by BRAG2 on liposomes.

Rac1 in liposomes uncovered a strong contribution of membranes to the efficiency of Trio that was not detected using isolated phospholipids.

Finally, we analyzed the specificity of the DH1-PH1 tandem of Trio by comparing its efficiency on RhoG and Rac1, its known substrates, with that on RhoA, the substrate of the second DH-PH tandem, and on a related GTPase, Cdc42. To our surprise, we observed that Trio potently activated RhoA-His and Cdc42-His on membranes, although with a lower exchange rate than RhoG-His and Rac1-His (Figure 3E). This is in striking contrast with the situation in solution where RhoA and Cdc42 were completely resistant to activation. A measure of the discrepancy between the solution and liposome assays is provided by the comparison of k_{obs} values determined at identical GTPase and GEF concentrations, which shows that Trio activates its poorer substrate, Cdc42, on membranes more efficiently than it does its favored substrate, RhoG, in solution (Figure 3G). Altogether, tethering Rho GTPases to membranes by a histidine tag provided quantitative information on the contribution of membranes to their regulation and uncovered a previously overlooked broader specificity.

Membrane-delimited activation of Rab1 by a bacterial RabGEF

Rab GTPases are master organizers of intracellular membrane traffic and organelle identity (reviewed in ref. [37]). As Rho GTPases, they are recruited to membranes by geranylgeranyl lipids covalently attached to their C-terminal extension, the sequence of which is highly variable among Rab GTPases. Many Rab regulators and effectors carry membrane-binding domains that are highly specific for given phosphoinositides, but the contribution of phosphoinositide-containing membranes to the efficiency of the activation/inactivation cycle has remained poorly studied due to the difficulty in generating and manipulating lipidated Rab GTPases. To investigate our His-tag tethering strategy in the Rab family, we selected human Rab1, a major regulator of membrane traffic at the ER (reviewed in ref. [38]), and *Legionella pneumophila* DrrA, a RabGEF that activates cellular Rab1 on the *Legionella*-containing vacuole during infection [39]. An important characteristic of DrrA is that it binds PI(4)P with exceptional affinity [40,41]; however, the contribution of PI(4)P-containing membranes to its GEF activity is not known. Rab1 fused to a 6-histidine tag in the C-terminus (Table 1) was purified to homogeneity and assessed for the presence of the His-tag and its ability to bind exclusively to liposomes containing Ni-lipids (Figure 4A–C). Likewise, DrrA bound strongly to liposomes containing PI(4)P and Ni-lipids but not to liposomes containing only Ni-lipids (Figure 4C). DrrA strongly activated Rab1-His both in solution and in the presence of liposomes containing both PI(4)P to recruit DrrA and Ni-lipids to tether Rab1-His (Figure 4D), although with different efficiencies (see below).

Next, we assessed whether membranes would broaden the specificity of DrrA as observed for Trio. We chose human Rab35, which regulates endocytic recycling (reviewed in ref. [42]) and bears resemblances to Rab1 that allow it to be the substrate of another *Legionella* effector, AnkX [43]. We fused full-length Rab35 to a C-terminal 6-histidine tag, purified it to homogeneity (Figure 4A) and controlled that it is recruited to Ni-lipid-containing liposomes (Figure 4B) and that it is efficiently activated by its specific GEF DennD in solution (Figure 4E). Remarkably, DrrA did not activate Rab35-His on liposomes (Figure 4E), highlighting a strict specificity that contrasts with the broadened specificity observed for the RacGEF Trio on membranes.

Finally, we quantified the contribution of membranes to the efficiency of DrrA by determining k_{cat}/K_m. To our surprise, the efficiency of DrrA on liposomes was reduced by 2.5 times compared with the efficiency determined in solution (Figure 4D and Table 2). Varying the concentration of liposomes did not modify the exchange rates, but the plateau of the reaction decreased with liposome concentration (Figure 4F), indicating that the fraction of activated Rab1-His decreases as the concentration of liposomes increases. To analyze whether this unexpected effect could result from the very high affinity of DrrA for PI(4)P leading to its slow dissociation, we compared the activation of liposome-bound Rab1-His by soluble DrrA and of soluble Rab1-His by liposome-bound DrrA (Figure 4G). In both cases, exchange rates were intermediate between the solution-only and the liposome-only rates. In contrast, the activation rate was further decreased when Rab1–

PORTLAND PRESS

Biochemical Journal (2017) **474** 1259–1272
DOI: 10.1042/BCJ20170015

liposomes and DrrA–liposomes were prepared separately, and this effect was reversed when Rab1-His was dissociated from liposomes by imidazole (Figure 4G). We conclude from this ensemble of experiments that DrrA is less active in the presence of membranes because it does not significantly dissociate from PI(4)P, such that it activates only Rab1 proteins that are in its immediate vicinity.

Discussion

In this work, we designed His-tagged versions of 11 small GTPases, including autoinhibited small GTPases of the Arf family and classical Rho and Rab GTPases, and we reconstituted their activation on membranes by membrane-binding GEFs. Using Arf1 and Arf6 for the validation of the approach, we found that the His-tagged GTPases recapitulated the activation of their myristoylated counterpart, thus validating the approach for quantitative biochemical assays. Importantly, we did not detect significant interference of the histidine tag with the reaction despite its location on a critical switch element, in contrast with larger tags that have been shown to impair biological functions of Arf GTPases in cells [44]. Next, we showed for a variety of systems that His-tagged GTPases provide valuable information on properties that were undetectable in solution. These systems included two ArfGEFs with opposite regulatory regimes: a RhoGEF that binds weakly to membranes and a RabGEF with exceptional affinity for phosphoinositides. Notably, we identified robust enhancement of ArfGEFs and a RhoGEF by membranes, a specificity broadening of a RacGEF that was not detectable in solution, and membrane-restricted activation of Rab1 by a bacterial RabGEF.

These findings have important biological consequences and open new perspectives for investigations. First, they reveal that all Arf isoforms are excellent substrates on membranes for two major endosomal ArfGEFs, ARNO and Brag2, a remarkable pan-family specificity that probably extends to the other members of these ArfGEF subfamilies. Thus, endosomal ArfGEFs do not select their substrates by a simple specificity rule, which suggests that several isoforms may be activated and mobilized in parallel in cells. This is consistent with previous observations that more than one Arf isoform has to be silenced to yield observable changes in organelle phenotypes [45].

In the case of Rho family GTPases, membrane tethering of RhoG showed that Trio is recruited to membranes in a RhoG-dependent manner, possibly through the engagement of the GTPase with the PH domain as seen in the Rac1–Trio co-crystal structure [36], and that this is accompanied by a large enhancement of its GEF activity. Our findings thus reconcile the conflicting observations that Trio bound isolated phospholipids only in the presence of unlipidated RhoG, yet phospholipid headgroups had no effect on its GEF efficiency [34]. Another unexpected observation is the broader specificity of Trio toward RhoA and Cdc42, which is undetectable in solution. Specificity broadening by membranes was observed before for EFA6, an ArfGEF that is strictly specific for Arf6 in solution (using truncated versions of Arf proteins to get around autoinhibition), but activates both myrAr1 and myrArf6 on membranes [10]. The presence in Trio of a second DH-PH tandem specific for the RhoA pathway makes it conceivable that the DH1-PH1 tandem generates RhoA-GTP on cellular membranes in small amounts due to its lesser efficiency when compared with RhoG and Rac1, possibly as part of a feedback mechanism which remains to be investigated. Finally, the apparent antagonistic effect of membranes on a bacterial RabGEF toward a cellular Rab GTPase highlights that the efficiency of GEFs is balanced by the strength with which they bind to the membrane. The extremely high affinity of DrrA for PI(4)P implies that its dissociation rate is very slow, effectively restricting its activity to Rab GTPases already bound in its immediate vicinity at the membrane surface. These characteristics endow the Legionella pathogen with a precise spatiotemporal control of Rab activation and its subsequent AMPylation on the *Legionella*-containing vacuole during infection.

Our comparison of myristoylated and His-tagged Arf GTPases highlights one limitation to keep in mind when using membrane-tethered GTPases. In the case of His-Arf1 and His-Arf6, we observed a slight increase in spontaneous nucleotide exchange, which we ascribe to the fact that the displacement of the autoinhibitory helix by membranes is facilitated in membrane-tethered Arf GTPases when compared with myristoylated GTPases which are in solution/membrane equilibrium. Accordingly, GEF efficiencies may appear lower than they actually are. Rho, Rab and Ras GTPases do not have autoinhibitory elements that maintain them in the cytosol, but they have to dissociate from their GDIs; the energetic cost of the membrane translocation step cannot be recapitulated in this set-up. Based on the case of the Arf GTPases, we believe that these effects remain small and do not compromise quantitative biochemical analysis.

Biochemical Journal (2017) **474** 1259–1272
DOI: 10.1042/BCJ20170015

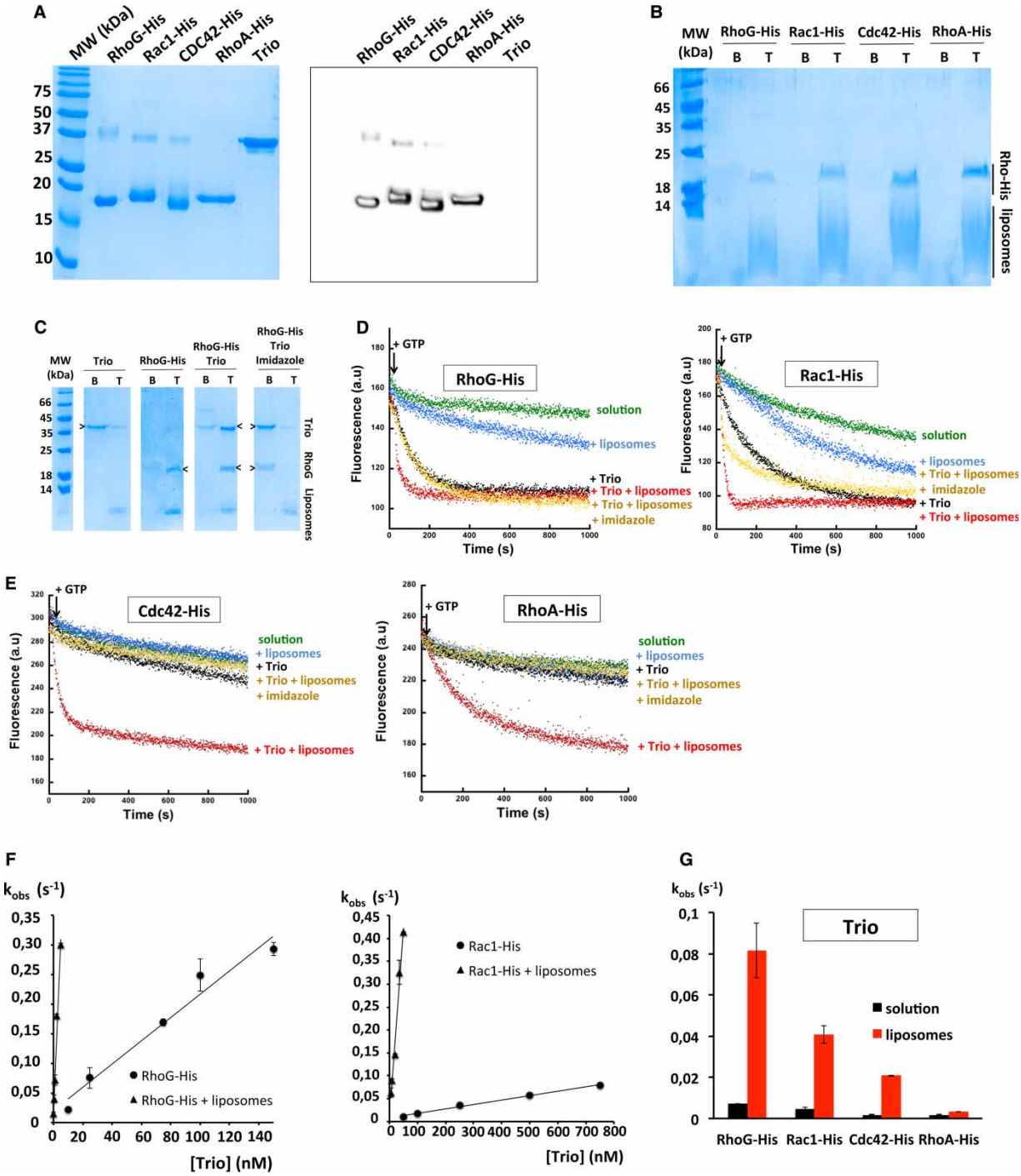

Figure 3. Membranes contribute to the efficiency and specificity of the RhoGEF Trio toward Rho family GTPases.

(**A**) Purity of Rho-His GTPases and of the GEF Trio and the presence of the histidine tag were checked by SDS–PAGE (left) and anti-His-tag western blot (right). (**B**) Binding of the Rho-His GTPases to Ni-liposomes was analyzed by liposome flotation. See Figure 1B for B and T labels. (**C**) Recruitment of Trio by liposome-bound RhoG-His, analyzed by liposome flotation. See Figure 1B for B and T labels. (**D**) Kinetics of activation of liposome-bound RhoG-His and Rac1-His (500 nM) by Trio (10 nM) measured by mant-GDP fluorescence. (**E**) Kinetics of activation of liposome-bound Cdc42-His and RhoA-His by Trio, measured as in (**D**). (**F**) Determination of k_{cat}/K_m of Trio for RhoG-His and Rac1-His in the presence and absence of liposomes. (**G**) Comparison of the activation rates (k_{obs}) of Rho-His GTPases by Trio in the presence and absence of liposomes.

PORTLAND PRESS

Biochemical Journal (2017) **474** 1259–1272
DOI: 10.1042/BCJ20170015

In conclusion, we anticipate that the His-tagged GTPases generated in this work will be of important use to reconstitute and characterize other GEFs, effectors and GAPs in the context of membranes. More generally, we propose fusion of histidine tags adjacent to lipidation sites is an easy implementary means to tether small GTPases to membranes, which allows quantitative biochemical analysis and opens broad applications to investigate how membranes co-operate with small GTPases and their partners to monitor and process cellular signals.

Materials and methods

Protein cloning, expression and purification

The sequences coding for full-length human Arf1, Arf3, Arf4, Arf5 and Arf6 were PCR-amplified with an additional sequence in 5′ encoding an N-terminal 6-histidine tag followed by a linker of two glycines. PCR products were cloned into the pET15b expression vector. The sequence coding for full-length human RhoG, Rab1 and Rab35 was PCR-amplified with an additional sequence in 3′ encoding a 6-histidine tag immediately following their C-terminal residue and cloned into the Gateway destination vector pDEST14. Full-length human Rac1, Cdc42 and RhoA with a 6-histidine tag immediately after their C-terminal residue have been described in ref. [46]. Untagged human ARNO containing the Sec7 and PH domains (residues 50–399) cloned into pET8c expression vector is a kind gift of Bruno Antonny (CNRS, Sophia-Antipolis, France). Human Brag2 (Sec7 and PH domains, residues 390–763) carrying an N-terminal 6-histidine tag followed by a TEV cleavage site has been described in ref. [7]. Human Trio containing the DH1 and PH1 domains (residues 1232–1550) is a kind gift from Anne Blangy (CNRS, Montpellier, France). The sequence was amplified by PCR and cloned into the Gateway destination vector pETG-20A to introduce a TEV protease cleavage site. *L. pneumophila* DrrA [GEF and PI(4)P-binding domains, residues 340–647] carrying a 6-His tag cleavable by the TEV protease is a kind gift from Lena Osterlein and Aymelt Itzen (MPI Dortmund, Germany) and has been described in ref. [40]. Human DennD1B (a construct lacking the 150–169 loop) is a kind gift from Karin Reinisch (Yale School of Medicine, Yale University, U.S.A.) and has been described in ref. [47]. All plasmids were confirmed by sequencing (GATC Biotech).

All GTPase constructs were expressed in *E. coli* Rosetta (DE3) pLysS in LB medium. Overexpression was induced overnight with 0.5 mM IPTG at 20°C. Bacterial pellets were lysed by lysosyme complemented with benzonase and an antiprotease inhibitor cocktail and disrupted at 1250 psi using a pressure cell homogenizer. The cleared lysate supernatant was loaded onto a Ni-NTA affinity chromatography column (HisTrap FF, GE Healthcare) and eluted with 250 mM imidazole. Purification was perfected by gel filtration on a Superdex 75 16/600 column (GE Healthcare) equilibrated with storage buffer [50 mM Tris, 300 mM NaCl, and 2 mM $MgCl_2$ (pH 8), supplemented with 2 mM β-mercaptoethanol and 5% glycerol for Arf and Rho GTPases]. Myristoylated Arf1 was obtained by co-expression of full-length human Arf1 and yeast *N*-myristoyltransferase as described in ref. [7]. Myristoylated Arf6 was obtained by *in vitro* myristoylation of full-length Arf6 carrying a C-terminal His-tag by recombinant myristoyltransferase as described in ref. [14].

ARNO was expressed in *E. coli* BL21 (DE3) Gold in LB medium. Overexpression was induced for 3 h by 0.5 mM IPTG at 37°C. Bacterial pellets were lysed as above and disrupted by sonication. The cleared lysate supernatant was loaded onto a Q-Sepharose anion exchange chromatography column and eluted with a 0–1 M NaCl gradient. Purification was perfected by gel filtration on a Superdex 200 16/600 equilibrated with storage buffer [50 mM Tris, 150 mM NaCl, 1 mM $MgCl_2$, and 1 mM DTT (pH 8)]. Brag2 was expressed and purified as described in ref. [7]. Trio was expressed and purified as described above for the small GTPases. The 6-His tag was cleaved by incubation with the TEV protease (1/4 w/w ratio) overnight at 4°C at low stirring. The cleaved tag was eliminated by passage over a Ni-NTA affinity chromatography column (Histrap FF, GE Healthcare) equilibrated with storage buffer [50 mM Tris, 500 mM NaCl, 10% glycerol, 2 mM β-mercaptoethanol and 2 mM $MgCl_2$ (pH 8)], and the protein was retrieved in the flowthrough. DrrA was expressed as in ref. [40], except that we used the *E. coli* BL21 (DE3) pG-KJE8 strain that expresses chaperones, in LB medium with 0.5 g/l L-arabinose and 2.5 mg/l tetracycline. The 6-His tag was cleaved by the TEV protease (1/10 w/w ratio) during overnight dialysis in storage buffer [20 mM HEPES, 100 mM NaCl and 2 mM β-mercaptoethanol (pH 7.4)] at 4°C. The cleaved tag was eliminated by a second Ni-NTA affinity chromatography step and the purity of cleaved protein was perfected on a Superdex 75 16/600 equilibrated with storage buffer. DennD was expressed and purified as described in ref. [47]. The presence of the His-tag on the small GTPases and the absence of the His-tag on their associated GEFs were checked by western blot with monoclonal antipolyhistidine peroxidase-conjugated antibody (Sigma; 1:5000).

Biochemical Journal (2017) **474** 1259–1272
DOI: 10.1042/BCJ20170015

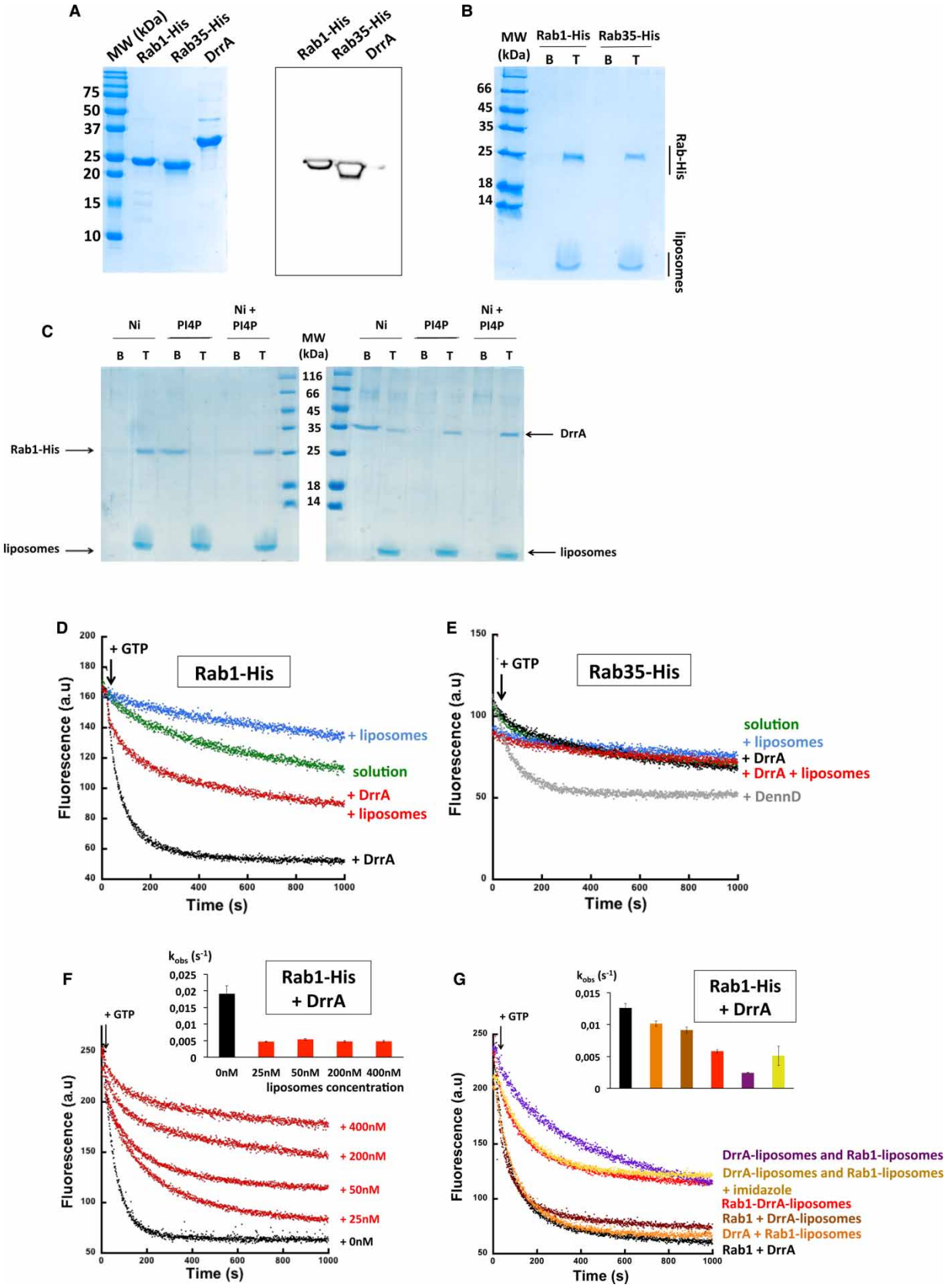

Figure 4. Membrane-delimited activation of human Rab1 by bacterial DrrA.

Part 1 of 2

(**A**) Purity of Rab-His GTPases and DrrA and the presence of the histidine tag were checked by SDS–PAGE (left) and anti-His-tag western blot

PORTLAND PRESS

Biochemical Journal (2017) **474** 1259–1272
DOI: 10.1042/BCJ20170015

Figure 4. Membrane-delimited activation of human Rab1 by bacterial DrrA. Part 2 of 2

(right). (**B**) Binding of the Rab-His GTPases to Ni-liposomes was analyzed by liposome flotation. Liposomes contained 91% PC, 4% PI4P, 5% DGS-NTA-Ni and 0.2% NBD-PE. See Figure 1B for B and T labels. (**C**) Selective binding of DrrA to PI(4)P-containing liposomes and of Rab1-His to Ni-lipid-containing liposomes. Liposome compositions were as follows: Ni-liposomes: 95% PC, 5% DGS-Ni-NTA, 0.2% NBD-PE; PI(4)P-liposomes: 96% PC, 4% PI(4)P, 0.2% NBD-PE; Ni + PI(4)P-liposomes: 91% PC, 4% PI(4)P, 5% DGS-NTA-Ni, 0.2% NBD-PE. See Figure 1B for B and T labels. (**D**) Kinetics of activation of liposome-bound Rab1-His (500 nM) by DrrA (25 nM), measured by mant-GDP fluorescence using Ni + PI(4)P liposomes. (**E**) Kinetics of activation of liposome-bound Rab35-His by DrrA, measured as in (**D**). (**F**) Kinetics of activation of liposome-bound Rab1-His by DrrA measured at increasing Ni + PI(4)P liposome concentrations. (**G**) Analysis of membrane-delimited activation of Rab1-His by DrrA. The set-up of the kinetics assays was varied as follows: Drra + Rab1: no liposomes; DrrA + Rab1–liposomes: liposomes containing only Ni-lipids; Rab1 + Drra–liposomes: liposomes containing only PI(4)P; Rab1–DrrA–liposomes: liposomes containing Ni-lipids and PI(4)P; DrrA–liposomes and Rab1–liposomes: Rab1 and DrrA were reconstituted separately on Ni+PI(4)P-liposomes, and the two pools of proteo-liposomes were mixed just before starting the exchange reaction; DrrA–liposomes and Rab1–liposomes + imidazole: as previous one in the presence of imidazole to dissociate Rab1-His from the liposomes.

Liposome synthesis and binding assays

Liposomes were prepared as described in refs [7,29], in a buffer containing 50 mM HEPES and 120 mM potassium acetate (pH 7.4). Except when indicated otherwise, experiments were carried out with liposomes containing 43% PC, 20% PE, 10% PS, 20% cholesterol, 2% $PI(4,5)P_2$ completed with 5% DGS-NTA-Ni lipids for the attachment of His-tagged GTPases and 0.2% fluorescent NDB-PE lipids to facilitate detection. Liposomes were extruded through a 0.2 μm pore size filter before use, and size distributions were checked by DLS on a DynaPro instrument (Wyatt).

For the liposome flotation assays, 2 μM proteins and 1 mM liposomes (lipids) were incubated in HKM buffer [50 mM HEPES, 120 mM potassium acetate and 1 mM $MgCl_2$ (pH 7.4)] at room temperature for 20 min in a total volume of 150 μl. The suspension was adjusted to 30% sucrose, overlaid with 200 μl of HKM containing 25% w/v sucrose and 50 μl of HKM containing no sucrose. The sample was centrifuged at 55 000 r.p.m. (240 000×***g***) in a Beckman swinging rotor for 1 h. The bottom (250 μl), middle (150 μl) and top (100 μl) fractions were manually collected from the bottom. The bottom and top fractions were analyzed by SDS–PAGE using Coomassie staining. The flotation of liposomes on the sucrose gradient after centrifugation and their separation in the collected fractions was checked by following the NBD-PE fluorescence using a ChemiDoc Imaging System (Biorad). All experiments were done in duplicate.

Nucleotide exchange assays

Nucleotide exchange kinetics were monitored by fluorescence on a Cary Eclipse fluorimeter (Varian) under stirring. In all experiments, proteins and liposomes were preincubated for 1 min under stirring before the exchange reaction was initiated by the addition of 100 μM GTP. When indicated, His-tagged GTPases were dissociated from Ni-lipid-containing liposomes by 250 mM imidazole. k_{obs} values were determined from a mono-exponential fit. Values of k_{cat}/K_m were determined by linear regression from k_{obs} values measured over a range of GEF concentrations following the Michaelis–Menten formalism as described previously [48]. For Arf GTPases, we monitored the increase in tryptophan fluorescence associated with the conformational changes induced by GTP binding, using excitation and emission wavelengths of 290 and 340 nm, as described in refs [7,26]. The reaction was performed at 37°C in HKM buffer containing 500 nM Arf GTPases and 10 nM GEF with or without 100 μM liposomes (lipids). For Rho and Rab GTPases, nucleotide exchange kinetics were monitored by the decay of mant-GDP fluorescence following its replacement by GTP, using excitation and emission wavelengths of 360 and 440 nm, respectively. Small GTPases were loaded with mant-GDP prior to nucleotide exchange by incubation of 250 μM GTPase with 1.5 mM mant-GDP and 10 mM EDTA for 30 min at room temperature. Nucleotide exchange was stopped by the addition of 75 mM $MgCl_2$. Removal of excess nucleotides and buffer exchange was done on a PD SpinTrap G-25 (GE HealthCare Life Science). Nucleotide exchange was carried out at 30°C (Rho GTPases) or 37°C (Rab GTPases) in HKM buffer using 500 nM Rho or Rab GTPases loaded with mant-GDP and either 10 nM Trio, 15 nM DrrA or 15 nM DennD, with or without 100 μM liposomes. All experiments were done in triplicate.

Biochemical Journal (2017) **474** 1259–1272
DOI: 10.1042/BCJ20170015

PORTLAND PRESS

Abbreviations

BRAG2, Brefeldin-resistant ArfGEF 2; DH, Dbl-homology; DLS, dynamic light scattering; EDTA, ethylenediaminetetraacetic acid; EFA6, Exchange factor for Arf6; ER, endoplasmic reticulum; GAPs, GTPase-activating proteins; GDI, guanosine nucleotide dissociation inhibitor; GEFs, guanine nucleotide exchange factors; His-tag, histidine tag; IPTG, isopropyl β-D-1-thiogalactopyranoside; mant-GDP, *N*-methylanthraniloyl-GDP; NBD-PE, N-(7-nitrobenz-2-Oxa-1,3-Diazol-4-yl)-1,2-dihexadecanoyl-sn-glycero-3-phosphoethanolamine; Ni-lipids, DGS-NTA-Ni, 1,2-dioleoyl-sn-glycero-3-[(N-(5-amino-1-carboxypentyl)iminodiacetic acid)succinyl] -nickel salt; PC, phosphatidylcholine; PE, phosphatidylethanolamine; PH, pleckstrin homology; PI(4)P, phosphatidylinositol 4-phosphate; PI(4,5)P2, PIP2, phosphatidylinositol 4,5 bisphosphate; PS, phosphatidylserine; TEV, tobacco etch virus.

Author Contribution

F.P. designed and performed experiments, analyzed data and drafted the manuscript. S.V. designed and performed experiments and analyzed data. Y.F. designed and performed experiments and analyzed data. I.L. performed experiments. S.B. performed experiments. M.Z. discussed data. G.P. analyzed data and supervised experiments. J.C. conceived and supervised the study and wrote the manuscript with input from the other authors.

Funding

This work was supported by grants to J.C. from Institut National du Cancer [INCA_7886], Fondation pour la Recherche Médicale [DEQ20150331694] and Agence Nationale de la Recherche [ANR-11-BSV1-0006 and ANR-14-CE09-0028] to F.P. from Ecole Normale Supérieure Paris-Saclay and to S.V. by Région Ile-de-France/ DIM MALINF.

Acknowledgements

We thank Lionel Duarte, Anne-Gaëlle Planson, Théo Desbordes, David Rémy and Raphaëlle Servant (CNRS and ENS Paris-Saclay) for preliminary experiments.

Competing Interests

The Authors declare that there are no competing interests associated with the manuscript.

References

1 Cherfils, J. and Zeghouf, M. (2011) Chronicles of the GTPase switch. *Nat. Chem. Biol.* **7**, 493–495 doi:10.1038/nchembio.608
2 Wang, M. and Casey, P.J. (2016) Protein prenylation: unique fats make their mark on biology. *Nat. Rev. Mol. Cell Biol.* **17**, 110–122 doi:10.1038/nrm.2015.11
3 Cherfils, J. and Zeghouf, M. (2013) Regulation of small GTPases by GEFs, GAPs, and GDIs. *Physiol. Rev.* **93**, 269–309 doi:10.1152/physrev.00003.2012
4 Liu, Y., Kahn, R.A. and Prestegard, J.H. (2009) Structure and membrane interaction of myristoylated ARF1. *Structure* **17**, 79–87 doi:10.1016/j.str.2008.10.020
5 Pasqualato, S., Renault, L. and Cherfils, J. (2002) Arf, Arl, Arp and Sar proteins: a family of GTP-binding proteins with a structural device for 'front-back' communication. *EMBO Rep.* **3**, 1035–1041 doi:10.1093/embo-reports/kvf221
6 Chardin, P., Paris, S., Antonny, B., Robineau, S., Béraud-Dufour, S., Jackson, C.L. et al. (1996) A human exchange factor for ARF contains Sec7- and pleckstrin-homology domains. *Nature* **384**, 481–484 doi:10.1038/384481a0
7 Aizel, K., Biou, V., Navaza, J., Duarte, L.V., Campanacci, V., Cherfils, J. et al. (2013) Integrated conformational and lipid-sensing regulation of endosomal ArfGEF BRAG2. *PLoS Biol.* **11**, e1001652 doi:10.1371/journal.pbio.1001652
8 Jian, X., Gruschus, J.M., Sztul, E. and Randazzo, P.A. (2012) The pleckstrin homology (PH) domain of the Arf exchange factor Brag2 is an allosteric binding site. *J. Biol. Chem.* **287**, 24273–24283 doi:10.1074/jbc.M112.368084
9 Folly-Klan, M., Alix, E., Stalder, D., Ray, P., Duarte, L.V., Delprato, A. et al. (2013) A novel membrane sensor controls the localization and ArfGEF activity of bacterial RalF. *PLoS Pathog.* **9**, e1003747 doi:10.1371/journal.ppat.1003747
10 Padovani, D., Folly-Klan, M., Labarde, A., Boulakirba, S., Campanacci, V., Franco, M. et al. (2014) EFA6 controls Arf1 and Arf6 activation through a negative feedback loop. *Proc. Natl Acad. Sci. U.S.A.* **111**, 12378–12383 doi:10.1073/pnas.1409832111
11 Franco, M., Chardin, P., Chabre, M. and Paris, S. (1996) Myristoylation-facilitated binding of the G protein ARF1GDP to membrane phospholipids is required for its activation by a soluble nucleotide exchange factor. *J. Biol. Chem.* **271**, 1573–1578 doi:10.1074/jbc.271.3.1573
12 Ha, V.L., Thomas, G.M.H., Stauffer, S. and Randazzo, P.A. (2005) Preparation of myristoylated Arf1 and Arf6. *Methods Enzymol.* **404**, 164–174 doi:10.1016/S0076-6879(05)04016-4
13 Glück, J.M., Hoffmann, S., Koenig, B.W. and Willbold, D. (2010) Single vector system for efficient N-myristoylation of recombinant proteins in *E. coli*. *PLoS ONE* **5**, e10081 doi:10.1371/journal.pone.0010081
14 Padovani, D., Zeghouf, M., Traverso, J.A., Giglione, C. and Cherfils, J. (2013) High yield production of myristoylated Arf6 small GTPase by recombinant N-myristoyl transferase. *Small GTPases* **4**, 3–8 doi:10.4161/sgtp.22895

PORTLAND PRESS

Biochemical Journal (2017) **474** 1259–1272
DOI: 10.1042/BCJ20170015

15 Grizot, S., Fauré, J., Fieschi, F., Vignais, P.V., Dagher, M.-C. and Pebay-Peyroula, E. (2001) Crystal structure of the Rac1–RhoGDI complex involved in NADPH oxidase activation. *Biochemistry* **40**, 10007–10013 doi:10.1021/bi010288k
16 Scheffzek, K., Stephan, I., Jensen, O.N., Illenberger, D. and Gierschik, P. (2000) The Rac-RhoGDI complex and the structural basis for the regulation of Rho proteins by RhoGDI. *Nat. Struct. Biol.* **7**, 122–126 doi:10.1038/72392
17 Hoffman, G.R., Nassar, N. and Cerione, R.A. (2000) Structure of the Rho family GTP-binding protein Cdc42 in complex with the multifunctional regulator RhoGDI. *Cell* **100**, 345–356 doi:10.1016/S0092-8674(00)80670-4
18 Robbe, K., Otto-Bruc, A., Chardin, P. and Antonny, B. (2003) Dissociation of GDP dissociation inhibitor and membrane translocation are required for efficient activation of Rac by the Dbl homology-pleckstrin homology region of Tiam. *J. Biol. Chem.* **278**, 4756–4762 doi:10.1074/jbc.M210412200
19 Rak, A., Pylypenko, O., Niculae, A., Goody, R.S. and Alexandrov, K. (2003) Crystallization and preliminary X-ray diffraction analysis of monoprenylated Rab7 GTPase in complex with Rab escort protein 1. *J. Struct. Biol.* **141**, 93–95 doi:10.1016/S1047-8477(02)00634-2
20 Bader, B., Kuhn, K., Owen, D.J., Waldmann, H., Wittinghofer, A. and Kuhlmann, J. (2000) Bioorganic synthesis of lipid-modified proteins for the study of signal transduction. *Nature* **403**, 223–226 doi:10.1038/35003249
21 Mejuch, T. and Waldmann, H. (2016) Synthesis of lipidated proteins. *Bioconjug. Chem.* **27**, 1771–1783 doi:10.1021/acs.bioconjchem.6b00261
22 Gureasko, J., Galush, W.J., Boykevisch, S., Sondermann, H., Bar-Sagi, D., Groves, J.T. et al. (2008) Membrane-dependent signal integration by the Ras activator Son of sevenless. *Nat. Struct. Mol. Biol.* **15**, 452–461 doi:10.1038/nsmb.1418
23 Medina, F., Carter, A.M., Dada, O., Gutowski, S., Hadas, J., Chen, Z. et al. (2013) Activated RhoA is a positive feedback regulator of the Lbc family of Rho guanine nucleotide exchange factor proteins. *J. Biol. Chem.* **288**, 11325–11333 doi:10.1074/jbc.M113.450056
24 Cabrera, M., Nordmann, M., Perz, A., Schmedt, D., Gerondopoulos, A., Barr, F. et al. (2014) The Mon1-Ccz1 GEF activates the Rab7 GTPase Ypt7 via a longin-fold-Rab interface and association with PI3P-positive membranes. *J. Cell. Sci.* **127**(Pt 5), 1043–1051 doi:10.1242/jcs.140921
25 Thomas, L.L. and Fromme, J.C. (2016) GTPase cross talk regulates TRAPPII activation of Rab11 homologues during vesicle biogenesis. *J. Cell Biol.* **215**, 499–513 doi:10.1083/jcb.201608123
26 Nawrotek, A., Zeghouf, M. and Cherfils, J. (2016) Allosteric regulation of Arf GTPases and their GEFs at the membrane interface. *Small GTPases* **7**, 283–296 doi:10.1080/21541248.2016.1215778
27 Jackson, C.L. and Bouvet, S. (2014) Arfs at a glance. *J. Cell Sci.* **127**(Pt 19), 4103–4109 doi:10.1242/jcs.144899
28 DiNitto, J.P., Delprato, A., Gabe Lee, M.-T., Cronin, T.C., Huang, S., Guilherme, A. et al. (2007) Structural basis and mechanism of autoregulation in 3-phosphoinositide-dependent Grp1 family Arf GTPase exchange factors. *Mol. Cell* **28**, 569–583 doi:10.1016/j.molcel.2007.09.017
29 Stalder, D., Barelli, H., Gautier, R., Macia, E., Jackson, C.L. and Antonny, B. (2011) Kinetic studies of the Arf activator Arno on model membranes in the presence of Arf effectors suggest control by a positive feedback loop. *J. Biol. Chem.* **286**, 3873–3883 doi:10.1074/jbc.M110.145532
30 Casanova, J.E. (2007) Regulation of Arf activation: the Sec7 family of guanine nucleotide exchange factors. *Traffic* **8**, 1476–1485 doi:10.1111/j.1600-0854.2007.00634.x
31 Heasman, S.J. and Ridley, A.J. (2008) Mammalian Rho GTPases: new insights into their functions from in vivo studies. *Nat. Rev. Mol. Cell Biol.* **9**, 690–701 doi:10.1038/nrm2476
32 Dransart, E., Olofsson, B. and Cherfils, J. (2005) RhoGDIs revisited: novel roles in Rho regulation. *Traffic* **6**, 957–966 doi:10.1111/j.1600-0854.2005.00335.x
33 Schmidt, S. and Debant, A. (2014) Function and regulation of the Rho guanine nucleotide exchange factor Trio. *Small GTPases* **5**, e983880 doi:10.4161/sgtp.29769
34 Skowronek, K.R., Guo, F., Zheng, Y. and Nassar, N. (2004) The C-terminal basic tail of RhoG assists the guanine nucleotide exchange factor trio in binding to phospholipids. *J. Biol. Chem.* **279**, 37895–37907 doi:10.1074/jbc.M312677200
35 Blangy, A., Vignal, E., Schmidt, S., Debant, A., Gauthier-Rouviere, C. and Fort, P. (2000) TrioGEF1 controls Rac- and Cdc42-dependent cell structures through the direct activation of rhoG. *J. Cell Sci.* **113**(Pt 4), 729–739 PMID:10652265
36 Chhatriwala, M.K., Betts, L., Worthylake, D.K. and Sondek, J. (2007) The DH and PH domains of Trio coordinately engage Rho GTPases for their efficient activation. *J. Mol. Biol.* **368**, 1307–1320 doi:10.1016/j.jmb.2007.02.060
37 Zhen, Y. and Stenmark, H. (2015) Cellular functions of Rab GTPases at a glance. *J. Cell Sci.* **128**, 3171–3176 doi:10.1242/jcs.166074
38 Yang, X.-Z., Li, X.-X., Zhang, Y.-J., Rodriguez-Rodriguez, L., Xiang, M.-Q., Wang, H.-Y. et al. (2016) Rab1 in cell signaling, cancer and other diseases. *Oncogene* **35**, 5699–5704 doi:10.1038/onc.2016.81
39 Murata, T., Delprato, A., Ingmundson, A., Toomre, D.K., Lambright, D.G. and Roy, C.R. (2006) The *Legionella pneumophila* effector protein DrrA is a Rab1 guanine nucleotide-exchange factor. *Nat. Cell Biol.* **8**, 971–977 doi:10.1038/ncb1463
40 Schoebel, S., Blankenfeldt, W., Goody, R.S. and Itzen, A. (2010) High-affinity binding of phosphatidylinositol 4-phosphate by *Legionella pneumophila* DrrA. *EMBO Rep.* **11**, 598–604 doi:10.1038/embor.2010.97
41 Del Campo, C.M., Mishra, A.K., Wang, Y.-H., Roy, C.R., Janmey, P.A. and Lambright, D.G. (2014) Structural basis for PI(4)P-specific membrane recruitment of the *Legionella pneumophila* effector DrrA/SidM. *Structure* **22**, 397–408 doi:10.1016/j.str.2013.12.018
42 Klinkert, K. and Echard, A. (2016) Rab35 GTPase: a central regulator of phosphoinositides and F-actin in endocytic recycling and beyond. *Traffic* **17**, 1063–1077 doi:10.1111/tra.12422
43 Mukherjee, S., Liu, X., Arasaki, K., McDonough, J., Galán, J.E. and Roy, C.R. (2011) Modulation of Rab GTPase function by a protein phosphocholine transferase. *Nature* **477**, 103–106 doi:10.1038/nature10335
44 Jian, X., Cavenagh, M., Gruschus, J.M., Randazzo, P.A. and Kahn, R.A. (2010) Modifications to the C-terminus of Arf1 alter cell functions and protein interactions. *Traffic* **11**, 732–742 doi:10.1111/j.1600-0854.2010.01054.x
45 Volpicelli-Daley, L.A., Li, Y., Zhang, C.J. and Kahn, R.A. (2005) Isoform-selective effects of the depletion of ADP-ribosylation factors 1-5 on membrane traffic. *Mol. Biol. Cell* **16**, 4495–4508 doi:10.1091/mbc.E04-12-1042
46 Vives, V., Cres, G., Richard, C., Busson, M., Ferrandez, Y., Planson, A.-G. et al. (2015) Pharmacological inhibition of Dock5 prevents osteolysis by affecting osteoclast podosome organization while preserving bone formation. *Nat. Commun.* **6**, 6218 doi:10.1038/ncomms7218
47 Wu, X., Bradley, M.J., Cai, Y., Kummel, D., De La Cruz, E.M., Barr, F.A. et al. (2011) Insights regarding guanine nucleotide exchange from the structure of a DENN-domain protein complexed with its Rab GTPase substrate. *Proc. Natl Acad. Sci. U.S.A.* **108**, 18672–18677 doi:10.1073/pnas.1110415108
48 Beraud-Dufour, S., Robineau, S., Chardin, P., Paris, S., Chabre, M., Cherfils, J. et al. (1998) A glutamic finger in the guanine nucleotide exchange factor ARNO displaces Mg^{2+} and the beta-phosphate to destabilize GDP on ARF1. *EMBO J.* **17**, 3651–3659 doi:10.1093/emboj/17.13.3651

Conclusions et perspectives

Durant ma thèse, j'ai pu étudier deux nouveaux systèmes de régulation des protéines FIC : par un changement d'ion et par les membranes.

J'ai pu montrer que la nouvelle petite protéine FIC à glutamate régulateur EfFIC est bien capable d'effectuer la réaction d'auto-modification en utilisant de l'ATP et du magnésium, comme la grande majorité des protéines appartenant à cette famille. Par une étude structurale dont les hypothèses ont été confirmées par tests d'activité *in vitro*, nous avons démontré que le remplacement du magnésium par du calcium comme ion majoritaire induisait un changement de la réaction catalysée de transfert d'AMP à dé-AMPylation, révélant la bifonctionnalité de cette protéine et son mécanisme contrôlé par un changement d'ion. Nous avons reproduit ces résultats avec HYPE, orthologue humain, et nous avons pu montrer que la bifonctionnalité de HYPE était également contrôlée par ce changement d'ion. Enfin, nous avons montré que la mutation du glutamate régulateur rend EfFIC constitutivement active pour la réaction de modification et donc que ce résidu est nécessaire à l'activité de dé-AMPylation. Ces derniers résultats justifient l'appellation « glutamate régulateur » à la place de « glutamate inhibiteur » couramment utilisée dans la littérature.

L'étude de l'activité EfFIC et de HYPE pourra être poursuivie en améliorant la méthode basée sur une protéine fluorescente liant le phosphate inorganique, ou en utilisant un dérivé d'ATP modifié sur la base azotée et permettant d'exploiter la variation d'anisotropie de fluorescence qui résulte de la fixation covalente de l'AMP à la protéine cible. Ainsi, une analyse de la cinétique de la modification et de la dé-modification pourra être réalisée.

Les études des FICs à glutamate réalisées jusqu'à présent utilisaient systématiquement la mutation de ce résidu afin d'améliorer l'efficacité de l'enzyme ; nos résultats montrent que cette mutation a également pour conséquences d'abolir toute possibilité de dé-modification, donnée qui n'était jusqu'à présent jamais prise en compte. Nos résultats pourraient donc être étendus à de nombreuse FIC de cette sous-famille et une expérience de modification avec la protéine mutante et de dé-modification avec la protéine sauvage comme réalisée dans Preissler *et al.* 2017.

Nos premiers résultats concernant l'oligomérisation d'EfFIC montrent une tetramérisation dans les conditions d'expérience utilisées. Cependant, une étude de l'oligomérisation par SEC-MALS, SAXS ou UCA pourrait révéler d'autres états de multimérisation en solution, ce

qui permettrait de comprendre les différents états observés par cristallisation. Nous pourrions alors comparer nos résultats avec ceux de l'étude d'oligomérisation de NmFIC publié par l'équipe de C. Dehio en 2015.

EfFIC et HYPE présentant tous deux une bifonctionnalité, une cible potentielle d'EfFIC pourrait être DnaK de *E. faecalis,* homologue à BIP, cible de HYPE, toutes deux membres de la famille des protéines chaperon HSP70. Le test de la modification de DnaK par EfFIC pourrait être mené à partir des protéines recombinante purifiées, en recherchant l'AMPylation de DnaK *in vitro* par $EfFIC^{WT}$ ou $EfFIC^{E190A}$. La confirmation de DnaK comme cible d'EfFIC permettrait d'émettre des hypothèses sur son activité *in vivo*. S'il s'avère que DnaK n'est pas la cible de cette FIC, une identification de sa cible par pull down comme décrit en partie I pourrait être réalisée.

Enfin, toutes les protéines FIC analysées jusqu'ici montrant une activité d'auto-modification ; une étude pourrait en être réalisée afin de comprendre si cette modification a un sens biologique. Pour cela, la mutation du résidu modifié d'une FIC bien caractérisée permettra d'observer les différences avec la protéine sauvage *in vitro* et *in cellulo* et ainsi de soulever des hypothèses sur l'importance de cette activité. Cette étude pourra également déterminer si cette modification est intra-moléculaire (auto-modification en cis) ou intermoléculaire (auto-modification en trans).

L'étude de la régulation d'AnkX par les membranes a permis de mettre en évidence son interaction avec les membranes et l'augmentation de son activité qui en résulte. Nous avons également montré que l'activité d'AnkX est plus forte sur la petite protéine G Rab35 que sur Rab1, contrairement à ce qui a été montré précédemment par le laboratoire de Goody (Goody 2016 Anal. Biochem.). Ces résultats différents peuvent s'expliquer car nous avons travaillé avec la forme Rab1a au lieu de Rab1b et que les différences entre ces deux protéines pourraient être significatives malgré 91.70% d'identité. Bien que les deux formes de Rab1 présentent le même pourcentage d'identité avec Rab35 (53,97% pour Rab1b et 53.17% pour Rab1a), les résidus non identiques entre Rab1a et Rab1b pourraient expliquer ces propriétés différentes. En effet, l'analyse d'alignements de séquences montre les peptides où Rab1a et Rab1b diffèrent (**Figure Conclusion A)**, le même peptide de Rab35 semble plus proche que celui de Rab1b (**Figure Conclusion B)** que celui de Rab1a (**Figure Conclusion C)**.

A

```
Q9H0U4 RAB1B_HUMAN      1   ---MNPEYDYLFKLLLIGDSGVGKSCLLLRFADDTYTESYISTIGVDFKIRTIELDGKTI      57
P62820 RAB1A_HUMAN      1   MSSMNPEYDYLFKLLLIGDSGVGKSCLLLRFADDTYTESYISTIGVDFKIRTIELDGKTI      60
                            ************************************************************

Q9H0U4 RAB1B_HUMAN     58   KLQIWDTAGQERFRTITSSYYRGAHGIIVVYDVTDQESYANVKQWLQEIDRYASENVNKL      117
P62820 RAB1A_HUMAN     61   KLQIWDTAGQERFRTITSSYYRGAHGIIVVYDVTDQESFNNVKQWLQEIDRYASENVNKL      120
                            ***********************************:***: **:****************

Q9H0U4 RAB1B_HUMAN    118   LVGNKSDLTTKKVVDNTTAKEFADSLGIPFLETSAKNATNVEQAFMTMAAEIKKRMGPGA      177
P62820 RAB1A_HUMAN    121   LVGNKCDLTTKKVVDYTTAKEFADSLGIPFLETSAKNATNVEQSFMTMAAEIKKRMGPGA      180
                            ******.*****:*** ***:**********************:****************

Q9H0U4 RAB1B_HUMAN    178   ASGG-ERPNLKIDSTPVKPAGGGCC                                  201
P62820 RAB1A_HUMAN    181   TAGGAEKSNVKIQSTPVKQSGGGCC                                  205
                            ::** *: *:**:***** :*****
```

B

```
Q9H0U4 RAB1B_HUMAN      1   MNPEYDYLFKLLLIGDSGVGKSCLLLRFADDTYTESYISTIGVDFKIRTIELDGKTIKLQ      60
Q15286 RAB35_HUMAN      1   MARDYDHLFKLLIIGDSGVGKSSLLLRFADNTFSGSYITTIGVDFKIRTVEINGEKVKLQ      60
                            *  :**:*****:*********.*******:*:: ***:**********:*::*:.:***

Q9H0U4 RAB1B_HUMAN     61   IWDTAGQERFRTITSSYYRGAHGIIVVYDVTDQESYANVKQWLQEIDRYASENVNKLLVG      120
Q15286 RAB35_HUMAN     61   IWDTAGQERFRTITSTYYRGTHGVIVVYDVTSAESFVNVKRWLHEINQNC-DDVCRILVG      119
                            ***************:****:**:********  **:.**:**:**:: . ::* ::****

Q9H0U4 RAB1B_HUMAN    121   NKSDLTTKKVVDNTTAKEFADSLGIPFLETSAKNATNVEQAFMTMAAEIKKRMGPGAASG      180
Q15286 RAB35_HUMAN    120   NKNDDPERKVVETEDAYKFAGQMGIQLFETSAKENVNVEEMFNCITELVLRAKKDNLAKQ      179
                            **.*  :****:.  * :**..:** ::*****: .***: *  ::  : :    . *.

Q9H0U4 RAB1B_HUMAN    181   -GERPNLKIDSTPVKPAGGGCC                                     201
Q15286 RAB35_HUMAN    180   QQQQQNDVVKLTKNSKRKKRCC                                     201
                              :: *  :. *  .     **
```

C

```
P62820 RAB1A_HUMAN      1   MSSMNPEYDYLFKLLLIGDSGVGKSCLLLRFADDTYTESYISTIGVDFKIRTIELDGKTI      60
Q15286 RAB35_HUMAN      1   ---MARDYDHLFKLLIIGDSGVGKSSLLLRFADNTFSGSYITTIGVDFKIRTVEINGEKV      57
                              *  :**:*****:*********.*******:*:: ***:**********:*::*:.:

P62820 RAB1A_HUMAN     61   KLQIWDTAGQERFRTITSSYYRGAHGIIVVYDVTDQESFNNVKQWLQEIDRYASENVNKL      120
Q15286 RAB35_HUMAN     58   KLQIWDTAGQERFRTITSTYYRGTHGVIVVYDVTSAESFVNVKRWLHEINQNC-DDVCRI      116
                            ******************:****:**:********  *** **:**:**:: . ::* ::

P62820 RAB1A_HUMAN    121   LVGNKCDLTTKKVVDYTTAKEFADSLGIPFLETSAKNATNVEQSFMTMAAEIKKRMGPGA      180
Q15286 RAB35_HUMAN    117   LVGNKNDDPERKVVETEDAYKFAGQMGIQLFETSAKENVNVEEMFNCITELVLRAKKDNL      176
                            **:** *  :***:   * :**..:** ::*****: .***: *  ::  : :    .

P62820 RAB1A_HUMAN    181   TAGGAEKSNVKIQSTPVKQSGGGCC                                  205
Q15286 RAB35_HUMAN    177   AKQQQQQQNDVVKLTKNSKRKKRCC                                  201
                            :    ::.*  :: *  .:    **
```

Figure conclusion :

Alignement des séquences de Rab1a et Rab1b (A), Rab1B et Rab35 (B) et Rab1a et Rab35 (C) réalisés par ClustalO.

La plus grande efficacité de phosphocholination de Rab35 et l'affinité pour les membranes sont deux propriétés d'AnkX qui sont en accord avec les résultats obtenus par Allgood *et al.* (2017) qui co-localisent AnkX avec Rab35 dans des cellules humaines, suggérant donc qu'AnkX cible Rab35 durant l'infection plutôt que Rab1a. Les études de Lem3, l'enzyme catalysant la réaction de déphosphocholination, menée dans notre laboratoire par Wenhua Zhang ainsi que celles publiées par l'équipe de R. S. Goody montrent une plus grande activité de dé-phosphocholination de Rab1a et Rab1b que de Rab35. Nous pouvons donc

émettre l'hypothèse suivante : l'activité de Lem3 corrigerait la phosphocholination sur la sérine 79 de Rab1 par AnkX, favorisant son AMPylation sur la sérine 78 par l'effecteur de Legionella Drra qui déclenche son recrutement à la surface de la LCV. Ces hypothèses peuvent être testées par l'analyse de localisation d'AnkX et Lem3 dans des cellules humaines infectées. Il est également possible d'étudier à l'aide de liposomes la spécificité membranaire de Lem3 et l'effet des membranes sur son activité.

Pour continuer l'analyse de l'activité d'AnkX, il peut maintenant être intéressant de déterminer si une activation est observée lorsque seule AnkX est localisée aux membranes, ce qui indiquerait que les membranes modifient directement les propriétés catalytiques de la toxine, et ne contribuent pas seulement à augmenter la probabilité de rencontre de l'enzyme et de son substrat. Enfin, l'étude de la modification de Rab35 par AnkX en présence de liposomes permettrait de confirmer la spécificité d'AnkX vis à vis de Rab35 par rapport à Rab1.

Comme nous sommes parvenus à purifier la forme $AnkX^{Cter}$, son interaction avec les liposomes pourra être étudiée, ce qui permettra peut-être de confirmer le rôle supposé du domaine C-terminal dans l'interaction avec les membranes.

L'étude de stabilisation du complexe $AnkX^{FL}$/Rab pourra être poursuivie et l'utilisation de formes courtes d'AnkX, afin de diminuer la flexibilité de la protéine, pourra être envisagée. Dans ce but, la production de la forme $AnkX^{\Delta Cter}$ devra être améliorée car les conditions actuelles de purification ne donnent pas un rendement et une pureté de la protéine suffisants pour mener une étude biochimique et structurale.

Un travail de mise au point plus poussé de l'utilisation du composé chimique nouvellement synthétisé, le Mant-CDC, pourrait nous permettre de trouver une condition d'utilisation de ce dérivé fluorescent de la CDP-choline permettant de détecter l'activité d'AnkX en cinétiques de fluorescence

Enfin, l'étude structurale mérite d'être poursuivie. Si une condition de stabilisation du complexe est trouvée, des essais de cristallisation pourront être réalisés ainsi qu'une analyse du complexe en solution par SAXS. Le profil de diffraction SAXS permettra de le comparer à celui avec la protéine entière ce qui donnera des informations sur la fixation de la petite protéine G par AnkX. Les cristaux de la forme $AnkX^{Cter}$ dernièrement obtenus seront améliorés et nous tenterons de résoudre le problème des phases d'une part par utilisation de métaux lourds (technique du remplacement isomorphe MIR) et d'autre part en marquant la protéine par de la sélénométhionine (technique du signal anomal SAD).

Enfin, une étude de la protéine en forme entière par microscopie électronique pourrait

être tentée à nouveau, AnkX^{FL} ayant théoriquement une taille compatible avec cette étude.

Ce projet a permis d'avancer sur l'étude de deux systèmes de régulation, très différents dans leurs modalités, de cette famille de protéines bactériennes. Sur les deux protéines ayant fait l'objet de ce travail, nous avons mis en évidence des nouveaux mécanismes de régulation qui montrent que l'étude des protéines FIC peut permettre « de belles surprises » malgré leur incroyable conservation structurale.

Titre : Structure et fonction de protéines bactériennes à domaine FIC

Mots clés : FIC, protéines, crystallographie, structure, biochimie.

Résumé : Les protéines à domaine FIC (Filamentation induced by cAMP) sont très répandues chez les bactéries où elles catalysent l'ajout d'une modification post-traductionnelle contenant un phosphate à une protéine cible, en utilisant différents co-substrats comme l'ATP. Certaines de ces protéines sont des toxines sécrétées par des pathogènes humains, mais la fonction de la plupart d'entre elles reste mystérieuse. Plus d'une dizaine de structures de protéines FIC ont été déterminées récemment, qui ont permis d'élucider leur mécanisme catalytique. Durant ma thèse, j'ai étudié la structure et les mécanismes de régulation de deux types de protéines FIC : les protéines FIC à glutamate inhibiteur, et la toxine AnkX de la bactérie pathogène Legionella pneumophila.
La première étude s'est intéressée à la protéine FIC de la bactérie pathogène Enterococcus faecalis (EfFIC), qui fait partie de la sous-famille des protéines FIC possédant un glutamate inhibiteur pour la fixation de l'ATP. J'ai résolu plusieurs structures cristallographiques d'EfFIC, qui ont permis de caractériser son site catalytique et la fixation de l'AMP et l'ADP. En utilisant une propriété fréquemment observée d'auto-AMPylation (modification par l'AMP), j'ai montré au moyen d'ATP radioactif qu'EfFIC possède une activité basale d'auto-AMPylation, et j'ai identifié une nouvelle activité de dé-AMPylation. En m'inspirant des métaux observés dans mes structures, j'ai montré que l'alternance entre les activités d'AMPylation et de de-AMPylation dépend de la nature du métal fixé dans le site actif et de la présence du glutamate. Ce glutamate régulateur est également présent chez une protéine humaine, HYPE, qui possède une double activité d'AMPylation et dé-AMPylation d'une chaperone du réticulum endoplasmique. Par un test de fluorescence, j'ai enfin montré que l'activité de HYPE était elle aussi régulée par les métaux. Ces résultats suggèrent un nouveau modèle de régulation partagé par des protéines FIC de la bactérie à l'homme.
La seconde étude a porté sur la toxine AnkX de Legionella pneumophila, qui est constitué d'un domaine FIC, de répétitions ankyrine et d'un domaine C-terminal et qui modifie les petites protéines G Rab1 et Rab35 (régulatrices du trafic cellulaire) par une molécule de phosphocholine (PC). En utilisant des liposomes de composition contrôlée, j'ai montré qu'AnkX interagit avec les membranes et j'ai identifié par mutagenèse son domaine d'interaction. Au moyen de petites GTPases Rab ancrées artificiellement à la surface de liposomes par une queue 6his remplaçant le lipide naturel, j'ai montré que l'activité d'AnkX est stimulée par la présence de membranes. J'ai ensuite mené une étude structurale d'AnkX par diffusion des rayons X aux petits angles (SAXS), qui permet d'obtenir des informations structurales en solution. L'analyse en SAXS montre que ces domaines s'organisent en forme de fer à cheval, suggérant un modèle d'association bi-partite du complexe AnkX/Rab aux membranes. L'ensemble de ces résultats conduit à un modèle dans lequel l'activité d'AnkX est régulée spatialement par les membranes, ce qui pourrait lui permettre de cibler à la fois les petites GTPases Rab cellulaires et le compartiment membranaire

Title : Structure and function of bacterial FIC proteins

Keywords : FIC, proteins, X-ray crystallography, structure, biochemistry

Abstract : FIC (Filamentation induced by cAMP) domain containing proteins are widespread in bacteria where they use different substrate such ATP to modify a target protein with a phosphate containing post-translational modification. Some of those proteins are secreted toxins from pathogens but the function of the majority stay unknown. In my thesis, I lead a structural and biochemical study of two type of FIC proteins: the auto-inhibited for ATP binding by a glutamate FIC sub-family and the *Legionella pneumophila* toxin AnkX.
For the first study, I focused on the pathogenic bacteria *Enterococcus faecalis* protein EfFIC that is an auto-inhibited FIC protein. I solved several crystallographic structures to characterize the active site and the AMP and ADP binding. Exploiting the classic auto-AMPylation (modification with an AMP molecule) mechanism and radioactive ATP, I demonstrated EfFIC activity and I identified a new de-AMPylation activity. Using metals found in my crystallographic structures, I showed that the AMPylation and de-AMPylation switch is controlled by the nature of the metal bound in the active site and that this switch is inhibitory glutamate-dependent. This glutamate is found in human HYPE that present a double AMPyaltion and de-AMPylation activity of the ER chaperone BIP. Using fluorescence assays, I showed that those two activities are regulated by metals as in EfFIC. Those results point on a new regulation model shared from bacteria to human.
The second study focused on *Legionella pneumophila* toxin AnkX that modifies small GTPases Rab1 and Rab35 with a phosphocholine (PC) molecule. Using controlled composition liposomes, I showed that AnkX interact with membranes and mapped the interaction domain by mutagenesis. With artificially anchored to nickel containing liposomes surface Rab GTPases, I demonstrated the stimulation of AnkX activity by the membranes. Preliminary results also suggest that Rab35 is a better substrate than Rab1a, giving information on AnkX function and localization during infection. I lead a small angle X-ray scattering (SAXS) study on AnkX that gave low-resolution structural information on AnkX in solution. The analyses of SAXS results show that AnkX is horseshoe shaped, suggesting an association with the membrane and Rab of AnkX model. In this model, membranes spatially regulate AnkX, allowing a targeting of Rab and cellular compartment targeting.

Université Paris-Saclay
Espace Technologique / Immeuble Discovery
Route de l'Orme aux Merisiers RD 128 / 91190 Saint-Aubin, France